

ABSTRACT

Title of Document: METABOLIC CHANGES ASSOCIATED
WITH ANDROGEN INDEPENDENT
GROWTH IN A MOUSE MODEL OF
PROSTATE CANCER

Philip Lloyd Martin, M.S., D.V.M., DACVP

Directed By: Siba Samal, Ph.D., Professor and Chairman

PTEN and *TP53* loss are common molecular alterations in aggressive prostate cancer that progresses to castrate resistant prostate cancer (CRPC). *PTEN/TP53* loss contributes to regulation of self-renewal and differentiation in prostate progenitor cells, the presumptive tumor and metastasis initiating cells for prostate cancer. *TP53* plays an important role in regulating normal cellular metabolism, and loss of function is responsible for metabolic alterations in tumor cells, including increased aerobic glycolysis. We use a novel model of *Pten/TP53* deleted prostate cancer to investigate properties of tumor and metastasis initiating cells, and metabolic alterations that contribute to the evolution of CRPC.

We employed a genetically engineered mouse model of *Pten^{-/-}TP53^{-/-}* prostate cancer to develop an orthotopic model derived from a clonal cell line from the parental heterogeneous prostate carcinoma. We used histopathology and immunohistochemistry to characterize the orthotopic primary tumors and metastases. We performed metabolomic screening followed by focused analysis of HK II enzyme levels, activity,

and cellular distribution in androgen replete and androgen deprived tumors. We also compared HK II levels in primary and metastatic human prostate cancer.

Tumor heterogeneity was due to transformation of tumor and metastasis initiating cells with biphenotypic potential capable of basal and luminal differentiation. There was epithelial-to-mesenchymal transition (EMT) in cells of the luminal lineage. The model was capable of androgen independent growth, which influenced the differentiation of metastasis initiating cells. CRPC had increased reliance on glycolysis with increased cytoplasmic and mitochondrial-associated HK II. These metabolic adaptations afforded CRPC increased ability to withstand metabolic stress. HK II levels in human metastases were markedly increased compared to primary tumors.

Pten/Tp53 loss in prostate cancer contributes to lineage plasticity in both tumor and metastasis initiating cells, contributing to heterogeneity observed in primary tumors and metastases. Increased glycolysis due to increased total and mitochondrial HK II is a metabolic adaptation that contributes to the evolution of aggressive disease, with progression to androgen independence, providing increased energy and carbon precursors for anabolic processes. Mitochondrial bound HK II blocks apoptosis and contributes to survival in the androgen deprived environment. Targeting this metabolic adaptation may provide improved treatment for this deadly disease.

METABOLIC CHANGES ASSOCIATED WITH ANDROGEN INDEPENDENT
GROWTH IN A MOUSE MODEL OF PROSTATE CANCER

By

Philip Lloyd Martin

Dissertation submitted to the Faculty of the Graduate School of the
University of Maryland, College Park, in partial fulfillment
of the requirements for the degree of
[Doctor of Philosophy]
[2014]

Advisory Committee:

Siba Samal, Ph.D., Professor and Chairman

Robert J. Dooling, Ph.D., Professor

Kathleen Kelly, Ph.D.

Meiqing Shi, D.V.M., Ph.D. Assistant Professor

R. Mark Simpson, D.V.M, Ph.D., DACVP

Xiaoping Zhu, D.V.M., Ph.D., Professor

© Copyright by
Philip Lloyd Martin
2014

Dedication

This work is dedicated to my wife Talia and my children: Alex, Avner, and Aviva. Their endless love and support gave me the strength and energy to persevere through the many years of this research project. I also dedicate this work to the prostate cancer patients of the past, present, and future (and their families), who may hopefully one day soon benefit from the findings of this research project.

Acknowledgements

- Kathy Kelly
- Mark Simpson, Josh Webster, Shelley Hoover, Jennifer Edwards
- Graduate Committee: Siba Samal, Kathy Kelly, Mark Simpson, Robert Dooling, Xiaoping Zhu, Meiqing Shi
- The Kelly Lab: Ben Barrett, Victoria Seng, Rachel Pierce, Ivy Yin, David Liu, Wassim Abou-Kheir, Orla Casey, Paul Hynes, Heather Tillman, Ross Lake, Yvona Ward, Daniel Camacho
- My wife Talia, and kids: Alex, Avner, and Aviva
- The NIH animal care staff and veterinarians
- The NIH Mouse Imaging Facility staff and veterinarians

Table of Contents

Abstract	
Title Page	
Copyright Page	
Dedication	ii
Acknowledgments	iii
Table of Contents	iv
List of Tables	v
List of Figures	vi
Chapter 1: Introduction	1
A. Epidemiology	1
B. Pathogenesis of human prostate cancer.....	2
C. Signaling pathways driving progression in prostate cancer	2
D. The role of androgen receptor signaling	3
II. Modeling human prostate cancer in the mouse	4
A. Comparison of human and mouse prostate glands	4
B. Genetically engineered mouse models of human prostate cancer	5
C. Orthotopic injection models of prostate cancer	7
III. Prostate cancer metabolism	9
A. General features of cancer metabolism	10
B. General features of prostate metabolism	10
C. Prostate cancer metabolism: androgen dependence	11
D. Prostate cancer metabolism in castrate resistant disease	12
E. Increased glycolysis in CRPC: The role of hexokinase II in energy production	13
F. Increased glycolysis in CRPC: the role of hexokinase II in pro-survival mechanisms	15
G. The role of AKT signaling in regulating hexokinase II	16
IV. Thesis goals and outlines	17
A. Experimental aims	17
B. Dissertation outline	18
Chapter 2: Prostate Epithelial Pten/TP53 Loss Leads to Transformation of Multipotential Progenitors and Epithelial to Mesenchymal Transition	21
I. Abstract.....	21
II. Introduction	22
III. Results	25
IV. Discussion	52
V. Materials and Methods	56
Chapter 3: Increased Total and Mitochondrial-Associated Hexokinase II Provides A Metabolic Adaptation to Growth and Survival in Androgen Deprived Conditions ...	65
I. Abstract.....	65
II. Introduction	66
III. Results	70
IV. Discussion	95
V. Materials and Methods	101
Chapter 4: Conclusion	107
Bibliography	110

List of Tables

Chapter 2. Prostate Epithelial *Pten/TP53* Loss Leads to Transformation of Multipotential Progenitors and Epithelial to Mesenchymal Transition

Table 1. Summary of immunohistochemical marker expression in wild type prostate epithelium and <i>PB-Cre4⁺Pten^{fl/fl}TP53^{fl/fl}</i> primary tumors or tumors arising from orthotopically transplanted tumor cell suspensions.....	32
Table 2. Summary of in-vitro and in-vivo phenotypes for <i>Pten/TP53</i> null prostatic carcinoma clonal cell lines.....	42
Table 3. Comparison of the prostatic carcinoma phenotypes derived from orthotopically transplanted Clone 1 and Clone 2 cells.....	48
Supplemental Table 1. The number and phenotype of lung metastases in individual mice orthotopically injected with Clone 1 cells under androgen replete and androgen deprived conditions.....	55

List of Figures

Chapter 2: Prostate Epithelial *Pten/TP53* Loss Leads to Transformation of Multipotential Progenitors and Epithelial to Mesenchymal Transition

Figure 1. Survival rate and tumor phenotype incidence for <i>PB-Cre4⁺; Pten^{fl/fl}; TP53^{fl/fl}</i> mice.	31
Figure 2. <i>PB-Cre4⁺; Pten^{fl/fl}; TP53^{fl/fl}</i> mice display a diversity of tumor phenotypes.	33
Figure 3. Orthotopic injection of <i>PB-Cre4⁺; Pten^{fl/fl}; TP53^{fl/fl}</i> mouse primary prostate carcinoma cells favors the development of adenocarcinoma.	38
Figure 4. Orthotopic prostatic intraepithelial neoplasia (oPIN) and orthotopic adenocarcinoma (oAC) resulting from injection of primary <i>PB-Cre4⁺; Pten^{fl/fl}; TP53^{fl/fl}</i> tumor cells.	39
Figure 5. Expression of differentiation and signaling markers in cultured wild type prostatic basal cells (see Materials and Methods) and in <i>Pten/TP53</i> deleted Clones 1 and 2 prostatic carcinoma cell lines.	44
Figure 6. Clonal orthotopic <i>PB-Cre4⁺; Pten^{fl/fl}; TP53^{fl/fl}</i> carcinomas demonstrate multi-lineage differentiation, metastasis, and epithelial to mesenchymal transition.	45
Figure 7. Androgen sensitivity and androgen independent tumor growth in <i>PB-Cre4⁺; Pten^{fl/fl}; TP53^{fl/fl}</i> Clone 1 orthotopic prostate carcinomas.	51
Figure 8. AR expression in Clone 1 orthotopic prostate carcinoma, recipient control prostate, and lung metastasis.	52
Figure S1. Co-expression of the neuroendocrine marker synaptophysin and cytokeratin 8 (CK8) in primary <i>PB-Cre4⁺; Pten^{fl/fl}; TP53^{fl/fl}</i> prostate carcinoma and orthotopic prostate carcinoma.	34
Figure S2. Epithelial to mesenchymal transition marker expression in sarcomatoid carcinoma.	35
Figure S3. Characterization of orthotopic prostatic carcinomas from Clone 2 including: bioluminescent imaging of lymphovascular invasion, epithelial to mesenchymal transition, and osseous metaplasia.	47

Chapter 3: Increased Total and Mitochondrial-Associated Hexokinase II Provides A Metabolic Adaptation to Growth and Survival in Androgen Deprived Conditions

Figure 1. Survival curves and histopathology of androgen replete and androgen deprived nude mice orthotopically injected with *Pten*^{-/-}*Tp53*^{-/-} prostate carcinomas.77

Figure 2. Metabolic analysis of androgen replete and androgen deprived *Pten*^{fl/fl},*TP53*^{fl/fl} orthotopic prostate carcinomas.80

Figure 3. Boxplots comparing metabolites that are increased in androgen deprived orthotopic *Pten*^{-/-}*Tp53*^{-/-} tumors similar to results reported for increased malignancy in human prostate cancer specimens.82

Figure 4. Androgen independent growth leads to increased expression of many genes involved in carbohydrate metabolism.84

Figure 5. Dual color immunohistochemistry demonstrates increased hexokinase II expression in androgen deprived orthotopic tumors relative to androgen replete tumors.87

Figure 6. Increased in-vitro and in-vivo cytoplasmic and mitochondrial or particulate hexokinase activity in androgen deprived tumor cells.93

Figure 7. Increased cell viability in response to metabolic stress in androgen deprived Clone 1 cells in-vitro.96

Figure 8. Hexokinase II levels in human prostate cancer primary and metastatic tumors. Tumors were scored semi-quantitatively for hexokinase II levels detected by immunohistochemistry on human prostate cancer tissue microarrays.98

Supplemental Figure 1. Frequency distributions for manual ki67 x hexokinase II quantification and Ariol™ system automated quantification90

Chapter 1: Introduction

I. Introduction to prostate cancer

A. Epidemiology

Prostate cancer is the second leading cause of cancer-related deaths in males, with approximately 1 in 6 males in the USA becoming affected [1, 2]. Prostate cancer will cause an estimated 29,480 deaths out of 233,000 new cases diagnosed in 2014 in the USA which is second only to lung cancer as the leading cause of cancer related deaths in men with an estimated 159,260 deaths out of an estimated 224,210 cases in 2014 [3]. Metastatic castrate resistant disease is usually the cause of death in these patients, as the primary tumors can be removed with surgical prostatectomy. The most common site of prostate metastasis is bone, with approximately 84% of patients presenting with metastasis having bone metastases followed by distant lymph nodes (10.6%), liver (10.2%), and thorax (9.1%) [4]. The development of mouse models that recapitulate the important features of progression to castrate resistant prostate cancer (CRPC) and metastasis are of paramount importance for the mechanistic study of this disease. This dissertation research describes the development of a novel mouse model of CRPC that is used to investigate the identity of tumor and metastasis initiating cells, and the metabolic changes that provide adaptation for the growth and survival of prostate cancer cells in the androgen deprived environment of CRPC.

B. Pathogenesis of human prostate cancer

Human prostate cancer usually follows a predictable pattern of initial prostatic intraepithelial neoplasia (PIN) with a slow progression to invasive carcinoma that can take up to 10 years, and in some cases the development of metastasis. In the early stages the tumors are usually androgen dependent yet progress to androgen independence with the development of invasive carcinoma and metastasis [5]. There has been intensive research into the molecular pathogenesis and genomics of prostate cancer. Many tumor suppressor genes have been implicated based on the region of chromosomal deletions in human prostate cancer specimens (ie: *RB*, *TP53*, *PTEN*, and *NKX3.1*). *PTEN* loss is often seen early (initiation), while p53 loss is often late in disease progression [6, 7]. *PTEN* deletions/mutations have been detected in 30% of primary and 64% of metastatic prostate carcinomas [8-10].

C. Signaling pathways driving progression in prostate cancer

Two of the major signaling pathway networks that have been implicated in driving human prostate cancer progression to castrate resistant prostate cancer (CRPC) are the AKT/mammalian target of Rapamycin (AKT/mTOR) and the ERK/MAPK signaling pathways [11]. Using mouse models as well as IHC analysis on human prostate cancer TMAs, Kinkade et. al, demonstrated the synergistic effect of the AKT/mTOR and the ERK/MAPK pathways in promoting the growth of CRPC [11]. In their investigation, p-AKT and p-ERK were elevated in human PIN in 28% and 40% of cases respectively, while in high-grade adenocarcinoma p-AKT and p-ERK were elevated in 79% and 68% of cases respectively. The mouse model described in this dissertation has upregulation of PI3K/AKT/mTOR signaling pathway as a result of *Pten* deletion, a

negative regulator of AKT. IHC results also have shown high levels of both nuclear and cytoplasmic pERK, suggesting that there is also activation of MAPK signaling.

D. The role of androgen receptor signaling

The growth of normal prostate epithelial cells, as well as the growth of neoplastic prostate cancer cells, is highly dependent upon the androgen receptor (AR) and its signaling mechanisms [12]. The first line of treatment in most cases of non-prostate confined, or metastatic prostate cancer, is blockage of normal AR signaling. However, in a small percentage of men the prostate cancer will adapt to the loss of AR signaling and progress to CRPC. There have been many mechanisms proposed, and confirmed, by which prostate cancer cells adapt to maintain androgen signaling networks in the presence of minimal castrate levels of circulating androgens [13]. There is a great deal known about the effects of androgen stimulation or withdrawal on human prostate cancer cells lines in vitro [14-16], and of the mechanisms of escape from androgen deprivation in CRPC specimens [12-15, 17, 18]. However, data is lacking regarding the selection process by which tumor cells subjected to androgen deprivation therapy eventually adapt to survive and proliferate despite the minimal castrate levels of androgens. In this dissertation we describe a novel mouse model which can be used to track the evolution of CRPC. Using this model, we identify that a change in tumor energy metabolism is associated with the adaptation of prostate cancer cells to the androgen deprived environment. Mouse models of androgen independent prostate cancer are crucial for investigating the effects of androgen withdrawal, as similar studies in humans are difficult if not impossible.

II. Modeling human prostate cancer in the mouse

A. Comparison of mouse and human prostate glands

In humans the prostate gland is an approximately walnut-sized organ which surrounds the urethra at the base of the bladder. Its normal function is the production of important secretions for the seminal fluid. The architecture of the human prostate can be divided into a central zone, the transitional zone, and the peripheral zone [19, 20]. The outermost peripheral zone is where most prostatic adenocarcinomas arise, while the more common benign prostatic hyperplasia arises from the transitional zone. The mouse prostate, in contrast, has a lobular architecture with paired ventral, anterior, and dorsolateral lobes. Each of these lobes have unique patterns of ductal branching, epithelial cell histology, gene and protein expression [21]. Both the mouse and the human contain the same three major epithelial cell types: luminal, basal, and neuroendocrine cells. In the human there is a continuous layer of basal cells which express CK5 and p63, which support the luminal cells which express CK8/CK18. Rarely in the epithelial cell layer there are synaptophysin + neuroendocrine cells as well. These epithelial cells lie on a basement membrane which is then supported by a large amount of fibro vascular stroma. The mouse, in contrast, does not have a complete basal cell layer, and there is only a thin layer of fibro muscular stroma that surrounds each gland. In the human, prostate adenocarcinoma is usually comprised of cells with a luminal (CK8/CK18) phenotype. However, other rare variations include basal cell carcinoma and neuroendocrine carcinoma of the prostate. Thus, when designing/characterizing mouse models of prostate cancer, one must pay close attention to the morphological and

molecular expression profile of the mouse prostate cancer to ensure its relevance to the human disease which we wish to model.

B. Genetically engineered mouse models of human prostate cancer

Transgenic mouse models provide the opportunity to study the molecular pathogenesis of prostate cancer in a model system with a defined genetic background that can be easily manipulated to test mechanistic hypotheses. The development of relevant mouse models of human prostate cancer is critical for the mechanistic study of prostate carcinogenesis as the data obtained from human specimens regarding the molecular mechanisms of carcinogenesis and metastasis is only correlative. In addition, there are only a limited number of human cancer lines available for study and these are from non-representative and variable genetic backgrounds. For example two of the commonly used human prostate cancer cell lines, LnCAP and PC3, were isolated from individual tumors over 30 years ago. The LnCAP cell line was isolated from a human prostate cancer lymph node metastasis and described in 1983 [22], while the PC3 cell line was isolated from a human prostate cancer bone metastasis and described in 1979 [23]. Many studies have used these cell lines in both basic and pre-clinical research [24-29]. Clearly improvements can be made.

Many investigations into the molecular pathology of human specimens give conflicting results due to tumor heterogeneity/multifocality or gene inactivation by a mechanism other than a coding region lesion (ie: promoter methylation, mutations in regulatory sequences, etc.) [6, 30]. In addition, the long term in-vitro growth of human prostate cancer cells may alter their characteristics and confound mechanistic studies [31].

The ideal mouse model should recapitulate both the human disease phenotype (morphology and disease progression) and molecular pathogenesis. Several transgenic mouse models have been developed which to some degree model human prostate carcinogenesis (although metastasis in these models is rare). A review of mouse models of prostate cancer was recently published which provides a comprehensive histopathological analysis of the most recently developed mouse models of prostate cancer [32]. A review of older mouse models of prostate cancer is provided in the consensus report from the Bar Harbor meeting of the Mouse Models of Human Cancer Consortium Prostate Pathology Committee [33]. Prostate specific deletion of *Pten* driven by the rat *Cre-Probasin4* (*PB-Cre4*) transgene has been shown in mice to lead to prostate adenocarcinoma that is capable of lymphatic invasion [34]. Chen et. al.[35] deleted both *Tp53* and *Pten* in the prostate which led to a more rapid progression to invasive adenocarcinoma than with *Pten* deletion alone, due to the role of *Tp53* loss in preventing tumor cell senescence. *Pten* deletions have also been combined with other deletions to provide a “second hit” such as with *p27^{-/-}* [36], *Nkx3.1* [37, 38], or *Smad4* [39].

In our mouse model of prostate cancer described herein, we also used deletion of *Tp53* and *Pten*; however we report important findings that were not described in the initial description of the model. We performed a thorough characterization of the histopathological progression of the model and describe previously unreported heterogeneity in histopathological phenotypes including: adenosquamous carcinoma, basal/squamous carcinoma, and sarcomatoid carcinoma [40]. We also demonstrate that the sarcomatoid carcinoma arises as a result of epithelial-to-mesenchymal transition (EMT) from adenocarcinoma of a luminal cell phenotype. In addition we also investigate

the role of *Tp53* loss in regulating the differentiation of tumor cell lineage, and identify the tumor and metastasis initiating cell as a bi-potential progenitor capable of differentiating along both basal and luminal cell lineages.

While *Tp53* is often thought of as the master regulator of cell cycle progression, there has been an increasing realization of the effects of *Tp53* in regulating cellular metabolism. *Tp53* has been shown to regulate cellular metabolic response to stress and the loss of this function has been shown to lead to characteristic features of tumor metabolism including increased glycolysis and increased glutaminolysis to fuel tumor energy production and anabolic reactions [41-43]. This characteristic tumor metabolic phenotype due to loss of *Tp53* forms the basis of our investigation into the metabolic adaptation of prostate cancer to CRPC.

C. Orthotopic injection models of prostate cancer

The utility of employing orthotopic injection to access the normal prostate microenvironment for growth and metastasis of injected cells has been demonstrated in numerous studies involving a variety of prostate cancer cell lines where growth in the subcutaneous tissue or renal sub-capsular space is slow and metastases non-existent, while orthotopically injected cells grow and metastasize readily [44-49]. Bastide, et. al. [47] found that 80% of Nod/Scid had metastases 8 weeks after orthotopic implantation of human PC-3 cells. Although very useful, orthotopic studies using human cell lines are limited due to the small number of human prostate cancer cell lines available, their unknown genetic background, as well as uncertainty regarding the effects of long term in-vitro culture.

Orthotopic injection of mouse prostate cancer cells offers significant advantages as an alternative to xenotransplantation of human prostate cancer cell lines. The main advantage of using mouse prostate tumor cells is the ability to engineer a specific constellation of molecular mutations which will enable a mechanistic study of the molecular pathogenesis of prostate cancer growth and metastasis. In addition, the problems of variability among human cell lines and of using long term culture adapted cells is largely eliminated. An additional potential benefit is the ability to use immunocompetent recipient mice, as modeling the interaction between cancer and the intact immune system is essential for an optimal cancer model.

Recent advances in in-vivo bioluminescent imaging have enabled the real-time assessment of tumor size and location as well as the presence of metastases. Orthotopic injection of bioluminescent human prostate cancer lines has been demonstrated to be a very efficient method to assay response of tumor and/or metastases to chemotherapy [50]. The development of a transplantable bioluminescent mouse orthotopic prostate cancer model is an important step in providing flexibility in a model with well-defined genetic parameters for investigating the molecular mechanisms of prostate cancer growth and metastasis.

Orthotopic injection also solves many of the problems with GEMs that often render them unsuitable for preclinical research. In mouse models of prostate cancer, the prostate specific promoters often result in multifocal expression of transgenes or Cre-lox targeted deletions of tumor suppressor genes. This often leads to diffuse transformation of the prostate epithelium and eventual obstruction of urinary outflow as the tumors invade and compress the urinary bladder, ureters, and urethra. Thus morbidity in the

mice is due to the secondary effects of the primary tumor, and not due to metastatic CRPC as is most common in humans. Some of the other problems associated with mouse prostate cancer models include not being able to reliably reproduce bone metastases, one of the most important metastatic sites in human prostate cancer, and having histology that is not representative of the human adenocarcinoma.

The *PB-Cre4; Pten^{-/-}; Tp53^{-/-}* model whose development and characterization is described within this dissertation project, [40] as well as the *Nkx3.1; Pten^{-/-}* [11] model have demonstrated progression to CRPC, however the model itself does not metastasize. Numerous mouse models of prostate cancer have been developed using a wide range of prostate specific promoters to drive increased expression or deletion of oncogenes or tumor suppressor genes [32, 51]. While many of these mouse models recapitulate most of the range of prostate cancer phenotypes observed in humans, they fail to reproduce one of the most important features associated with morbidity/mortality in humans: bone metastases. Some of the most relevant models incorporate common molecular lesions that are observed in humans including: *TMPRSS2-ERG* translocations [52], *Pten/Tp53* loss [40], *Pten/Smad4* [39] loss, and combining loss of the *Nkx3.1* homeobox gene with *Pten* loss which results in upregulation of both RAS-MAPK and PI3K-AKT signaling [11, 53].

III. Prostate cancer metabolism

A. General features of cancer metabolism

One consistent feature of the metabolic changes associated with carcinogenesis is an increase in aerobic glucose metabolism, named The “Warburg effect” after its discovery by Warburg [54]. Aerobic glycolysis is very inefficient at producing ATP with

only 2 molecules of ATP produced per molecule of glucose vs. 36 molecules of ATP produced with complete oxidation via oxidative phosphorylation [55]. However aerobic glycolysis provides carbon substrates for the upregulated anabolic processes required for rapidly growing tumor cells such as nucleic acid production via the pentose phosphate pathway, lipogenesis, and protein synthesis [56, 57]. In addition, the lactate that is formed can be converted back into pyruvate for the TCA cycle or provide carbons for amino acid synthesis, or can be made into Acetyl-CoA for use in de-novo lipogenesis [58]. The mechanism of the increased glycolysis associated with the Warburg effect has been demonstrated to be largely due to mitochondrial bound HK II, the first and rate limiting enzyme in glycolysis which allows escape from product inhibition (G-6-P) as well as the preferential access to mitochondrial ATP [59-61].

Some of the cell signaling mechanisms that have been shown to increase tumor glycolysis include: activation of PI-3 Kinase or disruption/deletion of *Pten* with activation of AKT [62-67]. The mechanisms of increased glycolysis due to AKT activation include: increased expression of surface membrane glucose transporters, increased mitochondrial binding by HK II, and activation of phosphofructokinase one of the key regulators of glycolytic rate [62]. As a large percentage of advanced prostate cancers display AKT activation [11], increased glycolysis and mitochondrial associated HK II would be expected. However, little research has been done on the activity and cellular distribution of HK II in prostate cancer.

B. General features of prostate metabolism

The energy metabolism of normal prostate epithelial cells differs from virtually all other epithelial cells in that large amounts of citrate are secreted into the prostatic

fluid, instead of being completely oxidized in the TCA cycle and used for oxidative phosphorylation. The result is a large amount of “wasted” energy as large numbers of ATP molecules that could have potentially been produced through complete oxidation of citrate are “lost” to the citrate in prostatic secretions. The mechanism of this truncated TCA cycle is due to zinc accumulation in the mitochondria of prostate cells, which inhibits the mitochondrial aconitase enzyme responsible for converting citrate into isocitrate in the TCA cycle [68].

C. Prostate cancer metabolism: androgen dependence

Androgens regulate the unique energy metabolism of normal prostate epithelium and primary prostatic adenocarcinomas which is based on lipid metabolism rather than the more common emphasis on glycolysis in most other tumor types. The lipid anabolic and catabolic processes in normal and transformed prostate epithelial cells are largely dependent upon the activity of the sterol regulatory element binding protein (SREBP). The SREBP is responsible for regulating the transcription of several genes involved in lipid metabolism. This is in part responsible for a reliance on lipid metabolism in primary androgen dependent prostate adenocarcinomas, including lipid uptake, lipogenesis, and utilization of lipids for energy production [16, 69, 70]

Primary prostate cancer, unlike most other tumors, does not rely on aerobic glycolysis but rather mitochondrial fatty acid β -oxidation (CPT1) as the dominant bioenergetic pathway [71]. Lipid metabolism in prostate cancer cells, especially lipogenesis, is androgen dependent, in part due to the indirect activation of the SREBP pathway by androgen receptor signaling [16, 70]. Lipid uptake is also androgen regulated as membrane lipid transporters (FABPpm) have been demonstrated to be

upregulated in response to androgen stimulation [69]. mTOR signaling also activates the SREBP [72, 73] and plays a role in regulating prostate cancer lipid metabolism [74]. Positron Emission Tomography (PET) studies indicate poor glucose uptake (F18-FDG) with increased lipid uptake/utilization (C11-acetate uptake) in clinical studies on primary prostate adenocarcinomas [75, 76]. The important role of androgens in regulating the energy metabolism of normal and primary prostate cancer led us to study the effects of androgen withdrawal on prostate cancer metabolism. We hypothesize that androgen depletion will result in a strong selection pressure to adapt to a carbohydrate based rather than a lipid based energy metabolism.

D. Prostate cancer metabolism in castrate resistant disease

Evidence from in-vivo and in-vitro studies in both humans and mouse models support a switch to an increased reliance on glycolysis instead of fatty-acid B-oxidation for energy metabolism in CRPC [16]. Of particular relevance to this dissertation research is the fact that androgen independent xenografts and cell lines increased F18-FDG uptake as well as increased expression of the GLUT1 glucose membrane transporters, as compared to androgen dependent cell lines and xenografts [77, 78]. The data suggesting increased reliance upon glycolysis as compared to fatty acid B-oxidation following androgen deprivation led us to hypothesize that for CRPC in our mouse model, increased glycolysis would be an adaptive mechanism in the androgen deprived environment. In addition to the energetic benefit, the increased carbon precursors from glycolysis can fuel anabolic processes such as shunting glucose-6-phosphate into the pentose phosphate pathway, and citrate into the cytoplasm for de novo lipogenesis. However, the results from studies on the effects of androgens on prostate cancer metabolism are often difficult

to interpret and give confounding results, likely due to the high degree of heterogeneity in prostate cancer. In fact, it has been shown that gene expression analysis of metabolic genes in the same cell lines from different labs have produced significantly different gene expression signatures [15]. This highlights the necessity of using metabolism gene expression and metabolite screening data as a guide for more refined assays designed to validate the general metabolic trends suggested by the broad spectrum metabolic screens. We propose that the most relevant way to model the changes in energy metabolism associated with castrate resistant prostate cancer (CRPC) is to use a genetically defined mouse model (containing common genetic lesions present in human CRPC). Here one can perform metabolic assays on the primary androgen dependent tumors and compare the results to those from androgen independent tumors that have been allowed to re-grow after initial androgen deprivation and evolution into CRPC through the selection process present in the androgen deprived environment.

E. Increased glycolysis in castrate resistant prostate cancer: the role of hexokinase II in energy production

The increased glycolysis associated with aerobic glycolysis in tumors (the Warburg effect) has been shown to be largely due to an increase in cytoplasmic and even more importantly mitochondrial associated HK II [59].

HK II catalyzes the irreversible first step in glycolysis:

Glucose + Mg-ATP \longrightarrow Glucose-6-phosphate + Mg-ADP [61]. Once phosphorylated, glucose is now trapped inside the cell and can be used for energy production via the glycolysis-TCA cycle-oxidative phosphorylation pathways. Alternatively glucose-6-phosphate can be shunted to the pentose-phosphate-pathway (PPP) for nucleic acid

production. Glucose-6-phosphate can be shunted out of the energetic pathways for other anabolic processes such as de-novo lipogenesis by the shunting of citrate out of the TCA cycle and into the cytoplasm. In mammals there are 4 hexokinase isoforms (1-4), with HK-1 and HK-2 being able to attach to the outer mitochondrial membrane, HK-3 is located in the perinuclear compartment, and HK-4 is located in the cytosol in certain organs such as the liver and pancreas [61]. HK-2 is the predominant isoform expressed by malignant tumors and in tumors is often located on the outer mitochondrial membrane voltage dependent anion channel (VDAC) [58, 79]. Several metabolic and cell-signaling pathways have been implicated in regulating HK II-mitochondrial VDAC binding including: intracellular lactate, pH, ATP/ADP ratio, glucose/glucose-6-phosphate ratio, AKT, and AMPK signaling [80-82]. Blocking PI3K-AKT signaling has been shown to inhibit the HK II-mitochondrial association in human hepatocellular carcinoma cell lines, as has PI3K independent activation of pAKT via AMPK signaling [83]. Insulin signaling has also been shown to participate in the binding of HK II to the VDAC [58]. In tumor cells glycolysis and oxidative phosphorylation can be spatially coupled through the binding of HK II to the VDAC on the outer mitochondrial membrane (OMM). This provides a dramatic energetic benefit by allowing HK II direct access to high concentrations of mitochondrial ATP through the OMM adenine nucleotide translocase exchange channel and VDAC [84], rather than relying on the lower concentration of ATP in the cytoplasm. In normal tissues that do not express significant levels of HK II such as the liver and pancreas, which express primarily the lower glucose affinity hexokinase IV isoform, one of the earliest metabolic adaptations associated with carcinogenesis is a switch from the hexokinase IV isoform to the expression of the higher glucose affinity

HK II isoform [60, 85-88]. Thus in human hepatocellular carcinoma cells, HK II is switched on while hexokinase IV is silenced [83]. In addition to the obvious energetic benefit to increasing glucose-6-phosphate production, this increased activity of HK II also provides increased carbon substrates to fuel nucleic acid production in the pentose phosphate pathway and for de-novo lipogenesis via the shuttling of citrate into the cytoplasm at the expense of fueling the TCA cycle. In addition, remaining bound to the outer mitochondrial membrane allows HK II to escape inhibition from its product glucose-6-phosphate [61].

F. Increased glycolysis in castrate resistant prostate cancer: the role of hexokinase II in pro-survival mechanisms

Perhaps just as important as the increased energy metabolism, and production of carbon substrates for anabolic processes required for rapidly growing tumor cells, is the fact that the binding of HK II to the VDAC directly inhibits the binding of several pro-apoptotic proteins (ie: Bax, Bak, Bad), and inhibits their oligomerization and initiation of apoptosis [89, 90]. Releasing the VDAC bound HK II via various inhibitors [91-93] strongly induces apoptosis in these previously resistant tumor cells. The attachment of HK II to the outer mitochondrial VDAC has been shown to be an adaptation to inhibition of glycolysis with 2-deoxyglucose, which is used to simulate low glucose conditions and metabolic stress in-vitro [94]. Increased HK II was shown by Ahn, et. al [83] to lead to increased survival in human hepatocellular carcinoma cells when exposed to the chemotherapeutic agent cisplatin.

This anti-apoptotic role of mitochondrial-associated HK II has been recognized as a potential drug target. Disrupting the HK II-mitochondrial interaction with compounds

such as 3-bromopyruvic acid, clotrimazole, bifanazole, methyl jasmonate, or a competitive peptide inhibitor has already demonstrated to be highly efficacious against tumors in animal models [95-98]. Targeting prostate cancer glycolysis with the inhibitory 2-Deoxyglucose has also been attempted in human clinical trials [99].

Inhibition of PI3K-AKT signaling dissociated mitochondrial bound HK II and led to increased apoptosis in human hepatocellular carcinoma cell lines [83]. The use of a HK II inhibitor has also been shown to have a synergistic effect in combination with a standard chemotherapeutic, cisplatin, in human colon cancer cells in vitro [100]

Despite the importance of HK II expression and cellular distribution in tumor metabolism and survival, no one has yet investigated the role of HK II in promoting prostate carcinogenesis or in the evolution of androgen independent growth. As we hypothesize that the evolution of CRPC will be associated with a switch to a more glycolytic phenotype in prostate cancer, it is logical to hypothesize that an increased glycolysis will be associated with increased total and mitochondrial-associated HK II.

G. The role of AKT signaling in regulating hexokinase II

As our mouse model demonstrates increased AKT activation due to the loss of the inhibitory effects of *Pten*, it is important to consider the role of PI3K/AKT signaling in HK II levels and cellular localization. Mitochondrial HK II is a major effector of AKT mediated tumor cell growth and survival [58, 90, 101]. Although the exact mechanism by which activated AKT increases mitochondrial-bound HK II is not currently known, circumstantial evidence points to AKT playing a role in maintaining the mitochondrial-HK II association and inhibiting the release of cytochrome c and blocking apoptosis [90]. This is based on the findings that AKT is necessary for maintaining mitochondrial

integrity and preventing cytochrome c release following apoptotic triggers. However, glucose is required for AKT signaling to prevent apoptosis. Cells in which AKT genes have been deleted lose the ability to maintain HK II bound to the outer mitochondrial membrane at the VDAC [102]. Similarly cells treated with a PI3-K inhibitor also had a reduced ability to maintain the mitochondrial-HK II association. Using drugs to dissociate HK II from the mitochondrial VDAC also ablated the anti-apoptotic effects of activated AKT. Even in the absence of the pro-apoptotic factors Bax and Bak, Majewski et. al, [102], showed that forced dissociation of HK II from the VDAC caused cytochrome c release into the cytoplasm and apoptosis. The role of activated AKT in regulating glycolysis via HK II levels and mitochondrial association is another piece of evidence leading to our hypothesis that CRPC in our *Pten*^{-/-}*Tp53*^{-/-} mouse model will be associated with increased total and mitochondrial associated HK II.

IV. Thesis Goals and Outline

A. There are two major aims of this dissertation research:

- 1) Develop and characterize a mouse model of *Pten*/*Tp53* deleted prostate cancer to investigate: the innate presence of castrate resistant prostate cancer (CRPC), the identity of tumor and metastasis initiating cells, and the lineage specific development of epithelial-to-mesenchymal transition.

Hypothesis: Orthotopically injected *Pten* and *Tp53* mouse prostate carcinoma will be capable of androgen independent (castrate resistant) growth and metastasis. The phenotypic heterogeneity: adenocarcinoma, adenosquamous carcinoma, basal/squamous carcinoma, and sarcomatoid carcinoma, each with

occasional neuroendocrine differentiation, that are observed in primary tumors and metastases are due to a multi-potent tumor and metastasis initiating prostate progenitor cell that is capable of differentiating along basal and luminal lineages with occasional neuroendocrine differentiation.

- 2) Determine if there are metabolic differences between androgen dependent and castrate resistant prostate cancer that may serve as adaptations for the evolution and survival of CRPC.

Hypothesis: CRPC will be associated with increased glycolysis as an adaptation to survival in androgen independent conditions in contrast to the reliance on lipid metabolism in androgen replete conditions. This increased glycolysis is adaptive not only to compensate for energetic needs, but also to provide carbon precursors for anabolic processes such as lipogenesis and nucleic acid synthesis via the Pentose phosphate pathway, as well as to prevent metabolic stress induced apoptosis.

B. Dissertation outline

The 2 chapters of this dissertation will be presented in the form of two separate manuscripts for publication:

- Chapter 1 describes the generation and characterization of the model. The initial thorough histopathological examination showed significant histopathological heterogeneity. This led us to investigate heterogeneity in lineage differentiation and phenotypic plasticity in tumor and metastasis initiating cells, as well as epithelial-to-mesenchymal transition (EMT). This manuscript has been published

in the American Journal of Pathology: *Prostate epithelial Pten/TP53 loss leads to transformation of multipotential progenitors and epithelial to mesenchymal transition* [40].

We performed our investigations on two well characterized clonal cells lines. The first, referred to as Clone 1, was a bipotential stem/progenitor cell line capable of differentiating along both luminal and/or basal lineages, with occasional neuroendocrine marker expression. The second, referred to as Clone 2, was a luminal progenitor cell line that produced adenocarcinoma with occasional neuroendocrine marker expression, with increasing EMT through progression to sarcomatoid carcinoma. Both of these clonal cell lines were capable of producing adenocarcinoma with a similar phenotype to that seen in most human prostate adenocarcinomas: CK8/CK18 luminal cells with occasional expression of neuroendocrine markers (ie: synaptophysin). The results of this investigation indicate that *Pten/TP53* loss in the mouse prostate epithelium leads to the expansion of multipotent tumor and metastasis initiating cells that are capable of differentiating along luminal and/or basal lineages, with occasional neuroendocrine differentiation.

Androgen deprivation led to the development of castrate resistant prostate cancer, and metastasis initiating cells that were primarily bi-potential progenitors expressing both basal and luminal markers, in contrast to androgen replete tumors where metastasis initiating cells were primarily of the luminal lineage. Epithelial-to-mesenchymal transition (EMT) was confirmed in cells of the luminal lineage derived from Clone 2 orthotopic tumors. These results highlight the role that *TP53* loss plays in regulating the

differentiation status of tumor and metastasis initiating cells, as well as its role in promoting EMT.

- Chapter 2 describes the investigation into the metabolic differences between androgen replete and androgen deprived orthotopic *Pten/TP53* mouse prostate carcinomas that were derived from Clone 1, the unique stem/progenitor cell line capable of multi-lineage differentiation. An initial metabolomic screen provided the rationale for this chapter's investigation as the preliminary results indicated an increased carbohydrate utilization in the androgen deprived tumors.

The results of this investigation indicate that increased glycolysis is associated with stem/progenitor cell mediated CRPC. This increased glycolysis is the result of increased cytoplasmic and mitochondrial HK II. Increased total and mitochondrial-associated HK II provides a novel metabolic adaptation for the evolution of CRPC due to increased energy production, increased production of anabolic precursors, and protection from apoptosis. This metabolic adaptation provides a new target in the fight against this deadly form of prostate cancer.

Chapter 2: Prostate Epithelial *Pten/TP53* Loss Leads to Transformation of Multipotential Progenitors and Epithelial to Mesenchymal Transition

I. Abstract

Loss of *PTEN* and loss of *TP53* are common genetic aberrations occurring in prostate cancer. *PTEN* and *TP53* contribute to the regulation of self-renewal and differentiation in prostate progenitors, presumptive tumor initiating cells for prostate cancer. Here we characterize the transformed phenotypes resulting from deletion of the *Pten* and *TP53* tumor suppressors in prostate epithelium. Using the *PB-Cre4⁺Pten^{fl/fl}TP53^{fl/fl}* model of prostate cancer, we describe the histologic and metastatic properties of primary tumors, transplanted primary tumor cells, and of clonal cell lines established from tumors. Adenocarcinoma was the major primary tumor type that developed, which progressed to lethal sarcomatoid carcinoma around 6 months of age. In addition, basal carcinomas and prostatic urothelial carcinoma were observed. We show that tumor heterogeneity resulted, at least in part, from the transformation of progenitors with biphenotypic potential. CK8+ luminal epithelial cells were capable of undergoing epithelial to mesenchymal transition in vivo to sarcomatoid carcinomas containing osseous metaplasia. Metastasis rarely was observed from primary tumors, but metastasis to lung and lymph nodes occurred frequently from orthotopic tumors initiated from a biphenotypic clonal cell line. Androgen deprivation influenced the differentiated phenotypes of metastases. These data show that one functional consequence of *Pten/TP53* loss in prostate epithelium is lineage plasticity of transformed cells.

II. Introduction

Prostate cancers display a range of clinical behavior, from slow-growing tumors of minor clinical significance to locally aggressive and ultimately metastatic disease. Human prostate adenocarcinoma has a mature luminal phenotype characterized by cytokeratin 8 (CK8) and androgen receptor (AR) expression and PSA production. Progressive prostate cancer (PC) is almost always treated with androgen deprivation therapy (ADT), but despite such treatment, approximately 10% of prostate cancers progress to metastatic disease [103]. Defining mechanisms of resistance to androgen deprivation and progression to metastasis would be significantly aided by the availability of genetically-defined models of prostate cancer progression.

One of the most common genetic alterations in prostate cancer is deletion of at least one copy of the *PTEN* tumor suppressor, which occurs in approximately 70% of human prostate cancers. Biallelic deletion of *PTEN* and the associated increase in AKT phosphorylation, which occurs in roughly 25% of PC, is correlated with resistance to ADT [104]. A recent genomic profiling study of mostly primary prostate cancers demonstrated that 21% of cases had either a hetero- or homozygous copy number loss of *TP53* [105]. Other large scale studies using combined immunohistochemistry and sequencing approaches have shown that *TP53* mutations occur in approximately 5% of primary tumors and at much higher frequencies in lymph node metastases (16%) and castrate-resistant (26%) tumors [106, 107]. Additionally, *TP53* mutations were found to be independent predictors of tumor recurrence in low and intermediate grade cancers. Thus, loss of *PTEN* and aberrations of *TP53* are implicated in aggressive forms of human PC [107].

Clinical and experimental evidence indicates that a major determinant of metastatic potential is the differentiated phenotype of the cancer cell of origin [108]. Multipotential progenitors as well as luminal progenitors are proposed cells of origin for prostate cancer [109]. Prostate cancer metastases are found most commonly in the bone, lymph nodes, liver, lungs, and dura mater [103, 110, 111]. Within bone metastatic sites there is a remarkable degree of phenotypic heterogeneity among tumor cells when comparing different patients as well as multiple sites within individual patients [103, 111]. This heterogeneity includes differences in morphology as well as immunophenotypes for differentiation markers. Most commonly, prostate cancer metastases tend to have a poorly differentiated morphology and not infrequently are composed of admixtures of mature luminal and neuroendocrine cells and occasionally contain biphenotypic intermediate cells expressing both basal and luminal cytokeratin markers [103, 112]. Thus, prostate cancer metastases develop from initiating cells with multi-lineage potential and/or from cells with significant phenotypic plasticity.

Modeling prostate cancer in mice generally involves the use of cell-type specific promoters to achieve over-expression of oncogenes or deletion of tumor-suppressors, mimicking commonly observed genetic aberrations in human prostate cancer. Deletion of floxed *Pten* alleles (*Pten^{fl/fl}*) initiated by pan prostate epithelial cell expression of *PB-Cre4* leads to the expansion of basal cells and the development of invasive adenocarcinoma with an intermediate/luminal phenotype [113]. On the other hand, deletion of *Pten* driven by PSA or NKX3.1 promoters in luminal progenitors also leads to PIN/adenocarcinoma [114, 115]. These data suggest that more than one differentiated cell type can serve as a target cell population for *Pten* deletion-mediated oncogenesis.

Previous investigations into the effect of combined genetic deficiencies in mouse models of prostate cancer have demonstrated that prostate epithelial cell-specific loss of *Pten* and *TP53* resulted in significantly more penetrant and rapidly developing PC than *Pten* deletion alone, while loss of *TP53* only did not lead to any notable phenotype [35]. It was proposed that the synergistic effect of *Pten/TP53* deletion results from a loss of *TP53* dependent cellular senescence secondary to *Pten* loss because *Pten/TP53* null PIN/adenocarcinoma tumors demonstrated many fewer senescent tumor cells than *Pten* null tumors [35]. Also significant, we have shown using in vitro analyses that *Pten* and *TP53* play a role in regulating self-renewal and differentiation of prostate stem/progenitor cells [116]. Therefore, we hypothesized that increased prostate progenitor amplification and deregulated differentiation contribute to the more aggressive and lethal phenotype of tumors initiated following *Pten/TP53* loss as compared to *Pten* loss only.

Increased numbers and/or plasticity of undifferentiated prostate epithelial cells might be expected to give rise to multiple tumor histologies. A longitudinal description of disease progression in the *PB-Cre4⁺; Pten^{f/f}; TP53^{f/f}* mouse model demonstrated a remarkable degree of cell lineage heterogeneity in primary tumors. We hypothesized that the epithelial heterogeneity derived from the transformation of a multi-potential progenitor cell. In addition, the occurrence of CK8+/Vimentin+ cells in tumors undergoing epithelial to mesenchymal transition (EMT), suggested an epithelial origin for the large spindle cell tumors that often caused morbidity/mortality in these mice. In order to investigate the origin and characteristics of primary tumor heterogeneity, clonal epithelial cell lines were established from tumors to evaluate the differentiation potential of clonally-derived tumor initiating cells. Upon in vivo inoculation, individual cell lines

recapitulated specific features of heterogeneous primary tumors, including EMT and biphenotypic basal and luminal epithelial differentiation. The biphenotypic line described here was androgen-sensitive and highly metastatic, characteristics that allow modeling of prostate cancer progression.

III. Results

A. PB-Cre4⁺; Pten^{fl/fl}; TP53^{fl/fl} mice develop adenocarcinoma with progression to sarcomatoid carcinomas but not metastasis.

As shown in Fig. 1A, *PB-Cre4⁺; Pten^{fl/fl}; TP53^{fl/fl}* mice demonstrated significantly earlier morbidity and mortality as compared to *PB-Cre4⁺; Pten^{fl/fl}* mice (Fig. 1A). A longitudinal pathological analysis (Fig. 1B) showed that *PB-Cre4⁺; Pten^{fl/fl}; TP53^{fl/fl}* mice developed severe mouse prostatic intra-epithelial neoplasia (mPIN) as early as 8 weeks with progression to adenocarcinoma by 12 weeks. All mice eventually succumbed by 30 weeks as the result of urinary tract obstruction by sarcomatoid carcinomas (Fig. 1). Mouse prostatic intraepithelial neoplasia (mPIN) lesions were comprised of large numbers of cyokeratin 8 (CK8) +/cyokeratin 5 (CK5) +/TP63- intermediate cells and CK8+/CK5-/TP63- luminal cells (Fig. 2C), with occasional foci containing small increases in CK8-/CK5+/TP63+ basal cells. CK8+/CK5- cells increased in proportion to CK8+/CK5+ cells in invasive adenocarcinoma relative to PIN (Table 1 and Fig. 2D), suggesting increased accumulation of differentiated luminal cells in adenocarcinoma. Co-expression of the neuroendocrine marker synaptophysin and CK8 were occasionally observed in focal regions of adenocarcinoma and mPIN (see Supplemental Figure S1A). At approximately 15-19 weeks, sarcomatoid carcinomas could be observed arising in the

wall of the anterior prostate, adjacent to poorly differentiated adenocarcinoma (Fig. 2G). As adenocarcinoma progressed to sarcomatoid carcinoma, there was a reduction/loss of E-cadherin and CK8 coupled with an increase in vimentin expression (Table 1). Occasional neoplastic spindle-shaped cells co-expressing CK8 and vimentin were observed, indicating epithelial to mesenchymal transition (see Supplemental Figure S2). Nuclear expression of the EMT marker, slug, was detected by IHC in sarcomatoid carcinomas (see Supplemental Figure S2), but was rarely detected in adenocarcinoma. Nuclear androgen receptor expression as determined by IHC decreased with disease progression. In mPIN, there was strong nuclear expression of AR in luminal cells. In adenocarcinoma, there was more heterogeneity relative to mPIN in the levels of AR expression, with loss of AR in occasional cells. AR was often very low or undetectable in spindle cell carcinoma (Table 1). At the time of death or euthanasia, distant metastases were not observed; however lymphovascular and perineural invasion was common (Fig. 2B&E), and small aggregates of tumor cells occasionally were detected in sublumbar lymph nodes and pulmonary capillaries.

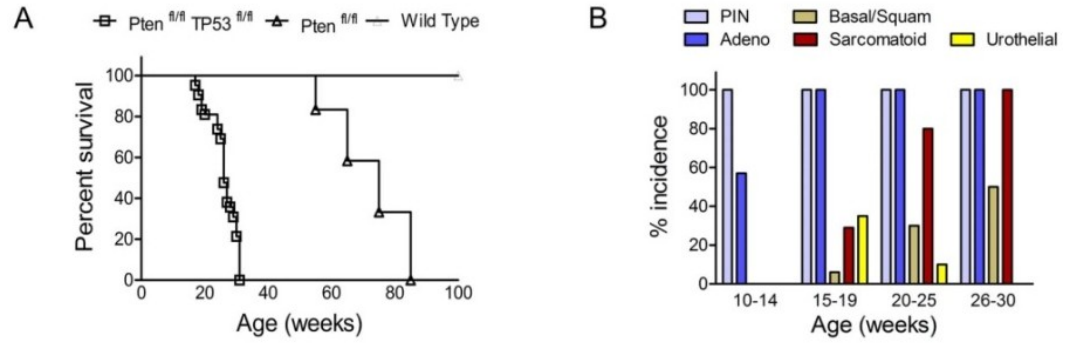


Figure 1. Survival rate and tumor phenotype incidence for $PB-Cre4^+; Pten^{fl/fl}; TP53^{fl/fl}$ mice. A) Kaplan-Meier curve showing the survival rates for $PB-Cre4^+; Pten^{fl/fl}; TP53^{fl/fl}$ (n=41) ($Pten^{fl/fl} TP53^{fl/fl}$) open squares, $PB-Cre4^+; Pten^{fl/fl}; TP53^{fl/fl}$ littermates (n=38) (Wild Type, straight line), and $PB-Cre4^+; Pten^{fl/fl}$ (n=12) ($Pten^{fl/fl}$, open triangle). B) Histogram showing the percentage of $PB-Cre4^+; Pten^{fl/fl}; TP53^{fl/fl}$ mice in each age group with a tumor containing the indicated phenotype (%incidence): 10-14 weeks (n=14), 15-19 weeks (n=17), 20-25 weeks (n=10), 26-30 weeks (n=12) : mouse prostatic intraepithelial neoplasia (PIN), Adenocarcinoma (Adeno), Basal/squamous carcinoma (Basal/squam), Spindle cell carcinoma (Sarcomatoid), and Urothelial carcinoma (Urothelial).

Table 1. Summary of immunohistochemical marker expression in wild type prostate epithelium and *PB-Cre4⁺Pten^{fl/fl}TP53^{fl/fl}* primary tumors or tumors arising from orthotopically transplanted tumor cell suspensions.

IHC Marker	Wild-type	mPIN	Adeno.	Sarcomatoid	Basal/Squamous
CK8	+++ in luminal cells	+++ ↑	+++ ↑	+/- ↓	+/-
CK5	+ in basal cells	++	+	-	+++
CK8+/CK5+	+/-	++	+	-	+/-
TP63	+ in basal cells	+(*)	+/-	-	+++
AR	+++	++↓	++↓	+/-↓	++↓
Synaptophysin	+, in rare neuroendocrine cells	+	+	+	+
Synapto./CK8+	+/-	+	+	+/-	+/-
Synapto./CK5+	-	+/-	+/-	-	+
E-cadherin	+++	+++	+++ (†)	-	+++
Vimentin	-	-	+/- (†)	+++	-
Vimentin/CK8+	-	-	+/-	+	-

Mouse prostatic intraepithelial neoplasia (mPIN), adenocarcinoma (Adeno.), sarcomatoid carcinoma (Sarcomatoid), and basal/squamous carcinoma (Basal/Squamous). +++ marker present in most or all cells (80%-100%), ++ marker present in many cells, however there are significant numbers of cells that lack expression (50%-80%), + marker present in a minority of cells (5%-50%), +/- marker is present in only rare populations of cells (less than or equal to 5%), - absence of marker. ↑Denotes increased and ↓denotes decreased IHC labeling intensity relative to epithelial cells in wild-type control prostate. Synapto.=synaptophysin. (*) In mPIN there are areas with minimal proliferation of TP63+ cells along the basal lamina, and rarely in the cell layer superficial to the basal cell layer, as well as areas lacking TP63+ cells. (†) In poorly differentiated adenocarcinoma there is often a decrease in intensity of E-cadherin labeling as well as the presence of rare vimentin + cells.

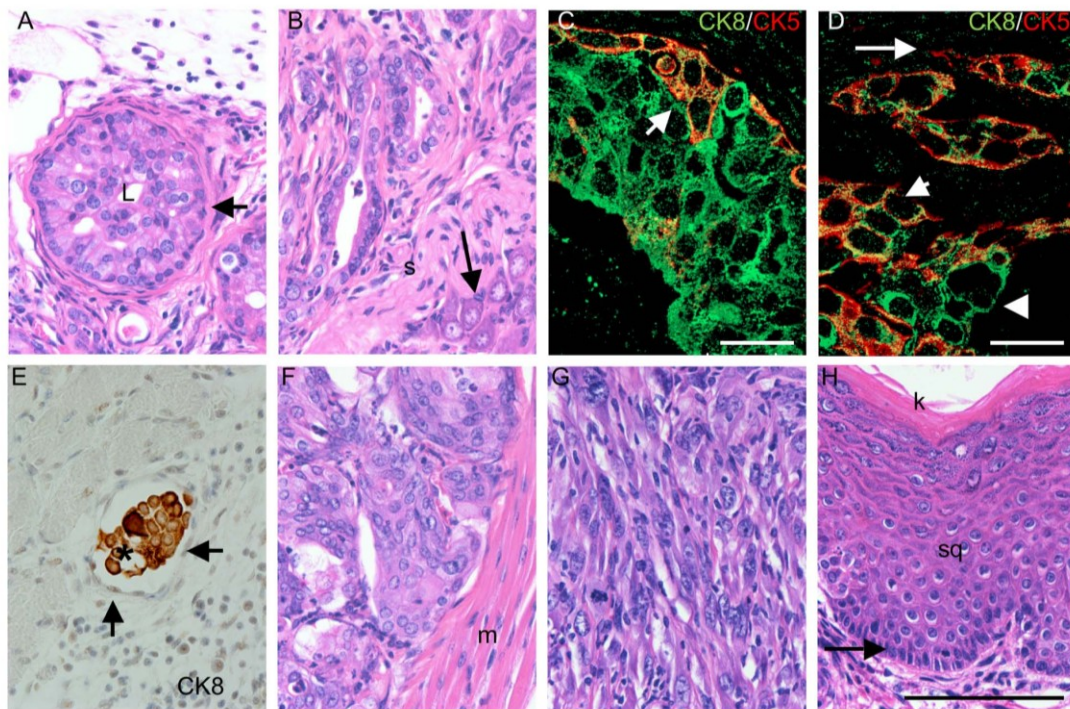
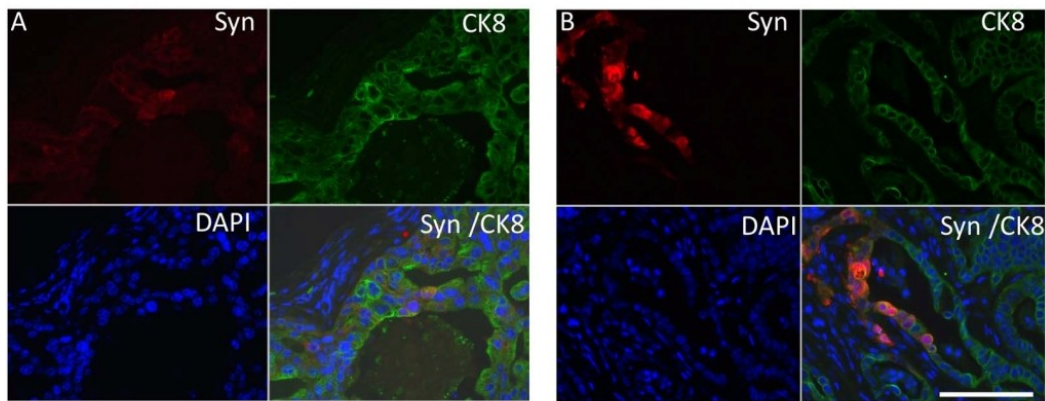


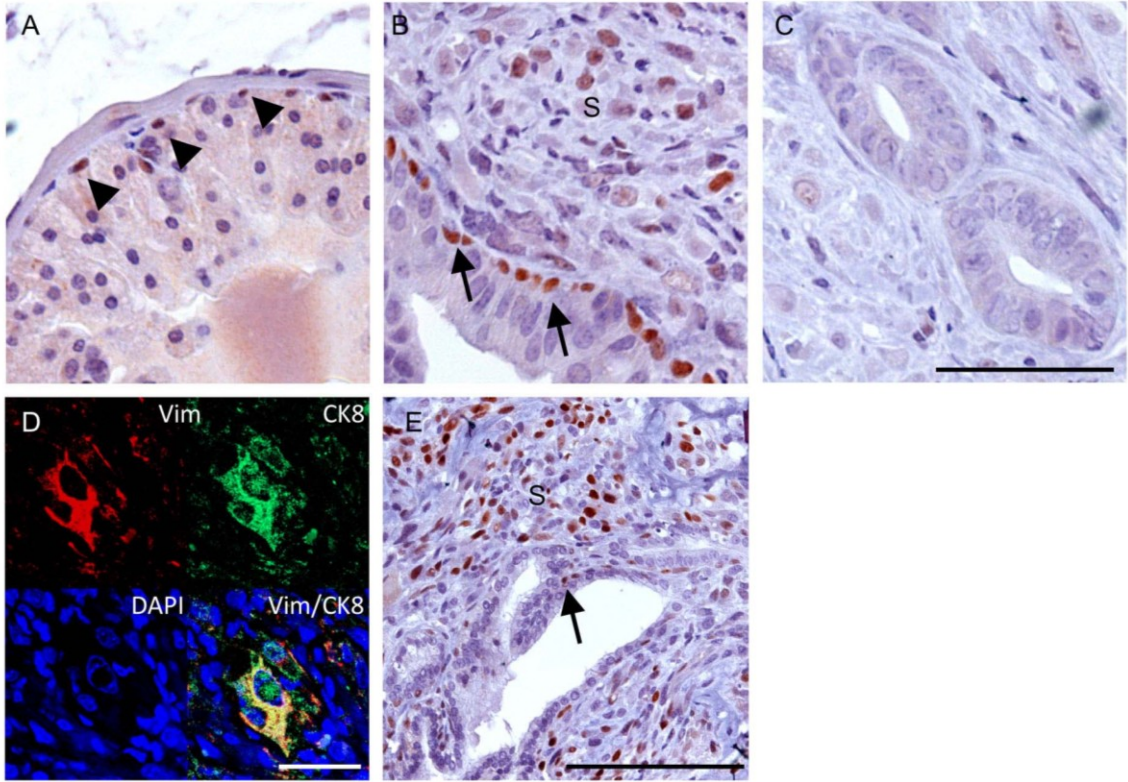
Figure 2. *PB-Cre4⁺; Pten^{fl/fl}; TP53^{fl/fl}* mice display a diversity of tumor phenotypes.

Panels A-F are different regions of tumor from a single mouse. A) High grade mouse prostatic intraepithelial neoplasia (mPIN), 14 week old mouse dorsal prostate. In an mPIN gland, the lumen (L) is almost completely occluded by a marked proliferation of neoplastic epithelium. The neoplasm does not invade the basement membrane and is bounded entirely by smooth muscle (arrow), H&E. B) Adenocarcinoma in periphery of the dorsal prostate. Neoplastic glands invade the stroma (s) adjacent to a prostatic nerve ganglion (arrow), H&E. C&D) Double immunofluorescence for CK8 (Green; Alexa Fluor 488) and CK5 (Red; Alexa Fluor 586) on mPIN (C) and adenocarcinoma (D). In mPIN (C) there are often cells with co-expression of CK5 and CK8 (arrow). In adenocarcinoma (D) there are cells with CK8/CK5 co-expression (short arrow), CK8+/CK5- cells (arrow head), and occasionally CK5+/CK8- cells (long arrow). E)

Vascular invasion. Tumor embolus (asterisk) within lumen of blood vessel is comprised of cells that label positive for CK8. Arrows indicate endothelial cells lining luminal surface of blood vessel, anti-CK8 and hematoxylin. F) Prostatic urothelial carcinoma in proximal prostatic ducts adjacent to the urethral muscularis (m). Note packets of prostatic urothelial carcinoma cells separated by a fine fibro vascular stroma, H&E. G) Sarcomatoid carcinoma in 28 week old mouse. Note streams of spindle shaped cells with large oval nuclei that lack glandular differentiation, H&E. H) Basal/Squamous carcinoma in anterior prostate of 28 week old mouse. Note palisading basal cells (arrow) on basement membrane with overlying stratified squamous epithelium (sq) and superficial keratin layer (k), H&E. Scale bar for A, B, E-H:100 μ m (Images taken at 400X). Scale bars in C&D: 20 μ m (Images taken at 630X).



S1. Co-expression of the neuroendocrine marker synaptophysin (Syn) and cytokeratin 8 (CK8) in primary *PB-Cre4⁺; Pten^{fl/fl}; TP53^{fl/fl}* prostate carcinoma and orthotopic prostate carcinoma. A) *PB-Cre4⁺; Pten^{fl/fl}; TP53^{fl/fl}* mouse primary prostate carcinomas have occasional regions where tumor cells co-express synaptophysin and CK8. B) Focus of synaptophysin and CK8 expression in orthotopic prostate carcinoma resulting from the injection of single cell suspension of *PB-Cre4⁺; Pten^{fl/fl}; TP53^{fl/fl}* mouse primary prostate carcinoma cells into the dorsal prostatic lobe of a nude mouse. Double immunofluorescence with anti-synaptophysin (Red; Alexa Fluor 586) and anti-CK8 (Green; Alexa Fluor 488), DAPI counterstain (200X), scale bar = 100 μ m.



S2. Epithelial to mesenchymal transition marker expression in sarcomatoid carcinoma. A-C) Slug expression in wild type mouse prostate (A) and in an individual 28 week old *PB-Cre4+*; *Pten^{fl/fl}*; *TP53^{fl/fl}* mouse primary prostate tumor (B&C) containing regions of mouse prostatic intraepithelial neoplasia (mPIN), adenocarcinoma, and sarcomatoid carcinoma. A) Wild type mouse prostate with low levels of slug expression in basal cells (arrow heads). B) Slug is expressed in mPIN basal cells (arrows) and in adjacent sarcomatoid carcinoma (S). C) Adenocarcinoma is generally negative for slug expression. A-C (400X), scale bar = 100 μ m. D) CK8 (Green; Alexa Fluor 488) and vimentin (Red; Alexa Fluor 586) double immunofluorescence demonstrating CK8 and vimentin (Vim) co-expression in a large multinucleated tumor cell within a region of sarcomatoid carcinoma in the same mouse tumor as B&C (DAPI counterstain) 630X, scale bar = 20 μ m. E) A Clone 2 orthotopic carcinoma containing regions of adenocarcinoma and sarcomatoid carcinoma and labeled with anti-slug. Slug expression is rare in adenocarcinoma (arrow) however is high in surrounding sarcomatoid carcinoma (S). Anti-slug IHC, DAB chromogen, with hematoxylin counterstain (200X) scale bar = 200 μ m.

B. Primary tumors contain additional minor components of other tumor phenotypes.

In addition to the development of adenocarcinoma with a luminal phenotype, *PB-Cre4⁺; Pten^{f/f}; TP53^{f/f}* tumors occasionally contained regions with a basal/squamous or urothelial phenotype (Fig. 2F&H). Basal/squamous regions often featured keratin production (Fig. 2H) and were characterized by CK5 and TP63 expression (Table 1). Occasionally in the most proximal regions of the prostatic lobes where the prostatic ducts traverse the urethral muscularis and communicate with the urethra, there was carcinoma with a urothelial pattern, referred to as prostatic urothelial carcinoma (CK5+/TP63+ with rare CK8+ cells) (Fig. 2F). However, no tumors of the urinary bladder or urethral transitional epithelium were observed in any mice. Frequently, basal/squamous carcinoma, adenocarcinoma, and prostatic urothelial carcinoma were present in the same tumor. All tumor types displayed heterogeneous expression of the neuroendocrine marker synaptophysin (see Supplemental Figure S1A). Chromogranin A was only rarely observed in isolated individual cells, indicating a not fully differentiated neuroendocrine phenotype. As anticipated, immunohistochemistry failed to detect TP53 or *Pten* expression in tumor cells of all histological types while *Pten* expression could be detected in adjacent reactive stroma.

C. Transplantation of *PB-Cre4⁺; Pten^{fl/fl}; TP53^{fl/fl}* tumor initiating cells does not lead to metastasis.

The rapid growth of primary tumors in this model led to early mortality, which might explain the lack of metastasis. To test the tumor-initiating capacity and metastatic potential of *PB-Cre4⁺; Pten^{fl/fl}; TP53^{fl/fl}* tumor cells, we injected into the dorsal prostatic lobe of nude mice single cell suspensions of primary mouse prostate tumors obtained from 12-16 weeks old *PB-Cre4⁺; Pten^{fl/fl}; TP53^{fl/fl}* mice. A constitutively-expressed luciferase construct was introduced by cross-breeding into the tumor model to provide a noninvasive marker for monitoring the growth and potential metastasis of transplanted cells [117]. Tumors from transplant recipients were harvested upon morbidity, an average of 27 weeks post-injection. Orthotopically transplanted tumor cells primarily formed orthotopic PIN (oPIN) and adenocarcinoma, which expressed markers similar to equivalent primary neoplasms (Figs. 3&4, Table 1 and see Supplemental Figure S1B). Basal/squamous carcinomas and prostatic urothelial carcinomas developed infrequently. Notably, although there were occasional foci of EMT with individual or small clusters of tumor cells acquiring spindle cell morphology, there were no discrete sarcomatoid carcinomas. There was widespread lymphovascular and perineural invasion in transplant recipients; however, metastases were not observed with either ex-vivo bioluminescent imaging of recipient mouse organs or by histopathological examination. The lack of metastasis in orthotopically-transplanted mice, in which there was an additional 12-16 weeks for orthotopic tumor development, supports the conclusion that pan-epithelial

Pten/TP53 deletions alone usually are not sufficient to drive prostate carcinoma metastasis.

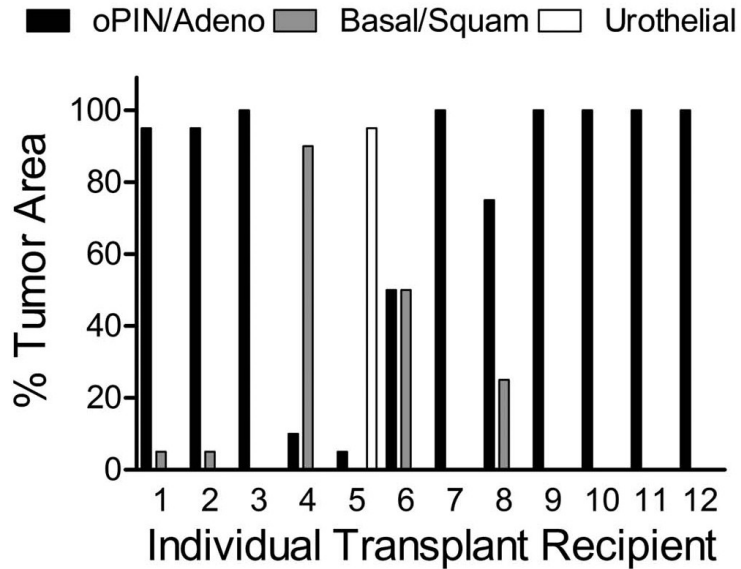


Figure 3. Orthotopic injection of *PB-Cre4⁺; Pten^{fl/fl}; TP53^{fl/fl}* mouse primary prostate carcinoma cells favors the development of adenocarcinoma. Orthotopic prostate carcinoma histological pattern as a percent of total tumor area for each individual orthotopic tumor, n=12 (oPIN/Adeno: mouse orthotopic prostatic intraepithelial neoplasia/adenocarcinoma; Basal/Squam: basal/squamous carcinoma; Urothelial: urothelial carcinoma). Nude mice were injected into one dorsal prostatic lobe with single cell suspensions of *PB-Cre4⁺; Pten^{fl/fl}; TP53^{fl/fl}* mouse primary mouse prostate carcinomas.

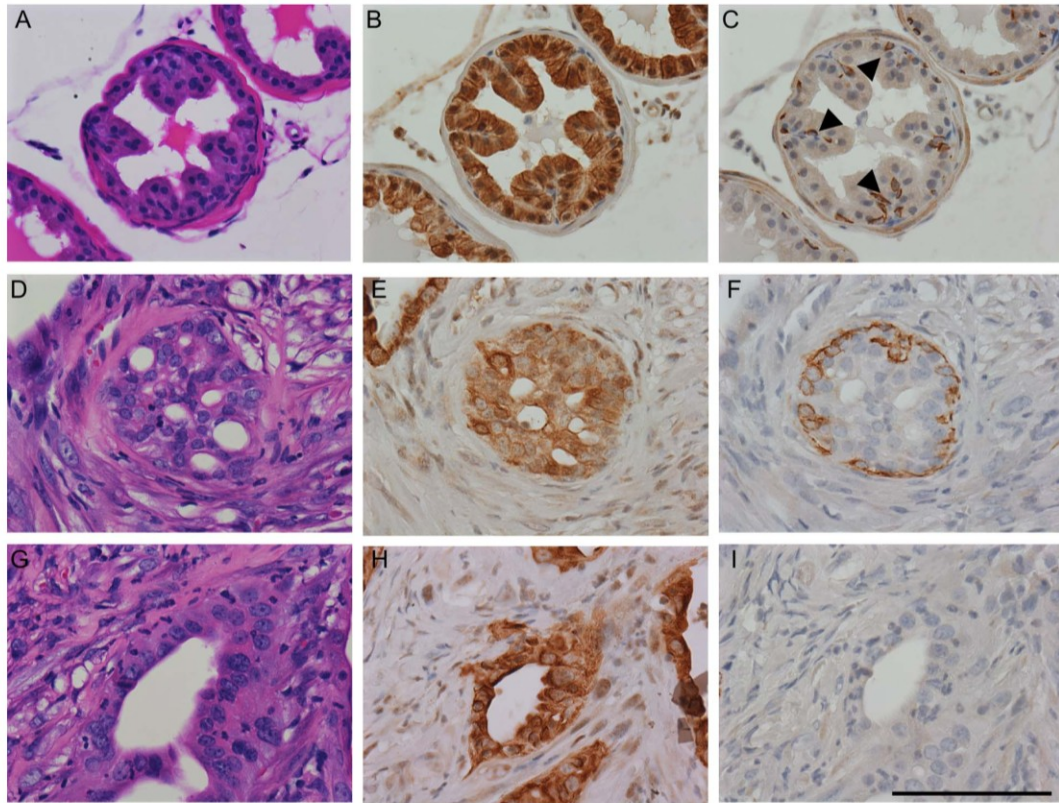


Figure 4. Orthotopic prostatic intraepithelial neoplasia (oPIN) and orthotopic adenocarcinoma (oAC) resulting from injection of primary *PB-Cre4⁺; Pten^{fl/fl}; TP53^{fl/fl}* tumor cells. Sequential serial sections of recipient nude mouse wild type prostate (A-C), oPIN (D-F), and oAC (G-I), were stained with H&E (A,D,G), CK8 (B,E,H), and CK5 (C,F,I). A) Recipient nude mouse wild type dorsal prostate. B) Luminal cells express cytokeratin 8 (CK8) while C) basal cells express cytokeratin 5 (CK5), (arrow heads). D) Orthotopic PIN with marked proliferation of neoplastic glandular epithelium in a cribriform pattern, E) most of the epithelial cells express CK8, F) There is a nearly complete basal cell layer comprised of CK5 expressing cells but no smooth muscle layer.

G) Orthotopic adenocarcinoma, H) the neoplastic epithelium expresses CK8, I) with loss of the CK5+ basal cell layer. All images taken at 400X, scale bar = 100 μ m.

D. Clonally derived cell lines produce tumors containing multiple lineages.

The tumor heterogeneity in primary and orthotopic prostate carcinomas could be the result of transformation of multiple, distinct, lineage-committed tumor progenitor cells and/or of tumor progenitors with multi-lineage potential. As one approach to begin addressing the differentiation potential of tumor-initiating cells, we derived several clonal cell lines from six separate orthotopic carcinomas. Clonal cell lines were immunophenotyped at passages 4 or 5 for CK5, CK8, and vimentin. The characteristics of 9 cell lines that were further expanded and tested for tumorigenicity are shown (Table 2). With the exception of clone 8 that was composed of CK8-/CK5+ cells, all the clones contained CK8+ cells and a variable percentage of double positive CK8+/CK5+ cells. Clonal cell lines appeared to produce continuously differentiating cells as individual colonies derived from single cells contained cells with heterogeneous marker expression. Cell suspensions were injected subcutaneously into nude mice. The basal cell phenotype clone did not form tumors, while 7/8 of the CK8+ clones were tumorigenic. Tumors with mixed histologies developed from 5/7 lines, and adenocarcinoma and sarcomatoid carcinoma developed from clones 6 and 7, respectively. Three cell clones (clones 1, 3, and 4) demonstrated the capacity for biphenotypic basal and luminal differentiation, suggesting origins of the cell lines with bipotential progenitors. In addition, the development of subcutaneous sarcomatoid carcinomas from three clonal epithelial cell lines (clones 2, 5, and 6) formally demonstrates the epithelial origin of spindle cell

tumors in this model (Table 2). Sarcomatoid carcinoma tumors frequently displayed osseous and cartilaginous metaplasia, implying mesenchymal differentiation to the osteoblast and chondrocyte lineages. One clone that produced biphenotypic tumors (Clone 1) and one clone that produced sarcomatoid carcinomas (Clone 2) were analyzed more extensively for the expression of lineage markers and for orthotopic tumorigenic and metastatic characteristics, as described below.

Table 2. Summary of in-vitro and in-vivo phenotypes for *Pten/TP53* null prostatic carcinoma clonal cell lines.

Clone	In-Vitro			Tumor#	In-Vivo
	CK5	CK8	Vimentin		Subcutaneous Tumor Phenotype
1	75%	100%	ND	101	Basal/squamous>adenocarcinoma
2	5%	100%	ND	301	Sarcomatoid/undiff./adeno.>basal/squamous
3	25-50%	100%	<1%	211	Basal/squamous>adenocarcinoma
4	90%	100%	ND	211	Basal/squamous>adenocarcinoma
5	75%	100%	<1%	211	Sarcomatoid>basal/squamous>adeno
6	75%	100%	<1%	222	Sarcomatoid
7	50-75%	75%	<1%	222	Adenocarcinoma
8	100%	0%	ND	222	No Tumor Growth
9	50-75%	100%	ND	222	No Tumor Growth

Average percent of cells expressing CK5, CK8, and vimentin determined by counting at least 200 cells per clonal cell line. ND; no cells detected expressing the marker in the entire well of an 8 well chamber slide containing approximately 1800 cells. <1%; less than 10 cells expressing the marker in the entire well of the chamber slide containing approximately 1800 cells. Undiff.=undifferentiated carcinoma, adeno.=adenocarcinoma.

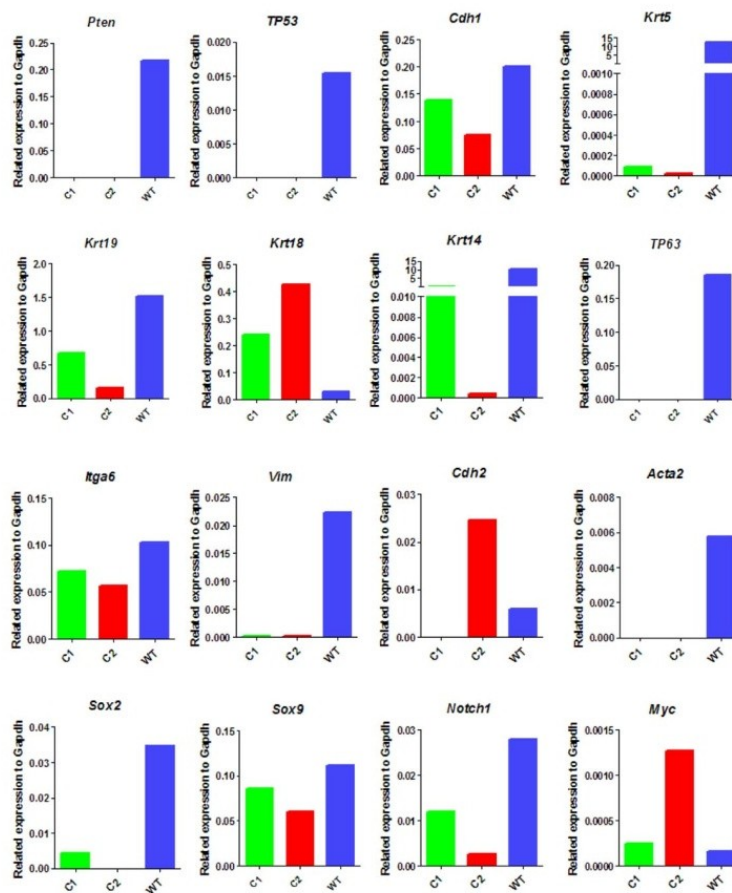
E. Analysis of sarcomatoid carcinoma-producing Clone 2

Clone 2 was comprised of primarily CK8+/CK5- cells with low numbers of CK8+/CK5+ cells. As shown in Fig. 5, the Clone 2 cell line was characterized for RNA expression of a variety of markers including epithelial lineage: *Krt5* (CK5), *Krt8* (CK8), *Krt18* (CK18), *Krt14* (CK14), *TP63*, and *Cdh1* (E-cadherin); mesenchymal lineage: *Vim* (vimentin), *Cdh2* (N-cadherin), *Acta2* (α -smooth muscle actin); progenitor: *Itga6* (α 6 integrin), *Sox2*, and *Notch1*; and prostate growth/differentiation: *Myc*, *Sox9* genes.

An immortalized basal phenotype (CK5+/TP63+) cell line derived from wild-type prostate is shown for comparison. Clone 2 showed a predominantly luminal epithelial expression pattern without evidence of *Vim* or *Acta2* expression. Interestingly, Clone 2 expressed both *Cdh1* and *Cdh2* as well as relatively elevated levels of *Myc* RNA (Fig 5A). As anticipated, Clone 2 cells demonstrated phospho-AKT and AR protein expression (Fig. 5B).

Clone 2 cells gave rise to orthotopic tumors that were primarily sarcomatoid carcinomas with occasional foci of adenocarcinoma (Fig. 6 and see Supplemental Figure S3C-D). Orthotopic carcinomas generally displayed diffuse low to moderate levels of cytoplasmic synaptophysin expression. Three Clone 2 orthotopic tumors harvested at 6 weeks were comprised of primarily adenocarcinoma containing a minority component of undifferentiated/early sarcomatoid carcinoma, while tumors harvested between 9 and 12 weeks were comprised of a majority of sarcomatoid carcinomas with occasional small foci of poorly differentiated adenocarcinoma, demonstrating increasing EMT with time and expansion of orthotopic tumors. Tumors cells that co-expressed CK8 and vimentin were readily observed (see Supplemental Figure S3C). Osseous and cartilaginous metaplasia were common in Clone 2 orthotopic tumors (Table 3, see Supplemental Figure S3D). Clone 2 rarely metastasized (Table 3); however, lymphovascular invasion was common and tumor emboli were occasionally observed in pulmonary capillaries, similar to the phenotype observed in late stages of the primary mouse model (see Supplemental Figures S3A&B).

A



B

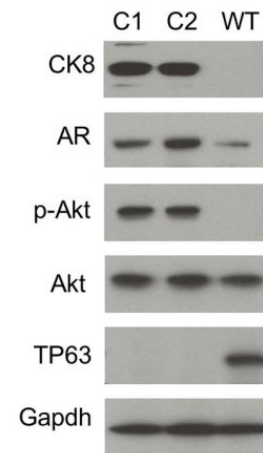


Figure 5. Expression of differentiation and signaling markers in cultured wild type prostatic basal cells (see Materials and Methods) and in *Pten/TP53* deleted Clones 1 and 2 prostatic carcinoma cell lines. **A)** Quantitative RT-PCR analysis of mRNA levels for various markers. **B)** Immunoblot analysis for selected markers. pAKT=AKT phosphorylated on Ser 473.

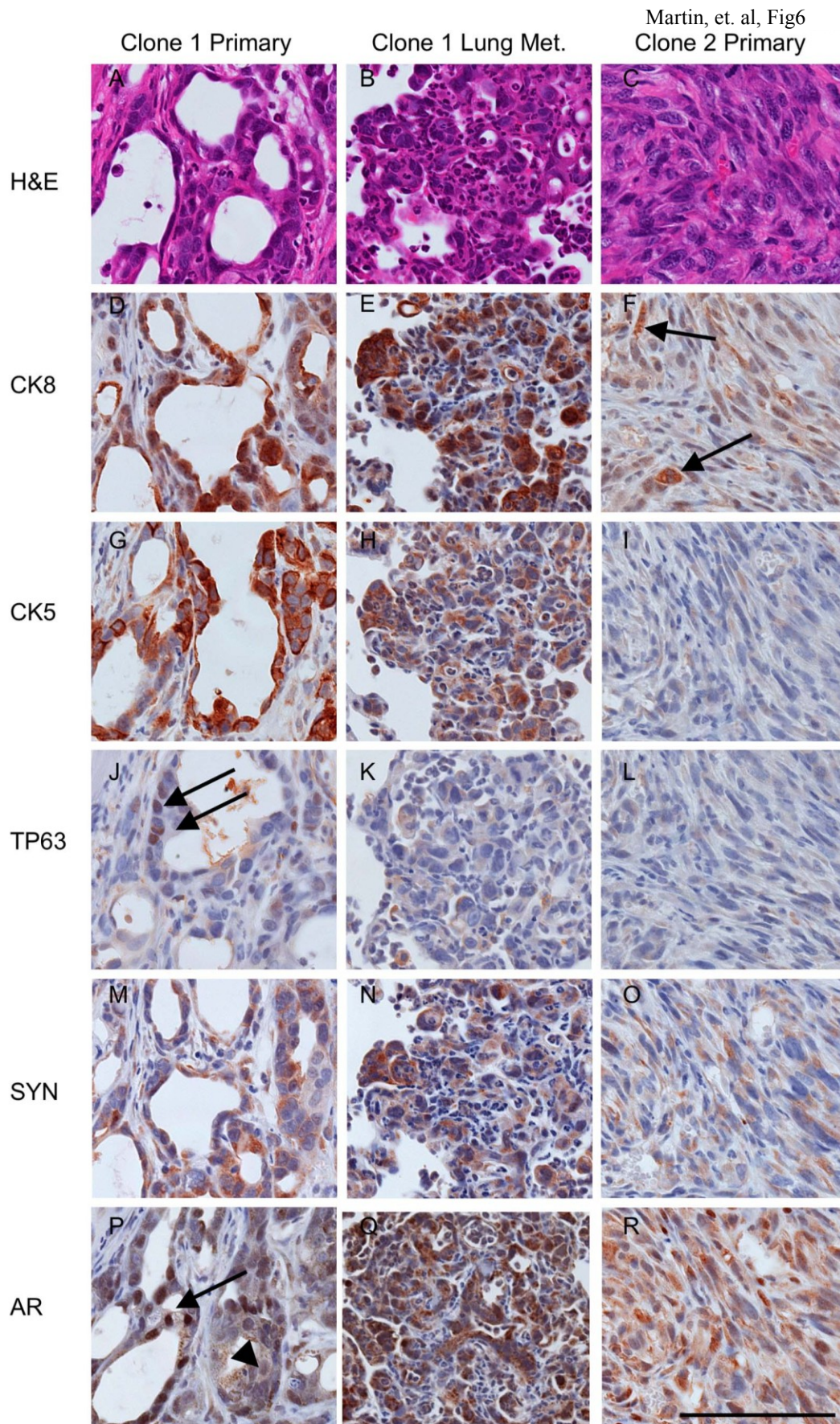
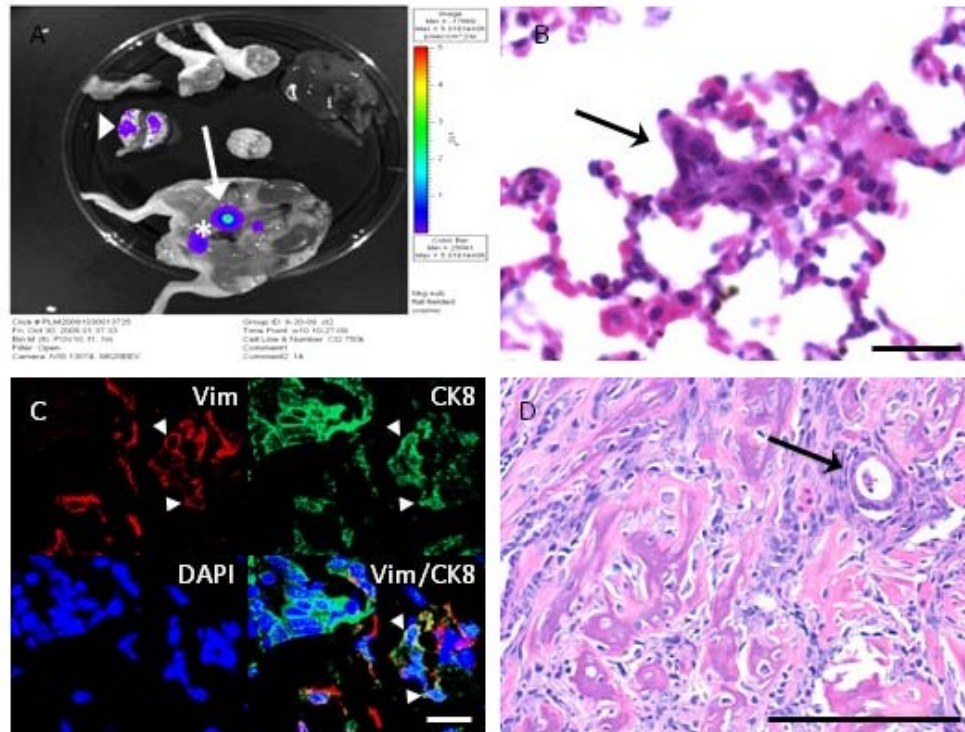


Figure 6. Clonal orthotopic *PB-Cre4⁺; Pten^{fl/fl}; TP53^{fl/fl}* carcinomas demonstrate multi-lineage differentiation, metastasis, and epithelial to mesenchymal transition. Sequential serial sections of a representative Clone 1 orthotopic prostate carcinoma (left column), a Clone 1 lung metastasis originating from this same primary carcinoma (middle column), and a Clone 2 sarcomatoid carcinoma (right column), staining with hematoxylin and eosin (H&E), and immunohistochemistry for cytokeratin 8 (CK8), cytokeratin 5 (CK5), TP63, synaptophysin (SYN), and androgen receptor (AR). Clone 1 gives rise to adenosquamous carcinomas **D)** with heterogeneous luminal cytokeratin 8 (CK8) expression, and **G)** basal cytokeratin 5 (CK5) expression. **J)** Definitive basal cells express nuclear TP63 (arrows). **M)** Heterogeneous synaptophysin (SYN) expression is observed in both adenocarcinoma and squamous portions of Clone 1 orthotopic tumors. **P)** Androgen receptor expression is heterogeneous ranging from strong nuclear expression (arrow) to weak nuclear and cytoplasmic expression (arrow head). **B)** Clone 1 orthotopic tumors commonly metastasize to the lungs where metastases display either a luminal phenotype or are biphenotypic. **E)** Shown is a luminal phenotype lung metastasis that co-expresses CK8, and **H)** CK5, but **K)** not TP63. **N)** Synaptophysin expression is common in Clone 1 lung metastases. **Q)** Androgen receptor expression in lung metastasis is generally low in the nucleus, yet high in the cytoplasm. **C)** Clone 2 orthotopic carcinomas undergo EMT to form sarcomatoid carcinomas with only occasional glandular differentiation. **F)** Sarcomatoid carcinomas lose cytokeratin expression leaving only occasional foci with weak CK8 expression (arrows). **I)** No CK5 or **L)** TP63 expression is observed. **O)** Weak cytoplasmic synaptophysin expression is common in clone 2 tumors. **R)** Androgen receptor expression is heterogeneous and

generally lower in Clone 2, with most tumor cells having weak or absent nuclear expression, and low cytoplasmic expression. All images taken at similar resolution (400X), scale bar = 100 μ m.



S3. Characterization of orthotopic prostatic carcinomas from Clone 2 including: bioluminescent imaging of lymphovascular invasion, epithelial to mesenchymal transition, and osseous metaplasia. A) Ex-vivo bioluminescent imaging of nude mouse orthotopically injected with Clone 2 cells demonstrates bioluminescent prostate carcinoma cells in sublumbar lymph node (arrow) as well as in the lungs (arrow head). Orthotopic prostate carcinomas are removed prior to ex-vivo imaging to enhance sensitivity as the high bioluminescent signal often obscures small signals originating from regional or distant tumor cells. There is a bioluminescent signal at the site of the removed orthotopic tumor demonstrating the presence of residual tumor cells (*). B) Histopathological analysis of the lungs from the mouse in A) demonstrating that the pulmonary bioluminescent signal is due to circulating tumor cells and tumor emboli (arrow), and not from actual metastases, (400X) scale bar = 20 μ m. C) CK8 (Green; Alexa Fluor 488) and vimentin (Red; Alexa Fluor 586) double immunofluorescence demonstrating several cells with CK8 and vimentin (Vim) co-expression in an orthotopic Clone 2 tumor (arrow heads), DAPI counterstain (400X), scale bar = 20 μ m. D) Region of osseous metaplasia in Clone 2 orthotopic prostate carcinoma surrounding entrapped adenocarcinoma gland (arrow), H&E, (200X) scale bar = 200 μ m.

Table 3. Comparison of the prostatic carcinoma phenotypes derived from orthotopically transplanted Clone 1 and Clone 2 cells.

Tumor Histology	Clone 1		Clone 2
	Adenosquamous Carcinoma		Sarcomatoid>Adenocarcinoma
	+Androgen	- Androgen	
Frequency of Lung Metastasis	7/8	9/9	1/12
Phenotype of Metastasis			N/A
Luminal Phenotype CK8+/CK5(+/-)/TP63-	5/5	3/5	
Biphenotypic CK8+/CK5+/TP63+	2/5	4/5	
Osseous/Cartilaginous Metaplasia	0/17		11/12

Ten mice orthotopically injected with Clone 1 cells were selected for immunophenotyping of lung metastases. Lung metastases were scored as a Luminal phenotype: all cells in the metastasis contain CK8 and/or CK5 and are negative for TP63, or Biphenotypic: all cells in the metastasis contain CK8 and/or CK5 and at least one cell is positive for TP63. >; in Clone 2 orthotopic tumors sarcomatoid carcinoma was the dominant histological pattern. + Androgen; subcutaneous androgen pellet was replenished at week 7 post orthotopic injection, - Androgen; subcutaneous androgen pellet was removed at week 7 post orthotopic injection. N/A; one mouse orthotopically injected with Clone 2 cells had a single small lung metastasis that did not appear in all three serial sections that were necessary for immunophenotyping.

F. Analysis of biphenotypic Clone 1 in androgen replete and deprived conditions

The initial characterization of Clone 1 at passage 4 demonstrated mostly double-positive CK5+/CK8+ cells (Table 2). As Clone 1 was cultured in vitro, CK5 expression decreased. At passage 25, Clone 1 cultures consisted of 95% CK8+/CK14+/CK5- cells and 5% CK8+/CK14+/CK5+ cells, and quantitative PCR analyses of the same culture revealed expression of luminal (*Krt18*) and basal (*Krt14* with low levels of *Krt5*) cytokeratins but not the definitive basal marker *TP63*. Other basal/progenitor-associated markers such as *Notch1*, *Sox2*, and *Itga6* were expressed (Fig. 5A). Western blot analyses showed high constitutive levels of pAKT, detectable androgen receptor, and no detectable TP63 (Fig. 5B).

Clone 1 subcutaneous tumors displayed adenocarcinoma histology and AR expression, two characteristics of human androgen-dependent prostate cancer. To analyze androgen-dependent growth and development of the castrate-resistant phenotype, Clone 1 orthotopic tumor growth was performed in androgen replete conditions and in conditions that mimic patient treatment regimens giving rise to castrate-resistant prostate cancer. Specifically, prior to orthotopic injections of Clone 1 cells, mice were castrated and implanted with testosterone pellets. Orthotopic tumor growth was detected with in-vivo bioluminescent imaging, usually between 4 and 6 weeks after inoculation. At 7 weeks post injection, mice were randomized into two cohorts. Testosterone pellets were removed from half (n=9), while the remaining half (n=8) were reimplanted with new testosterone pellets. Tumors were harvested upon death or morbidity of individual animals in both cohorts. The removal of subcutaneous androgen pellets usually led to a

temporary halt in orthotopic tumor growth and a reduction in tumor mass as assayed by in-vivo bioluminescent imaging and by manual palpation. Androgen deprivation led to a survival benefit as the mice in which the testosterone pellets had been removed survived up to 15 weeks post injection, while all of the androgen replete mice were moribund by week 9 post injection (Fig. 7A). In addition, quantitative PCR analyses of RNA extracted from tumors revealed in androgen deprived mice loss of androgen-dependent gene expression as shown for *Nkx3.1* and *Msb* in Fig. 7B.

Clone 1 orthotopic tumors grown in an androgen replete environment were composed of both CK8+ adenocarcinoma and TP63+ basal/squamous carcinoma components, demonstrating biphenotypic differentiation (Fig. 6). Synaptophysin expression in both adenocarcinoma and basal/squamous carcinoma was heterogeneous. In androgen deprived tumors there were often foci of fibrosis and chronic inflammation, indicative of tumor regression. However, Ki-67 immunohistochemistry identified multifocal regions of proliferation consistent with androgen independent tumor growth (data not shown). Interestingly, the histological phenotypes of the androgen deprived tumors were similar to the androgen replete tumors with the exception of the amount and distribution of androgen receptor, which is discussed below (Fig. 8). These data show that androgen deprivation of established tumors did not lead to the selective survival of either adenocarcinoma or basal/squamous carcinoma.

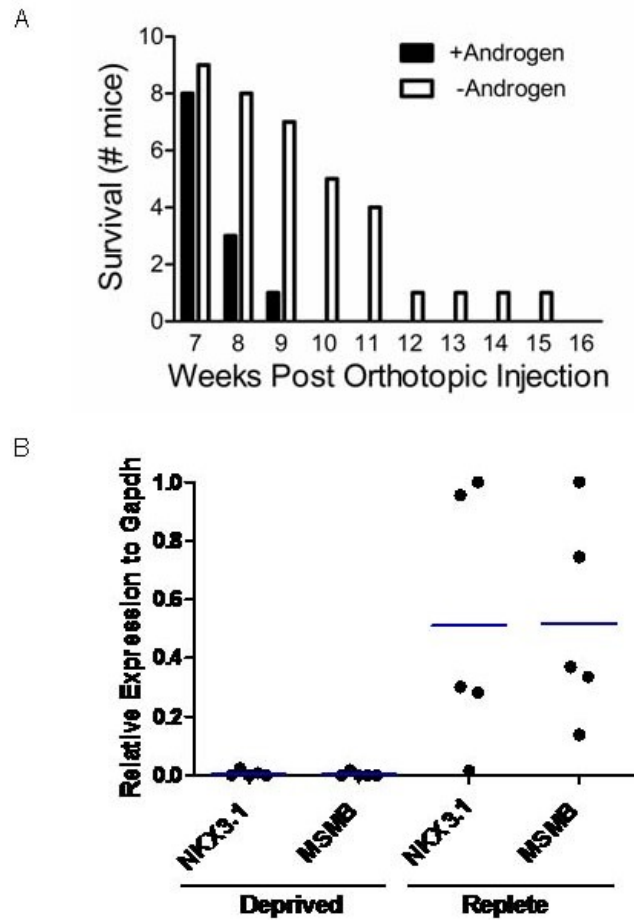


Figure 7. Androgen sensitivity and androgen independent tumor growth in *PB-Cre4⁺; Pten^{fl/fl}; TP53^{fl/fl}* Clone 1 orthotopic prostate carcinomas. **A)** Androgen pellets were either replenished (+Andro) or removed (-Andro) at seven weeks post orthotopic injection. Animals were removed from study when moribund. **B)** RNA samples extracted from Clone 1 tumors grown in androgen replete (n=5) or deprived (n=5) animals were assessed for *Nkx3.1* and *Msb* expression levels by QRT-PCR. Samples were normalized to *GAPDH*. The androgen deprived tumors came from orthotopically injected mice that were euthanized between 19 and 33 days following the removal of subcutaneous androgen pellets.

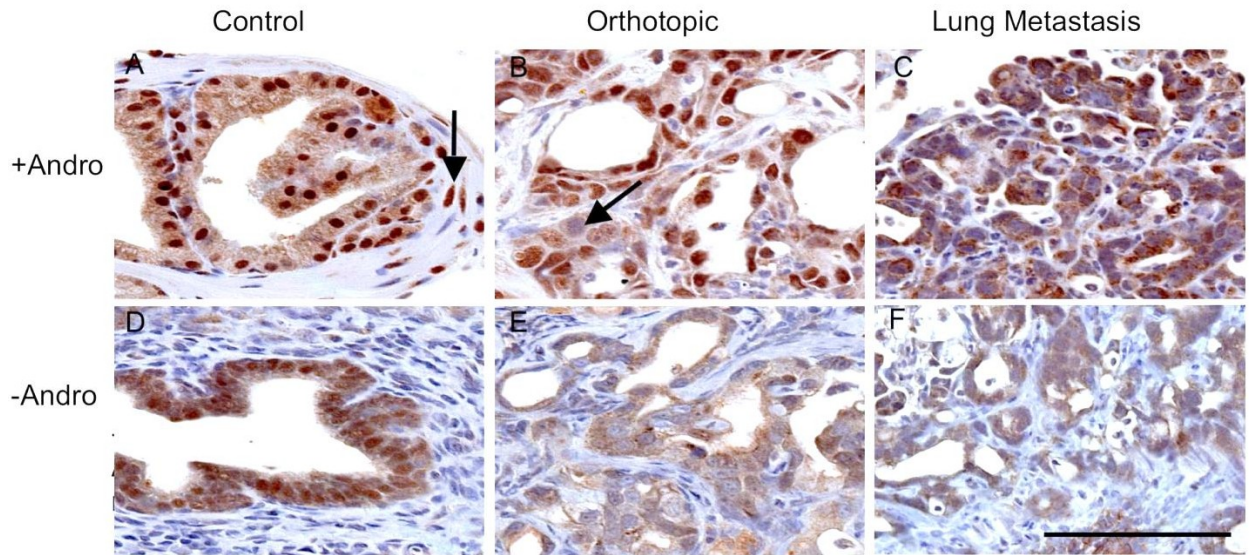


Figure 8. AR expression in Clone 1 orthotopic prostate carcinoma, recipient control prostate, and lung metastasis. Recipient nude mice had androgen pellets replenished (+ Andro): panels A,B,C or removed (-Andro): panels D,E,and F at week 7 post orthotopic injection. The tumor shown was taken from a mouse that survived 20 days after the androgen pellet was removed. **A)** Recipient dorsal prostate showing expression in epithelial cells and occasionally in stromal cells (arrow). **B)** Androgen replete orthotopic carcinoma harvested 50 days post orthotopic injection demonstrating strong nuclear expression and occasional reduced or absent expression (arrow). **C)** Lung metastasis from same mouse as in B. AR expression was primarily cytoplasmic with a granular appearance. AR expression decreased in **D)** control (recipient) nude mouse prostate, **E)** adjacent orthotopic carcinoma, and **F)** lung metastasis. All images taken at 400X, scale bar = 100 μ m.

G. Clone 1 metastases

Of interest, Clone 1 metastasized to the lungs in 9/9 androgen-deprived mice and in 7/8 androgen-replete mice (Table 3, see Supplemental Table 1). Lung metastases were immunophenotyped in five animals each from androgen-deprived and androgen-replete conditions. There was phenotypic cellular heterogeneity within individual metastases and among different metastases in the same mouse (see Supplemental Table 1). All metastases contained CK8+ cells and displayed adenocarcinoma or an undifferentiated/solid carcinoma morphology. However, some metastatic colonies contained TP63+ cells while others did not. There was an observable phenotypic variability in lung metastases comparing androgen deprived and androgen replete conditions, shown in Table 3 as a fraction of mice harboring at least one metastatic lesion of the indicated phenotype. Quantification of total metastases with respect to Immunophenotype demonstrated a statistically-significant increase in the total number of metastases containing TP63+ cells in androgen deprived mice (see Supplemental Table 1). Therefore, it appears that androgen deprivation effected either the selection of or differentiation of metastasis-initiating cells. The number of lung metastases per mouse was not statistically different as a result of androgen deprivation (see Supplemental Table 1) although this may be due to prior metastatic seeding and the presence of a significant tumor burden at the time of androgen withdrawal.

An interesting phenotypic difference between primary tumors and lung metastases was observed with respect to AR staining patterns. Androgen-replete orthotopic carcinomas displayed heterogeneous nuclear AR levels, ranging from high levels to significantly reduced levels and occasional nuclei with undetectable AR (Fig. 8).

Remarkably, lung metastases that developed in animals with implanted testosterone pellets had minimal levels of nuclear AR as compared to the primary tumors, implying distinct AR-dependent signaling in primary tumors as compared to metastases, even under androgen replete conditions (Fig. 8C). As expected for androgen deprivation, nuclear AR levels in orthotopic tumors and in nude mouse recipient prostates were markedly reduced, accompanied by an increase in granular cytoplasmic labeling (Fig. 8D-F). Androgen deprived lung metastases usually had overall reduced levels of total AR, with minimal to undetectable nuclear AR levels and low granular cytoplasmic expression levels. These data suggest that the metastatic cells have a distinct and possibly reduced AR-dependent signaling program relative to the primary tumor.

Supplemental Table 1. The number and phenotype of lung metastases in individual mice orthotopically injected with Clone 1 cells under androgen replete and androgen deprived conditions.

Mouse #	N	Luminal Phenotype (no TP63+ cells)	Biphenotypic (TP63+ cells present)
+Androgen			
1-4	2	2	0
1-7	14	14	0
1-8	2	2	0
1-14	5	2	3
1-17	5	4	1
1-3	2	ND	ND
1-5	2	ND	ND
1-6	0	ND	ND
-Androgen			
1-1	9	0	9
1-10	1	0	1
1-11	7	5	2
1-12	2	1	1
1-13	11	11	0
1-2	2	ND	ND
1-9	14	ND	ND
1-15	6	ND	ND
1-16	17	ND	ND

All lung metastases were counted as detailed in the materials and methods. Immunohistochemistry for CK8, CK5, and TP63 were performed on sequential serial sections from 5 androgen replete (+Androgen) and 5 androgen deprived (-Androgen) mice. Individual lung metastases were scored as being either luminal phenotype: cells in the metastasis contain CK8 and/or CK5 and are negative for TP63, or being biphenotypic: all cells in the metastasis contain CK8 and/or CK5 and at least one cell is positive for TP63. Androgen deprivation led to a statistically significant increase in lung metastases that were biphenotypic ($p < 0.0212$, Fisher's exact test). There was no significant difference in the number of lung metastases per mouse between the androgen replete and androgen deprived conditions ($p = 0.1576$, unpaired t-test). N: total number of lung metastases per mouse; ND: immunophenotype not determined.

IV. Discussion

Loss of *PTEN* and loss of *TP53* are common genetic aberrations in human prostate cancer [105]. A major finding described here from the pathological analysis of the *PB-Cre4⁺; Pten^{fl/fl}; TP53^{fl/fl}* model of prostate cancer is the time-dependent development of heterogeneous histologies. This most likely reflects the synergistic effect of *Pten* and *TP53* loss on increased prostate epithelial progenitor/stem cell self-renewal and differentiation plasticity. The significant intertumoral and intratumoral morphological and lineage heterogeneity described here for the *PB-Cre4⁺; Pten^{fl/fl}; TP53^{fl/fl}* model has not been observed in *PB-Cre4⁺; Pten^{fl/fl}* mice by us or by others [34].

The tumor suppressor TP53 functions pleiotropically in cells to negatively regulate growth through a variety of mechanisms including increased senescence, which previously was shown to be significantly decreased in *PB-Cre4⁺; Pten^{fl/fl}; TP53^{fl/fl}* prostate tumors[35]. More recently it has been appreciated that TP53 plays an important role in the proliferation and differentiation of stem/progenitor cells [35, 118, 119]. TP53 inhibits self-renewal in nontransformed and transformed somatic stem cells, and we have demonstrated that *Pten/TP53* null prostate progenitors have significantly increased self-renewal ability in vitro [116]. These data suggest that the rapid growth and aggressive nature of the carcinoma in the *PB-Cre4⁺; Pten^{fl/fl}; TP53^{fl/fl}* model is due not only to decreased senescence in bulk differentiated tumor cells but also to increased progenitor amplification.

TP53 also suppresses pluripotency and cellular dedifferentiation in induced pluripotent stem (iPS) cells [119]. In neural stem cells, the combined effects of losing *PTEN* and TP53 lead to impaired differentiation, although loss of either gene alone is

insufficient for such a phenotype [120]. Similarly in the *PB-Cre4⁺; Pten^{fl/fl}; TP53^{fl/fl}* model, at least some tumor initiating cells demonstrate multipotency and/or differentiative plasticity. Upon orthotopic transplantation, clonally derived TP63-negative Clone 1 cells gave rise to TP63+ basal and TP63-negative luminal phenotype tumor cells with focal neuroendocrine marker expression. These data imply either the transformation of a bipotential progenitor or plasticity of a committed progenitor to dedifferentiate. Lineage marking studies in normal prostates have demonstrated that the development of most TP63-negative luminal epithelial cells involves a TP63+ precursor [121]. However, studies of clonal, immortalized human prostate cancer cell lines are similar to the results described here [122]. That is, clonal human TP63-negative tumor-derived cells gave rise to tumors containing cells of multiple lineages, including TP63+ cells. Taken together, we suggest that TP53 loss of function in prostate cancer contributes not only to abnormal cell cycle control but also to increased differentiative plasticity of the tumor cells. The origin of the increased plasticity may be stochastic or alternatively, may be a result of transformation of a progenitor that precedes TP63+ basal cells in lineage commitment.

We also have presented evidence that sarcomatoid carcinomas develop from CK8+ prostate epithelial cells in the *PB-Cre4⁺; Pten^{fl/fl}; TP53^{fl/fl}* model. Given the previous observation that *TP53* loss in the context of *Pten* deletion results in decreased senescent markers in carcinoma cells, it is of interest to note that the bypass of senescence and the acquisition of an EMT phenotype have been correlated [35, 123, 124]. In other model systems, loss of senescence was attributed to oncogenic signaling acting in concert with transcription factors such as TWIST and ZEB1 that are known to regulate EMT.

Therefore, it will be relevant to determine in the *PB-Cre4⁺; Pten^{fl/fl}; TP53^{fl/fl}* model whether transcription factors that regulate sarcomatoid carcinoma development at late stages initially inhibit senescence in adenocarcinoma.

We observed osteogenic elements in some primary sarcomatoid carcinomas and in almost all Clone 2 orthotopic carcinomas. Human sarcomatoid carcinoma of the prostate is a rare but aggressive disease with poor prognosis [125]. The human tumors share many histological characteristics with the mouse tumors described here. These include diverse epithelial lineages, including basal and neuroendocrine phenotypes, as well as heterologous elements such as osteosarcoma and chondrosarcoma. TP53 has been demonstrated to control the proliferation and differentiation of mesenchymal stem cells with loss of TP53 leading to accelerated differentiation toward osteogenic lineages [126]. It is possible that the loss of *TP53* in *PB-Cre4⁺; Pten^{fl/fl}; TP53^{fl/fl}* epithelial cells predisposes EMT-derived mesenchymal cells to differentiate toward osteo- and/or chondrogenic cells.

The development of a mouse model of prostate cancer metastasis is important given the lack of models for advanced disease. Using pathological analyses of *PB-Cre4⁺; Pten^{fl/fl}; TP53^{fl/fl}* animals with end-stage disease and bioluminescent imaging of transplanted tumor cells, we observed lympho-vascular invasion and circulating tumor cell/emboli in pulmonary capillaries. However, we conclude that the deletion of *Pten* and *TP53* in prostate epithelial cells is not sufficient to allow metastatic colonization. Sarcomatoid carcinomas were rarely metastatic from primary tumors or following orthotopic growth of Clone 2. Similar invasive but non-metastatic phenotypes for mouse mammary EMT-phenotype tumors have been described [127]. Although the ability to

undergo EMT correlates with progression and metastasis in various experimental models, it is important to distinguish reversible, or transient, EMT from the apparently irreversible EMT that occurs in sarcomatoid carcinoma. A reasonable hypothesis is that terminal mesenchymal differentiation that occurs in sarcomatoid carcinoma is associated with a loss of the ability to undergo a mesenchymal to epithelial (MET) transition that contributes to metastatic colonization.

A significant finding was that Clone 1, which produces biphenotypic tumors containing adenocarcinoma and basal/squamous carcinoma, is highly metastatic, most likely as a result of additional acquired genetic or epigenetic alterations. Immunophenotypic analysis of Clone 1 lung metastases demonstrated that they were either of a transit amplifying/luminal phenotype (CK8+/ CK5(+ /-)/ TP63-) or were biphenotypic, containing metastases with both TP63+ and TP63- cells. The relative abundance of these two metastatic phenotypes changed depending upon the androgen status of the mouse, with an increased percentage of biphenotypic metastases in androgen deprived animals (Table 3 and see Supplemental Table 1). This suggests that androgen-deprivation in this model selects for the growth and/or differentiation of cells with basal lineage commitment. Although human prostate cancer metastases rarely contain TP63+ cells, the demonstration that metastasis-initiating cells have differentiative plasticity driven by androgen deprivation suggests the possibility that a related mechanism is a contributing factor to the development of castrate-resistant prostate cancer. Interestingly, metastases demonstrated reduced nuclear AR compared to most regions of the primary orthotopic tumor, and the role of AR-dependent signaling in metastatic colonization is of interest for future studies. A clonal prostate carcinoma cell line with multi-epithelial

lineage differentiation potential and a high metastatic rate will be useful for studying the molecular mechanisms driving androgen independent growth and prostate cancer metastasis.

V. Materials and Methods

Animal Breeding

Pb-Cre4⁺ mice [B6.D2-Tg(Pbsn-Cre)4Prb, #01XF5] were obtained from the Mouse Models of Human Cancers Consortium Mouse Repository (Frederick, MD), *Pten*^{fl/+} mice (C;129S4-*Pten*^{tm1Hwu}/J, #004597) were obtained from The Jackson Laboratory (Bar Harbor, ME), *P53*^{fl/+} mice (B6; 129-*Trp53*^{tm1Brn}) were obtained from Anton Berns [128] and Luciferase + (FVB.Luc⁺, L2685) were obtained from the Contag Laboratory [117]. Tumor-bearing *Pb-Cre4*⁺; *Pten*^{fl/fl}; *P53*^{fl/fl} male mice were produced by breeding 6-10 week old *Pb-Cre4*⁺; *Pten*^{fl/fl}; *P53*^{fl/fl} males to *Luc*⁺ *Pb-Cre4*⁺; *Pten*^{fl/fl}; *P53*^{fl/fl} females. Animals were bred, housed, and used in accordance with the Policy on Humane Care and Use of Laboratory Animals (Office of Laboratory Animal Welfare, NIH, Bethesda, MD).

The following primer sets were used to detect the transgenes for the purposes of genotyping: *Trp53* F: 5'-CACAAAACAGGTTAAACCCAG-3' and *Trp53* R: 5'-AGCACATAGGAGGCAGAGAC-3'; *Pten*^{fl/fl} F: 5'-CAAGCACTCTGCGAACTGAG-3' and *Pten*^{fl/fl} R: 5'-AAGTTTTTGAAGGCAAGATGC-3'; *Pb-Cre4* 01: 5'-ACCAGCCAGCTATCAACTCG-3' and *Pb-Cre4* 02: 5'-TTACATTGGTCCAGCCACC-3'. This primer set was combined with *Pb-Cre4* 03: 5'-CTAGGCCACAGAATTGAAAGATCT-3' and *Pb-Cre4* 04: 5'-GTAGGTGGAAATTCTAGCATCATCC-3' to detect the wild type IL-2 allele that served as an internal control. *Luc* F: 5'-CCAGGGATTCAGTCGATGT-3' and *Luc* R:

5'-AATCTGACGCAGGCAGTTCT-3'. For all primer pairs, the thermocycler was run for 35 cycles with an initial 94°C incubation for 3 minutes followed by 94°C melting (30 seconds), 60°C annealing (1 minute), and 72°C extension (1 minute). PCR products were run on a 1.5% agarose gel.

Orthotopic Transplantation

Single cell suspensions of primary prostate tumor cells from the dorsal and ventral prostatic lobes of *Pb-Cre4⁺;Pten^{fl/fl};P53^{fl/fl}* mice were prepared and injected into the dorsal prostate as described [116]. For orthotopic injection of cell lines, 750,000 cells resuspended in 10 µl of prostate harvest media were injected into one of the anterior prostatic lobes of recipient nude mice. Orthotopically injected nude mice were manually palpated weekly and imaged with the Xenogen Ivis (Caliper Life Sciences, Mountain View, CA) bioluminescent imaging system every two weeks as described [129]. Mice were euthanized upon signs of morbidity and/or when distended urinary bladders (indicative of urinary obstruction by prostate tumors) were easily palpable. In order to test for androgen independent growth, the transplant recipient nude mice were castrated through an abdominal incision at the time of orthotopic injection and a 90-day release 5mg testosterone pellet (Innovative Research of America, Sarasota, FL) was implanted subcutaneously in the cervical region. Mice were randomized into two groups at week seven post orthotopic injection. One group (n=9) had the subcutaneous testosterone pellets removed, and the other group had the androgen supply replenished by implantation of a second subcutaneous testosterone pellet (n=8).

Derivation of wild type basal cell line

The prostatic lobes from wild type mice were dissected from the urogenital tracts and prepared as described [116] except that the tissue digestion was stopped at the organoid stage before the trypsin digestion. The organoids were washed once with PBS and resuspended in WIT-P medium (Stemgent, San Diego, CA), passed several times through a 19-gauge needle, and plated into a 6-well Primaria plate (BD Biosciences, San Jose, CA). The cells were passaged every 7 days for 6 passages. The resulting established cell line was composed of morphologically uniform cells, and 100% of the cells expressed CK5 but not CK8 as determined by both flow cytometry and immunofluorescence.

Derivation of Clonal Cell Lines

Orthotopic carcinomas were aseptically harvested and washed briefly in sterile prostate harvest media DMEM (Invitrogen) supplemented with 10% fetal bovine serum, 1% penicillin/streptomycin (Invitrogen), gentamycin (Lonza, Walkersville, MD): 300 μ l of a 50mg/ml solution/500ml, and amphotericin B (Lonza): 30 μ l of a 250ug/ml solution/500ml. A 2-3mm cube of the tumor was minced and divided into 3 aliquots. Each aliquot was placed in a 10-cm Primaria tissue culture dish containing one of the three following medias: 1) PrEGM media (Lonza) containing 5×10^{-9} M dihydroxytestosterone (Steraloids Inc., Newport, RI) referred to hereafter as PrEGM/DHT, or 2) PrEGM/DHT, 5% fetal bovine serum, and 5% 3T3 conditioned media, or 3) PrEGM/DHT and 5% 3T3 conditioned media. 3T3 conditioned media was produced by incubating 3T3 fibroblasts in prostate harvest media for 2 days. The conditioned culture media was collected, clarified, filtered through a 0.4 μ m filter, and stored at -80C until use.

Cultures were incubated for one week or until there was growth on the dish, at which time cells were washed, trypsinized, and passaged two times before being plated at serial dilutions onto 10-cm Petri dishes. Cell cultures were maintained in the same culture media throughout the procedure. Single well-spaced colonies demonstrating an epithelial morphology were harvested using gene choice cloning rings (PGC Scientific Corp., Frederick, MD) and placed into a single well of a 24 well Primaria plate. On average, less than 10% of colonies were capable of expansive growth and establishment. Between passages 4-5, double immunofluorescence was performed for CK5/CK8 and CK8/vimentin. Clones that demonstrated detectable CK5-/CK8-/vimentin+ cells, or greater than 1% CK8+/vimentin+ cells were excluded from further analysis. Forty clonal cell lines were produced from 6 separate orthotopic tumors. Nine of these cell lines, derived from 4 separate orthotopic tumors, were selected for tumorigenesis assays. Clone 1 was grown in PrEGM/DHT with 5% serum and 5% 3T3 conditioned media. Clones 2,3,4,5,7, and 9 were grown in PrEGM/DHT. Clone 8 was grown in PrEGM/DHT with 5% 3T3 conditioned media.

Subcutaneous tumorigenesis assay

Single cell suspensions (1×10^6) of clonal cell lines were injected subcutaneously with or without Matrigel™ (BD Biosciences, San Jose, CA) into the flank region of nude mice (n=3 mice per cell line, with 3 tumors injected with matrigel and 3 tumors injected without matrigel). Cells were resuspended and injected in 200 μ l of prostate harvest media. For the contralateral flank, the cells were resuspended in a mixture of 100 μ l of prostate harvest media and 100 μ l of Matrigel™. Subcutaneous tumors were harvested when they reached approximately 1cm in diameter.

Histology

Primary prostate, subcutaneous, and orthotopic tumors were harvested and fixed with 4% paraformaldehyde overnight, rinsed well in PBS, and transferred to 70% ethanol prior to standard histological processing, sectioning and staining (Histoserve Inc., Germantown, MD). All prostates were sectioned as described [33], allowing for the examination of all prostatic lobes, the seminal vesicles, bladder, and urethra. Several sections of the tumor, two sections through each lung lobe, and the sublumbar lymph nodes were placed together on the same slide. For the purpose of histopathological analysis of disease progression, for each mouse, two H&E sections separated by 200 μm were analyzed. For the purposes of immunophenotyping the lesions, sequential serial sections were used for all immunohistochemical staining. Two serial sections (separated by 200 μm) of the liver, kidneys, spleen, brain, head, and decalcified longitudinal sections of the lumbar spine as well as fore and hind limbs were analyzed from each animal to assay for metastasis. All slides were analyzed blindly and histopathological analysis was done by a board certified veterinary pathologist (P. Martin and M. Simpson). To quantify the percentage of orthotopic tumor area with a certain histological pattern, the area was estimated by using the number of 200X fields comprised by the particular histological pattern/total 200X fields analyzed, averaged over the two 200 μm step sections. Bright field images were taken using an upright Zeiss Axioplan microscope.

Immunohistochemistry

Unstained slides were deparaffinized, and antigen retrieval was performed in a citrate buffer (DAKO targeted antigen retrieval solution) in a steamer at 100°C for 15 min,

followed by a 15 min incubation at room temperature. Blocking was performed with Cyto Q Background Buster reagent (Innovex Biosciences, Richmond, CA) for 30 min at room temperature for rabbit primary antibodies, and for 1hr for mouse primary antibodies. Primary antibody incubation was performed overnight at 4°C, followed by secondary antibody incubation at room temperature for 30 min. Secondary goat anti-rabbit biotinylated IgG (E0432), and goat anti-mouse biotinylated IgG (E0433), used at 1:200 dilution were from Dako (Carpinteria, CA). The ABC peroxidase kit (Vector Laboratories, Burlingame, CA) was used followed by DAB (Dako) for chromagen visualization. All slides were counterstained with hematoxylin. Primary antibodies and the concentrations used are as follows. The following primary antibodies were obtained from Abcam (Cambridge, MA): anti-Ki-67 (ab15580), 1/600; anti-CK8 (ab59400), 1:50; anti-synaptophysin (ab52636), 1:250; anti-Chromogranin A (ab15160), 1:10,000; and anti-PTEN (ab9559), 1:100. Additional antibodies were anti-CK5, 1:1000, from Covance (PRB-160P), San Diego, CA; anti-TP63, 1:400, from Millipore (MAB4135), Billerica, MA; anti-AR (sc-816), 1:200, from Santa Cruz Biotechnology, Santa Cruz, CA. The following antibodies were obtained from Cell Signaling (Danvers, MA): anti-E-cadherin (3195), 1:100; anti-pAKT (9271), 1:50; anti-TP53 (2527), 1:250, and anti-Slug (9585). At least 3 tumors from each experimental group (primary tumor, orthotopic transplant of primary tumor cells, and clonal orthotopic tumors both +/- androgen) were analyzed for immunohistochemical phenotyping.

Immunofluorescence

Double immunofluorescence was performed on tissue sections using the same protocol as used for IHC with the following exceptions: The secondary antibodies were Alexa

Fluor 488 conjugated goat anti-mouse IgG (A11001) and Alexa Fluor 586 conjugated goat anti-rabbit IgG (A11011), 1:200, (Invitrogen, Carlsbad, CA). Slides were mounted with vectashield hard mount with DAPI (Vector Laboratories, Burlingame, CA). The same primary antibodies at the concentrations indicated were used as for immunohistochemistry with the following exceptions: anti-cytokeratin 8 (CK8), 1:400 from Covance (MMS-162P), San Diego, CA; anti-vimentin, 1:50 from Santa Cruz (sc-7557), Santa Cruz, CA; anti-smooth muscle actin, 1:100, Abcam (ab5694), Cambridge, MA. For immunofluorescence of cell lines grown in vitro, adherent cells were fixed in 4% paraformaldehyde (PFA) in PBS for 10 min, followed by permeabilization with 0.5% Triton X-100 in PBS for 2 min. Non-specific sites were blocked by incubation in 2% BSA in PBS for 30 min. Cells were then incubated overnight at 4°C with the specified primary antibodies in 2% BSA/PBS. Cells were washed three times with PBS containing 0.1% Tween-20, incubated with Alexa Fluor 488 conjugated goat anti-mouse IgG and Alexa Fluor 586 conjugated goat anti-rabbit (1:200) in 2% BSA for 30 min at room temperature, and finally washed and mounted using the anti-fade reagent Fluoro-gel II with DAPI. Fluorescent images were captured using a Zeiss Observer.Z1 laser confocal microscope and an upright fluorescent Zeiss Axioplan microscope. In order to estimate the number of cells expressing CK8/CK5 or CK8/vimentin, two micrographs were taken at 200X for each combination of markers and the percentage of positive cells were counted and data was reported as the average of the two micrographs.

Reverse Transcriptase PCR

The following primer sets were used to detect mRNA for the purposes of assaying gene expression: *Nkx3.1* F: 5'-GGAGAGGAAGTTCAGCCATC-3' and

Nkx3.1 R: 5'-TGGCAAAGACAATGGTGAGT-3'; *Msmb*
 F: 5'-CACCTGCTGTACCAACGCTA-3' and *Msmb* R: 5'-
 CAACTCGACAGGTCTTCCCT-3'; *Pten* F: 5'-TTGAAGACCATAACCCACCA-3'
 and *Pten* R: 5'-TTACACCAGTCCGTCCCTTT-3'; *TP53* F: 5'-
 TGGTGGTACCTTATGAGCCA-3' and *TP53* R: 5'-AGGTTCCCCTGGAGTCTTC-
 3'; *Cdh1* F: 5'-GAC AACGCTCCTGTCTTCAA-3' and *Cdh1* R: 5'-
 ACGGTGTACACAGCTTTCCA-3'; *Krt5* F: 5'-AACGTCAAGAAGCAGTGTGC-3'
 and *Krt5* R: 5'-TCCAGCTCTGTCAGGTTGTT-3'; *Krt19* F: 5'-
 TATGAGATCATGGCCGAGAA-3' and *Krt19* R: 5'-CGTGA CTTCGGTCTTGCTTA-
 3'; *Krt18* F: 5'-CTGGTCTCAGCAGATTGAGG-3' and *Krt18* R: 5'-
 CTCCGTGAGTGTGGTCTCAG-3'; *Krt14* F: 5'-GATGACTTCCGGACCAAGTT-3'
 and *Krt14* R: 5'-TGAGGCTCTCAATCTGCATC-3'; *TP63* F: 5'-
 CAGTCAAGGACTGCCAAGTC-3' and *TP63* R: 5'-CATCACCTTGATCTGGATGG-
 3'; *Itga6* F: 5'-ACGGTGTTTCCCTCAAAGAC-3' and *Itga6* R: 5'-
 GAAGAAGCCACACTTCCACA-3'; *Vim* F: 5'-AAACGAGTACCGGAGACAGG-3'
 and *Vim* R: 5'-TCTCTTCCATCTCACGCATC-3'; *Acta2* F: 5'-
 TTTCATTGGGATGGAGTCAG-3' and *Acta2* R R: 5'-
 CCTGACAGGACGTTGTTAGC-3'; *Cdh2* F: 5'-ATGCCCAAGACAAAGAAACC-3'
 and *Cdh2* R: 5'-CTGTGCTTGGCAAGTTGTCT-3'; *Sox2* F: 5'-
 ATGCACA ACTCGGAGATCAG-3' and *Sox2* R: 5'-TATAATCCGGGTGCTCCTTC-
 3'; *Sox9* F: 5'-CTCCGGCATGAGTGAGGT-3' and *Sox9* R: 5'-
 GCTTCAGATCAACTTTGCCA-3'; *Notch1* F: 5'-TGGAGGACCTCATCAACTCA-3'
 and *Notch1* R: 5'-GTTCTGCATGTCCTTGTTGG-3'; *Myc* F: 5'-

TTCTCTCCTTCCTCGGACTC-3' and *Myc* R: 5'- TCTTCTTCAGAGTCGCTGCT-3';
Gapdh F: 5'- CAGAACATCATCCCTGCATC-3' and *Gapdh* R: 5'-
CTGCTTCACCACCTTCTTGA-3'. For reverse transcription, 3ug of total RNA was
used with the SuperScript III kit (Invitrogen, Carlsbad, CA). The amplification step used
the SYBR green PCR master mix (Applied Biosystems, Bedford, MA). For all primer
pairs, the thermocycler was run for 40 cycles with an initial 95°C incubation for 10
minutes, followed by 95°C melting for 15 seconds, 55°C annealing for 30 seconds, and
72°C extension for 30 seconds.

Western Blotting

For protein detection, the following primary antibodies at the indicated
concentrations were used in an overnight 4°C incubation: anti-rabbit CK8 (Abcam,
ab59400), 1/1000; anti-rabbit AR (Millipore, #06-680), 1/500; anti-rabbit p-AKT (Cell
Signaling, #4060), 1/1000; anti-rabbit AKT (Cell Signaling, #4691), 1/1000; anti-mouse
TP63 (Millipore, NAB-4315), 1/500; anti-mouse GAPDH (Novus Biochemicals,
Littleton, CO: NB300-221), 1/4000. Secondary antibodies (1:2000) were anti-rabbit IgG
(#386325) or anti-mouse IgG (#381254) (GE Healthcare, Piscataway, NJ), incubated at
room temperature for 1 hour.

Chapter 3: Increased Total and Mitochondrial-Associated Hexokinase II Provides A Metabolic Adaptation to Growth and Survival in Androgen Deprived Conditions

I. Abstract

Background. *PTEN* and *TP53* loss are common molecular alterations in human castrate-resistant prostate cancer. We used a mouse model of *Pten* and *Tp53* prostate carcinoma to investigate the metabolic changes that occur with the development of castrate-resistant disease.

Methods. Castrated nude mice with subcutaneous testosterone pellets were orthotopically injected with a clonal *Pten*^{-/-}*Tp53*^{-/-} mouse prostate carcinoma cell line. Half of the mice had removal of testosterone pellets at 4 weeks post injection. A broad spectrum metabolomic screen was performed on the resulting tumors to identify potential differences in energy metabolism associated with androgen independent growth. Gene expression analysis and direct enzyme activity measurements were used to investigate differences in the transcription, activity, and cellular distribution of key metabolic enzymes. 2-deoxyglucose treatment and a competitive peptide inhibitor of HK II-mitochondrial binding were used to compare the ability of the parental and ARKD cell lines to proliferate under metabolic stress. Human tissue microarrays of primary and metastatic prostate cancer were immunostained with HK II to validate our findings of increased HK II as a metabolic adaptation to survival in androgen depleted conditions.

Results. The metabolomic screen identified depletion of carbohydrates, increased glycogen breakdown products, and an increase in lactate in androgen deprived relative to androgen replete tumors, suggesting an increased reliance on glycolysis in androgen depleted conditions. mRNA expression analysis showed increased transcription of genes involved in glycolysis, TCA cycle, glycogen metabolism, and PPP in androgen deprived

tumors. Enzyme activity assays showed increased cytoplasmic and mitochondrial-associated HK activity in androgen deprived tumors relative to androgen replete tumors. Quantitative dual color IHC confirmed that HK II expression was increased in the castrate resistant tumors in both proliferating and non-proliferating cells. This increased mitochondrial associated HK II allowed for increased survival in low glucose conditions (2-deoxyglucose treatment) as well as increased ability to withstand the negative effects of the competitive inhibition of HK II-mitochondrial binding. HK II immunohistochemistry demonstrated a large increase in HK II expression in human metastatic CRPC relative to the low grade primary tumors.

Conclusion. These findings suggest that increased total and mitochondrial associated HK II is one metabolic adaptation that can promote androgen independent growth in prostate carcinoma, and is responsible for increased carbohydrate utilization in androgen deprived tumors. Increased total and mitochondrial associated HK II provides for increased resistance to metabolic stress in androgen deprived tumors, and provides evidence for the selective advantage of increased total and mitochondrial HK II in vivo. This increased HK II-mitochondrial association provides an additional potential target for the treatment of castrate resistant prostate cancer.

II. Introduction

Despite current advances in prostate cancer treatment most cases of castrate resistant prostate cancer (CRPC) remain ultimately terminal. Several mechanisms have been proposed and confirmed, by which prostate cancer cells evade the first line androgen deprivation therapy including: increased androgen receptor expression, AR gene amplification, increased utilization of adrenal androgens, and intra-tumoral

steroidogenesis, as well as others [13]. These mechanisms help to explain how tumor cells are able to maintain androgen dependent signaling networks despite minimal levels of circulating androgens. Metabolic alterations may also play a role in prostate cancer progression and recent research [130-139] has revealed changes in several metabolic pathways. However, there is still a large degree of uncertainty regarding the metabolic changes associated with the development of CRPC. The large degree of genotypic and phenotypic heterogeneity observed in primary tumors and metastases reflects the numerous mechanisms by which prostate cancer cells adapt to evade androgen deprivation therapy, and contributes to the ultimate treatment failure of CRPC metastatic disease. Determining the metabolic changes that evolve in the development of CRPC are critical and may allow more focused treatment options for patients with certain tumor genotypes and/or metabolic phenotypes.

Although the genomics of prostate cancer are very heterogeneous, *PTEN* deletions and or mutations have been identified in up to 30% of primary tumors and 64% of metastatic prostate carcinomas [8, 9, 140]. An extensive genomic/mRNA expression analysis of primary and metastatic prostate cancer specimens by Taylor et. al.[10] showed altered PI3K signaling in approximately one half of the primary tumors and all of the metastases. Thus PI3K-AKT pathway plays a significant role in prostate cancer progression, metastasis, and CRPC [11, 53, 141]. AKT activation is associated with increased glycolysis in via several mechanisms: including increased expression of glucose transporters, and expression and mitochondrial localization of HK II [83]. Therefore it is reasonable to hypothesize that CRPC would have increased levels of glycolysis. However, unlike most tumors which employ aerobic glycolysis as the major

bioenergetic pathway, primary prostate carcinomas rely on fatty acid β -oxidation [71]. This feature is consistent with the low uptake of F18-FDG in PET imaging of most primary prostate carcinomas, the majority of which are low grade slow growing indolent tumors. However, increased F18-FDG uptake has been demonstrated in androgen independent tumors, metastases, xenografts, and cell lines [77, 78, 142-145]. While there have been several studies that have addressed the role that androgens play in regulating prostate cancer metabolism in-vitro [146-149] there is still uncertainty as to the effects of androgen withdrawal on prostate cancer in-vivo. More importantly, it has yet to be determined whether there are metabolic alterations that prostate tumor cells undergo that may serve as adaptations to survival in the androgen deprived environment.

The metabolomic approach has been applied to prostate cancer and has successfully identified several biomarkers that are altered between normal and malignant tissue such as: decreases in citrate and polyamines, increased choline, glycerophospholipids, lactate, and several pathways of amino acid metabolism [139, 149]. This approach has also identified several biomarkers that correlate with disease progression and metastasis such as sarcosine, uracil, kynurenine, glycerol-3-phosphate, leucine, and proline [137]. McDunn, et, al,2013 [134] used metabolomic screening of prostate cancer needle biopsies to develop a panel of metabolites that correlated with characteristics of disease aggressiveness: Gleason score, extra capsular invasion, and seminal vesicle/lymph node involvement. The results indicated significant heterogeneity as there was stratification into 3 general metabolite “signatures” of aggressive prostate cancer. These studies demonstrate the significant heterogeneity in prostate cancer metabolomics and highlight the utility of using mouse models with specific and common molecular lesions (ie:

Pten/Tp53 deletion) to identify mechanistic correlations between tumor genotype, metabolic signature, and disease progression. In addition, these studies in general do not specifically address the metabolomic changes occurring with castrate resistant tumor growth.

The increased aerobic glycolysis that is one of the characteristic changes in tumor metabolism (the Warburg effect) has been shown to be largely due to increased expression and mitochondrial localization of the first enzyme in glycolysis, HK II (HK II) which phosphorylates glucose to glucose-6-phosphate [60]. HK II binding to the outer mitochondrial membrane Voltage Dependent Anion Channel (VDAC) in tumor cells has been shown to inhibit the binding of pro-apoptotic factors Bax and Bad [59-61, 85, 91, 92, 150] and blocking apoptosis. The mechanism of this increased cytoplasmic and mitochondrial HK II has been demonstrated to be AKT dependent [39, 54, 57] making it a potential important metabolic adaptation in castrate resistant prostate cancer, which often demonstrates significant PI3K-AKT activation [10] However, there is a lack of research into the changes in HK II levels and cellular distribution that occur with the evolution of castrate resistant prostate cancer.

The purpose of the current study was to determine whether there are changes in energy metabolism that accompany the evolution of androgen independent prostate cancer in-vivo. We used a well characterized mouse model of human prostate cancer that is based on *PTEN/TP53* deletion [40], two common molecular lesions observed in human androgen independent prostate cancer [10]. We show an increased reliance on carbohydrate metabolism as well as increased expression and activity of cytoplasmic and mitochondrial-associated HK II in androgen deprived tumors relative to androgen replete

tumors. This metabolic adaptation afforded the androgen deprived cells an increased ability to withstand the metabolic stresses associated with a low glucose environment and treatment with a specific HK II-mitochondrial binding inhibitor. In addition, we show that increased HK II levels correlated with human prostate cancer progression to CRPC and metastasis. These data demonstrate that increased total and mitochondrial-associated HK II is an adaptive metabolic mechanism that can contribute to the evolution of androgen independent prostate cancer.

III. Results

A. Androgen withdrawal leads to an increased survival time in mice with *Pten*^{-/-}*Tp53*^{-/-} clonal orthotopic tumors, however mice eventually succumb to androgen independent carcinomas.

In order to investigate metabolic changes associated with the progression to androgen independent (castrate resistant) prostate cancer, we developed a mouse model featuring *Pten*^{-/-} and *Tp53*^{-/-} deletions, two of the most common genetic alterations found in human castrate resistant disease. The model is based on the orthotopic injection of a clonal *Pten*^{-/-}*Tp53*^{-/-} cell line (Referred to as “Clone 1”) derived from a prostatic adenocarcinoma from a *Probasin-Cre4* (*PB-Cre4*); *Pten*^{fl/fl}; *Tp53*^{fl/fl} mouse, described previously [40]. Briefly, nude mice were injected with 500,000 Clone 1 cells under the thin capsule surrounding the anterior prostate gland. At the time of surgery mice were castrated and either implanted with a subcutaneous 5mg testosterone capsule (low dose DHT experiment) or a 12.5mg testosterone capsule (high dose DHT experiment). Mice in the low dose experiment had their DHT capsules either removed (n=9; referred to as androgen deprived), or replenished (n=8; referred to as androgen replete) at week 7 post orthotopic injection. At this 7 week time point most of the tumors were able to be

palpated in anesthetized mice (approx. 2-5mm in diameter). Mice were allowed to continue on study until signs of morbidity due to urinary obstruction from large prostate carcinomas. Mice in the high dose DHT experiment had their 12.5mg testosterone capsule either removed (n=7) or remained intact (n=8) at week 4 before tumors were palpable, and were allowed to continue on study until signs of morbidity due to urinary obstruction were observed (Fig. 1A).

In the low dose DHT experiment androgen replete mice (subcutaneous DHT capsule left intact) succumbed to disease faster (median 8 weeks) than the androgen deprived mice (median 11.5 weeks; $p=0.0012$) (Fig1A). In the high dose DHT experiment androgen replete mice also succumbed faster (median 8 weeks) than the androgen deprived mice (median 10 weeks; $p=0.0004$) (Fig1A). In the two androgen replete cohorts there was a trend in the higher dose DHT experiment towards increased rate of disease progression as compared to mice in the low dose DHT experiment ($p=0.1272$). Similarly for the androgen deprived cohorts there was a trend towards increased rate of progression in the androgen deprived mice in the high dose DHT experiment (median 10wks) as compared to androgen deprived mice in the low DHT experiment (median 11.5wks; $p=0.0633$).

Similar to previously reported clone 1 orthotopic *Pten*^{-/-}*Tp53*^{-/-} tumors [40] the histological appearance was adenocarcinoma admixed with a minority basal/squamous component (Fig1B). Androgen deprivation led to an increased proportion of basal/squamous foci in the androgen deprived tumors (Fig1 C). In both low and high dose androgen experiments there was frequent lymphovascular invasion, with the lung being the most common site of distant metastasis (Fig1D). The metastatic rate in the low

dose DHT experiment was 5.6 lung mets/mouse in the androgen replete mice and 6 lung mets/mouse in the androgen deprived mice ($p=0.8952$). In the high dose DHT experiment the metastatic rate was 2.25 lung mets/mouse in the androgen replete mice and 2.20 lung mets/mice in the androgen deprived mice ($p=0.97$).

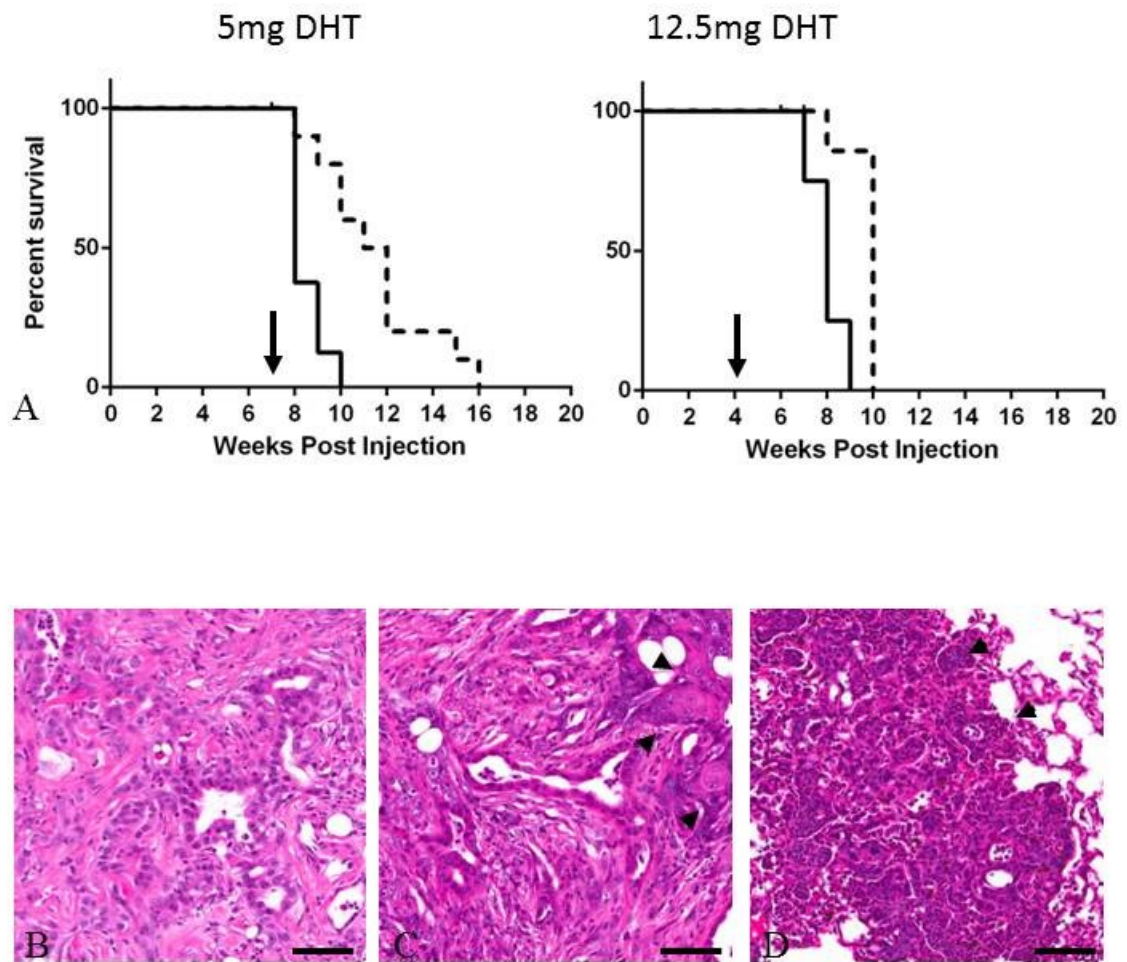


Figure 1. Survival curves and histopathology of androgen replete and androgen deprived nude mice orthotopically injected with *Pten*^{-/-}*Tp53*^{-/-} prostate carcinomas. (A) Low dose DHT mice had a 5mg subcutaneous testosterone pellet implanted at the time of castration and orthotopic cell injection surgery. The testosterone capsules were later removed from 9 mice at week 7 post injection (arrow) when orthotopic tumors were easily palpable (bold line-androgen replete). 8 mice remained “intact” and were replenished with a new 5mg testosterone capsule (broken line-androgen deprived). All of the intact mice were removed from study by week 10 with large orthotopic tumors (>1cm diameter) and

failure/difficulty to urinate during palpation. Removal of the testosterone pellet led to temporary tumor regression, and an approximate 2.5 week average increased survival time ($p=0.0012$). In the high dose DHT experiment mice were implanted with a 12.5mg subcutaneous testosterone pellet, which was then removed in 7 mice at week 4 post-orthotopic injection (arrow), when most orthotopic tumors were not yet palpable. With the high dose testosterone capsule all androgen replete (intact) mice were removed from the study by week 9 post injection. Androgen deprivation in the high dose experiment led to a two week increase in median survival time ($p=0.0004$). B) Orthotopic prostate tumors in androgen replete mice were primarily adenocarcinomas with occasional basal/squamous foci. C) The tumors in androgen deprived mice had increased foci of basal/squamous differentiation (arrow heads). D) Lung metastases were common in both androgen deprived and androgen replete mice. The metastases were often surrounded by dense infiltrates of neutrophils (arrow heads). Bar = 100um.

B. A metabolomics screen identified significant differences in carbohydrate metabolism and the tricarboxylic acid cycle (TCA) in androgen deprived orthotopic tumors.

In order to determine if there were significant metabolic differences between intact and androgen deprived orthotopic tumors we performed a broad spectrum metabolomic screen (Metabolomics™) on flash frozen orthotopic tumor samples collected at necropsy from both the low and high dose DHT experiments previously described. Significant differences in carbohydrate metabolism and the TCA cycle were more common in the high DHT dose mice as compared to the low dose DHT mice. Thus we focused our analysis on metabolic differences between androgen replete and androgen

deprived tumors in the high dose DHT experiment (Fig. 2A). The most consistent changes in metabolism between intact and androgen deprived orthotopic tumors were decreases in carbohydrates that can be converted into glucose-6-phosphate for glycolysis. Tumor fructose, mannitol, and sorbitol levels were decreased in androgen deprived tumors compared to those measured in tumors from the androgen replete mice. Evidence for glycogen metabolism to fuel glycolysis in androgen deprived tumors was demonstrated by significant increases in the glycogen breakdown products maltotetraose (2.86 fold increase) and maltotriose (7.93 fold increase) compared to the androgen replete tumors.

In the TCA cycle there was a significant decrease in citrate levels in the androgen deprived tumors as compared to the androgen replete tumors (Fig 2B). However, despite this decrease in citrate, the first intermediate in the TCA cycle, there were significant increases in the later intermediates: succinate, fumarate, and malate in the androgen deprived mice relative to the androgen replete mice. Levels of aspartate and glutamate were also increased in the androgen deprived tumors relative to the androgen replete tumors suggesting replenishment of TCA cycle intermediates via anaplerosis, ie: glutaminolysis to replenish α -ketoglutarate and aspartate conversion to oxaloacetate.

Pathway	Biochemical Name	6mo DHT	12.5mo DHT
Fructose, mannose, galactose, starch, and sucrose metabolism	fructose	0.02	0.09
	6'-sialyllactose	0.98	1.37
	maltose	1.43	1.73
	mannitol	0.08	0.08
	mannose	0.34	0.28
	sorbitol	0.08	0.04
	maltotriose	1.98	2.88
	maltotetraose	2.25	7.85
Glycolysis, gluconeogenesis, pyruvate metabolism	1,6-anhydroglucitol (1,6-AG)	0.98	1.69
	glycerate	0.27	0.07
	glucose-6-phosphate (G6P)	1.94	1.40
	glucose	0.60	0.48
	isobar: fructose 1,6-diphosphate, glucose 1,6-diphosphate	0.98	0.60
	phosphoglycerate (2 or 3)	0.78	0.60
	lactate	0.85	1.28
	glucuronate	1.38	1.17
	arabitol	0.78	0.40
	ribitol	0.78	0.46
Nucleotide sugars, pentose metabolism	ribose 5-phosphate	0.31	2.08
	isobar: ribulose 5-phosphate, xylulose 5-phosphate	1.20	1.66
	UDP-glucuronate	0.38	1.43
	xylitol	0.88	1.28
	citrate	0.77	0.36
Krebs cycle	dis-acconitate	0.76	0.28
	succinate	0.34	1.28
	succinylsuccinylamine	0.73	1.26
	fumarate	1.08	1.61
	malate	1.02	1.83
Oxidative phosphorylation	acetylphosphate	0.90	1.29
	phosphate	1.08	1.37
	pyrophosphate (PPi)	1.07	1.36
Alanine and aspartate metabolism	alanine	1.18	1.81
	beta-alanine	1.07	1.68
	N-acetylalanine	1.48	1.85
	N-acetyl-beta-alanine	1.88	2.05
	aspartate	1.37	1.78
	N-acetylaspartate (NAA)	3.89	2.71
Glutamate metabolism	5-ureidopropionate	3.41	2.06
	glutamate	1.02	1.38
	glutamate, gamma-methyl ester	1.42	1.68
	glutamine	1.18	1.30
	gamma-aminobutyrate (GABA)	0.43	0.12
	N-acetylglutamate	2.83	2.87

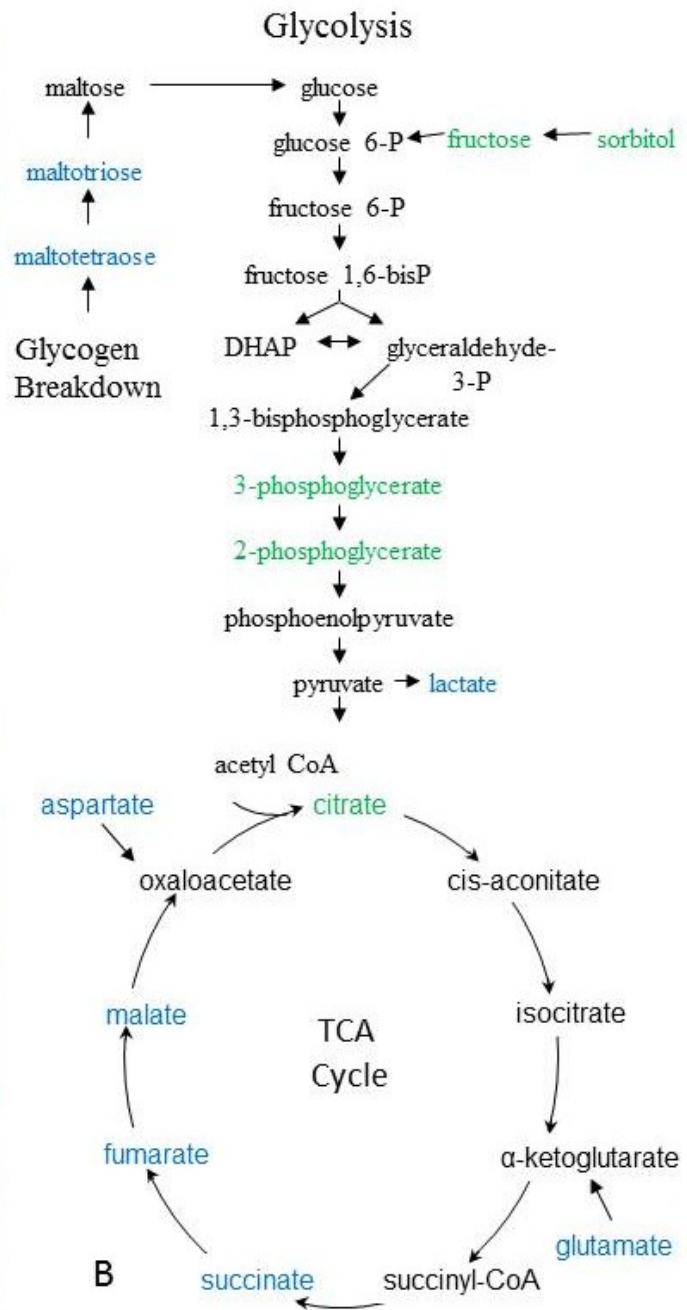


Figure 2. Metabolic analysis of androgen replete and androgen deprived *Pten^{fl/fl};TP53^{fl/fl}* orthotopic prostate carcinomas . A) Heat map depicting metabolic changes in androgen deprived orthotopic tumors relative to androgen replete tumors in several key energetic pathways. Values indicate fold of change in androgen deprived tumors relative to androgen replete tumors. Shaded cells indicate $p \leq 0.05$ (red indicates that the mean

values are significantly higher in androgen deprived tumors; green values significantly lower). Blue print indicates strong trend ($0.05 < p < 0.10$) for increase in androgen deprived tumors relative to androgen replete tumors. Light green print indicate strong trend ($0.05 < p < 0.10$) for decrease in androgen deprived tumors relative to androgen replete tumors. 5mg DHT; Low dose DHT experiment: Androgen replete: n=7, Androgen deprived: n=6. 12.5mg DHT; High dose DHT experiment: Androgen replete n=7, Androgen deprived: n=6. B) Integrated model of metabolic changes in glycolysis and the tricarboxylic acid (TCA) cycle in high dose DHT experiment. Blue indicates increase in androgen deprived tumors relative to androgen replete tumors, green indicates decrease in androgen deprived tumors relative to androgen replete tumors.

In order to determine whether the metabolic changes associated with progression to androgen independent growth in our murine model are similar to those reported for malignant progression in human prostate cancer, we compared our results to several published reports of metabolic changes associated with progression in human prostate cancer (Fig 3). Several metabolic alterations with androgen deprivation in this murine *Pten*^{-/-}*Tp53*^{-/-} orthotopic tumor model mirror those observed with progression in human prostate cancer specimens including: increased sarcosine[137], spermine [133], glutamine [133], glutamate [133], alanine [133], proline/hydroxyproline[137], uracil[137], and leucine [137] (Fig. 3). However it should be noted that these studies on human prostate cancer specimens were not focused on the metabolite changes that occur with androgen deprived CRPC.

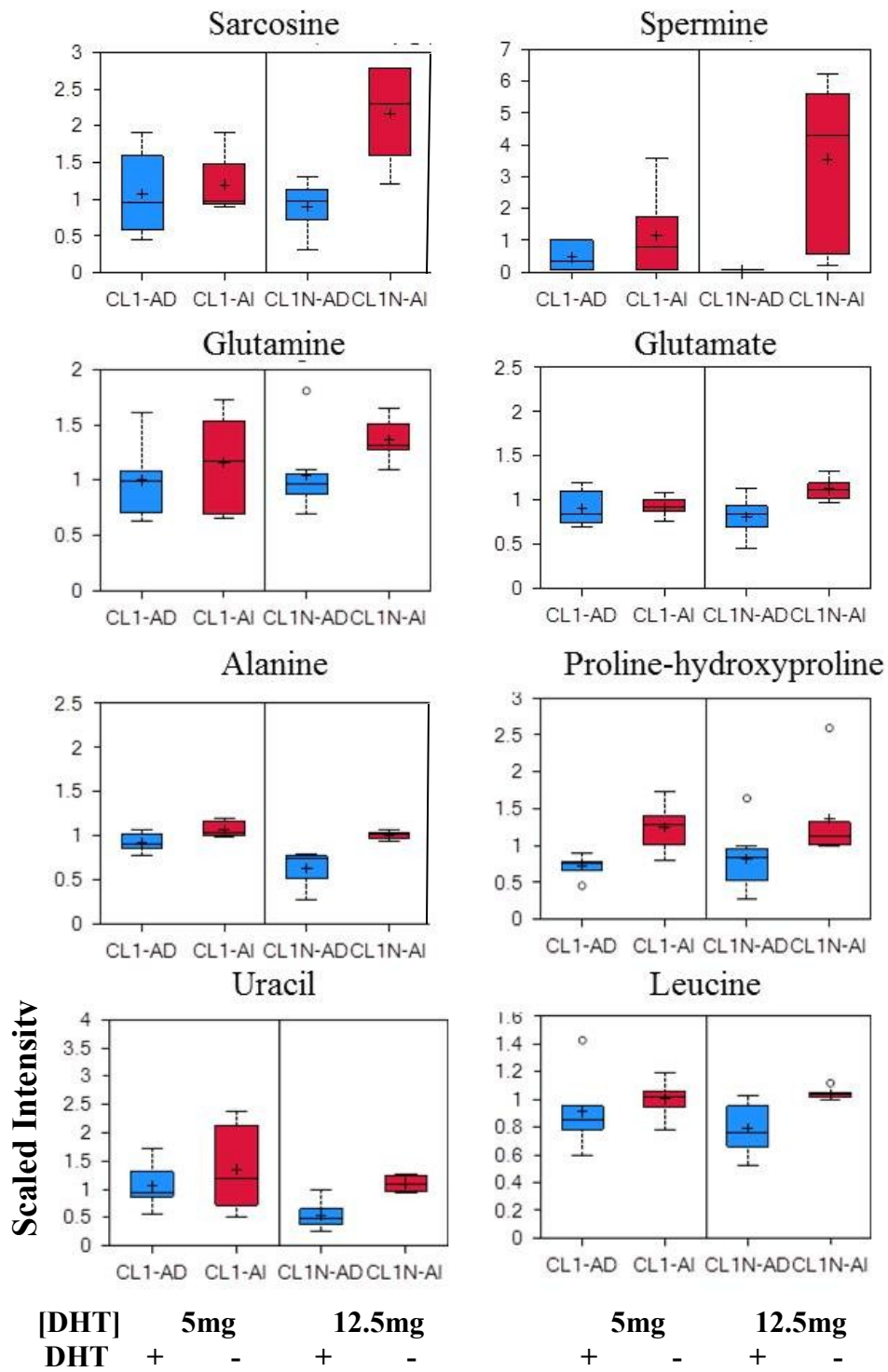


Figure 3. Boxplots comparing metabolites that are increased in androgen deprived orthotopic *Pten*^{-/-}*Tp53*^{-/-} tumors similar to results reported for increased malignancy in

human prostate cancer specimens. Values (y-axis) are scaled intensities representing relative biochemical amounts (Metabolon™). DHT concentrations of 5mg = low dose androgen, 12.5mg = high dose androgen, DHT + = androgen replete tumors; - = androgen deprived tumors. Androgen replete tumors are blue bars (CL1-AD) and androgen deprived tumors are red bars (CL1-AI). Box and whisker plots represent: + = mean; central line in box = median; box represents upper and lower quartile above and below mean; whiskers represent maximum and minimum values (range); empty circles represent outliers.

C. Androgen deprivation leads to upregulation of many genes involved in key energetic pathways related to carbohydrate metabolism

In order to determine if there were transcriptional differences associated with the metabolomic differences observed in androgen deprived orthotopic tumors, we performed a focused metabolic gene expression analysis (Qiagen™) on tumors from the high dose DHT experiment. The expression of several genes in each pathway: glycolysis, glycogen metabolism, TCA cycle, and pentose phosphate pathway were significantly increased in the androgen deprived tumors relative to the intact tumors (Fig 4). In fact all of the significant changes were in the direction of increased expression in androgen deprived tumors relative to androgen replete tumors.

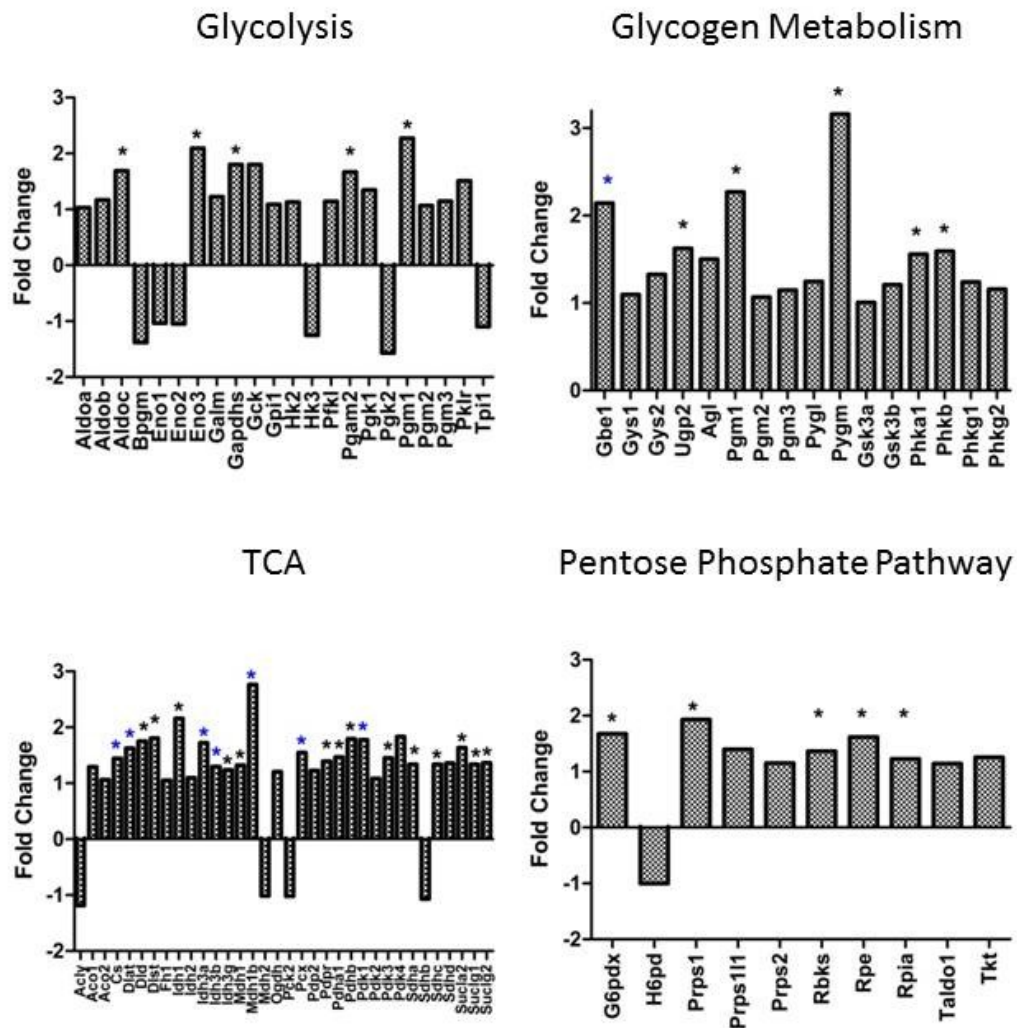


Figure 4. Androgen independent growth leads to increased expression of many genes involved in carbohydrate metabolism. The Qiagen™ Glucose Metabolism RT-PCR array was used to analyze the expression of 84 genes involved in glycolysis, TCA cycle, glycogen metabolism/gluconeogenesis, and the pentose phosphate pathway. Bars represent mean fold change in gene expression in androgen deprived orthotopic prostate carcinomas (n=5) relative to androgen replete tumors (n=5) *(Black) $p < 0.05$ *(Blue) $0.10 > p > 0.05$.

D. Androgen deprivation in orthotopic tumors and Clone 1 cells in-vitro leads to increased cellular levels of hexokinase II

Based on evidence from the metabolomics screen and gene expression analysis which suggested increased utilization of carbohydrates for energy metabolism in androgen deprived orthotopic tumors, we hypothesized that this would be accompanied by increased amounts and/or activity of Hexokinase enzyme activity, specifically HK II the major isoform responsible for the Warburg effect in most tumor cells [59]. Androgen deprived prostate carcinomas in this model have a large degree of heterogeneity in cellular proliferation with multifocal quiescent regions with low or no proliferation adjacent to rapidly proliferating regions with abundant nuclear Ki67 expression. Thus, in order to quantify and compare cellular HK II levels in both proliferating and non-proliferating regions of androgen replete and androgen deprived tumors we employed dual color immunohistochemistry. Cytoplasmic levels of HK II were detected with DAB while nuclear Ki67 was detected with Impact™ NovaRed, allowing for the semi quantitative scoring of HK II levels in both proliferating and non-proliferating cells (0=negative, 1=minimal/mild, 2=moderate, 3=strong). This dual color IHC demonstrated increased levels of HK II in both proliferating and non-proliferating cells in androgen deprived tumors relative to the androgen replete tumors (Fig 5). In proliferating (Ki67+) tumor cells the average per cell HK II score was approximately 34% greater in androgen deprived tumors relative to androgen replete tumors ($p < 0.0001$, Mann-Whitney U-Test). In non-proliferating (Ki67-) tumor cells the average per cell HK II score was approximately 17% greater in androgen deprived tumors vs. androgen replete tumors

($p < 0.0001$) (Fig 5G). In both androgen replete and androgen deprived tumors the mean per cell HK II scores in proliferating cells were significantly higher than in non-proliferating cells: 72% greater in androgen replete tumors and 92% greater in androgen deprived tumors ($p < 0.0001$). Thus androgen deprivation leads to a greater increase in the magnitude of HK II levels in proliferating cells vs. non-proliferating cells. The frequency distribution of per cell HK II scores also reflected this significant increase in HK II levels in androgen deprived tumors, regardless of cellular proliferation status (Supplemental figure 1A). We also employed an automated quantification (Using the Ariol™ Scanning/Analysis System) of the dual IHC to support and confirm the semi-quantitative histopathological scoring of increased HK II in androgen deprived tumors. Linear regression analysis was used to compare the relationship between tumor region of interest (ROI) proliferation (%cells Ki67+) and ROI % area positive for HK II in androgen replete and androgen deprived tumors. Each tumor was divided into 150um square ROIs so that the entire tumor was analyzed in a non-biased method. This analysis revealed a positive linear correlation between ROI proliferation and HK II levels in both conditions, with a statistically significant ($p < 0.001$) steeper slope in the androgen deprived tumors (supplemental figure 1B). Thus when controlling for the reduced rate of cellular proliferation in androgen deprived tumors, they have a significantly higher level of HK II. The effect of androgen deprivation on HK II levels in the clone 1 cells in-vitro was also assessed by western blot. 48 hours of androgen deprivation led to a significant increase in total cellular HK II levels (Fig5H).

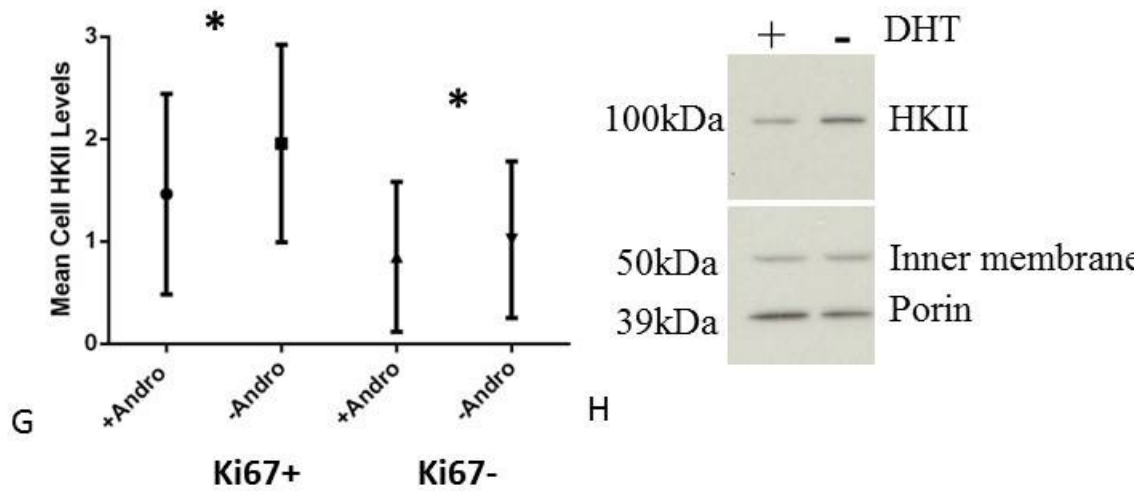
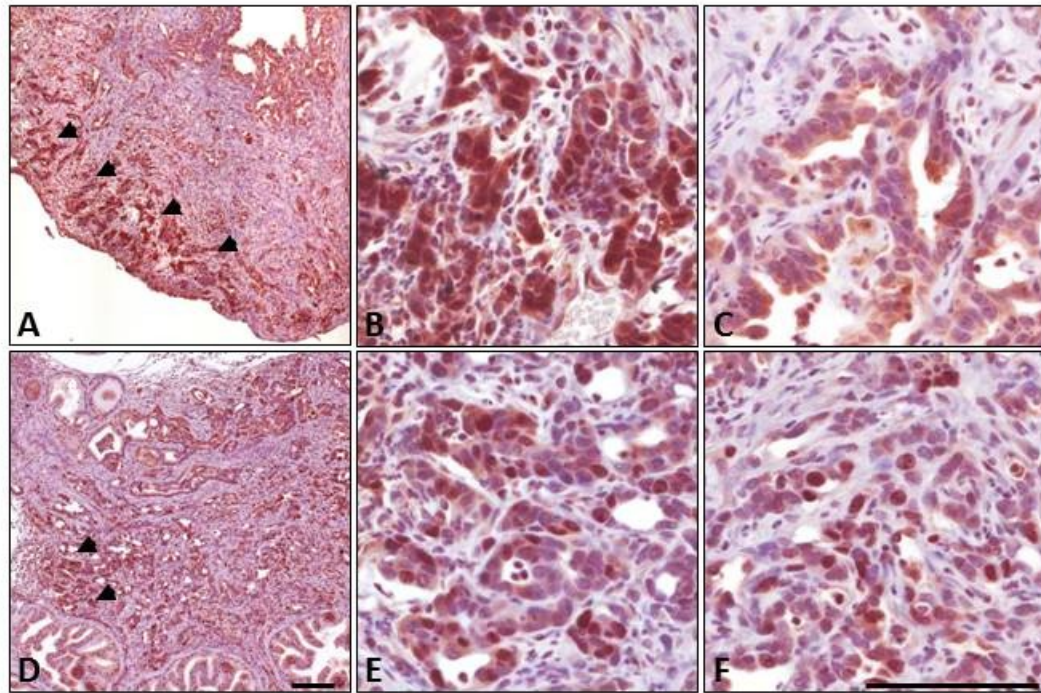
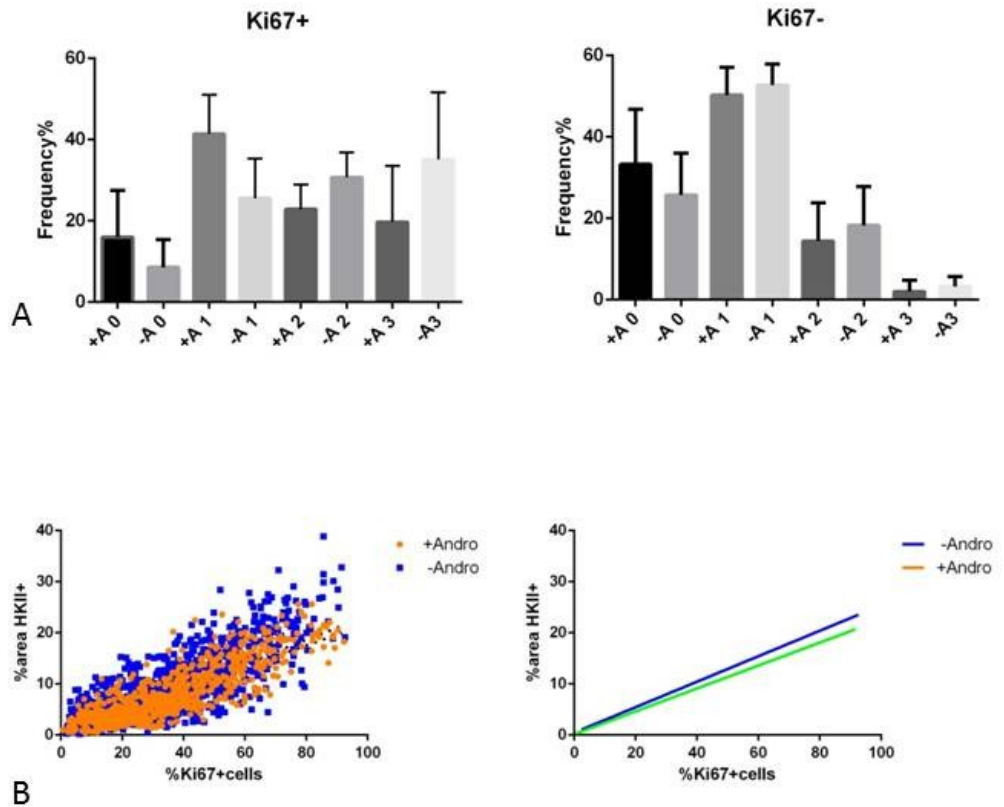


Figure 5. Dual color immunohistochemistry demonstrates increased HK II expression in androgen deprived orthotopic tumors relative to androgen replete tumors. Androgen deprived tumors (A,B,C) and androgen replete tumors (D,E,F) both demonstrate increased HK II expression with increased proliferation (Ki-67), however the magnitude of this response is higher in androgen deprived tumors. A) Androgen deprived tumors have a prominent increase in HK II expression in the higher proliferating regions at the

periphery of the tumors (arrow heads), 10X. B) High HK II expression in peripheral tumor region with high proliferation, 40X. C) Lower HK II expression in interior region of same tumor with no proliferating cells rate, 40X. Note that the cytoplasmic HK II levels are higher in the non-proliferating region of the androgen deprived tumor than in the proliferating region of the androgen replete tumor (F). D) Androgen replete tumors often have moderate increases in HK II expression at the tumor periphery (arrow heads), however the increase in HK II at the proliferating tumor periphery is not as prominent as in the androgen deprived tumors, 10X. E) Moderately increased HK II expression at periphery of androgen replete tumor, 40X. F) Low HK II expression in proliferating region in interior of same androgen replete tumor, 40X. Note that several proliferating cells have no or minimal HK II expression, while the non-proliferating cells in the androgen deprived region in (C) have mild to moderate levels. Dual color immunohistochemistry with anti-HK II: cytoplasmic (DAB) and anti-Ki-67: nuclear (ImmPACT NovaRED). G) Increased relative amounts of cellular HK II in androgen deprived (-Andro) orthotopic tumor proliferating and non-proliferating cells relative to the androgen replete tumor cells (+Andro). Dual color immunohistochemistry was used to label proliferating cells as well as the levels of HK II. For each orthotopic tumor 100 Ki67+ cells and 100 Ki67- cells were randomly chosen and scored semi-quantitatively for cytoplasmic HK II levels (0=negative, 1=minimal/mild, 2=moderate, 3=strong). In androgen deprived tumors (-Andro) there is a significantly higher HK II expression in both proliferating (Ki67+, $p < 0.0001$) and non-proliferating (-Ki67, $p < 0.0001$) tumor cells as compared to androgen replete (+Andro) tumor cells (Mann-Whitney U test). H) Increased total cellular HK II in androgen deprived (-DHT) clone 1 cells (24hrs of

androgen withdrawal) relative to androgen replete cells (+DHT). Mitochondrial inner membrane protein (50kDa) and porin (39kDa) used as protein loading controls to control for possible differences in mitochondrial amounts between androgen replete and androgen deprived tumors. Bar = 100um.



Supplemental Figure 1. A) Frequency distribution of semiquantitative scoring of HKII levels for proliferating and non-proliferating cells. +A = androgen replete tumors, -A = androgen deprived tumors. B) Automated quantification of the linear relationship between % region of interest that is positive for HKII expression, and % of ROI proliferating cells. The androgen deprived mice (-Andro) had a significantly higher slope ($p < 0.001$).

E. Androgen deprivation leads to increased total hexokinase enzyme activity in-vitro as well as in vivo, with increased levels in the mitochondrial cellular compartment.

In order to determine if the observed increases in HK II enzyme expression were associated with increased enzyme activity levels, we performed direct total hexokinase enzyme activity assays on clone 1 cells grown in-vitro, as well as on the androgen replete and androgen deprived orthotopic tumors. We also fractionated the cells into cytoplasmic and mitochondrial compartments in order to investigate sub-cellular differences in hexokinase activity. In clone 1 cells grown in-vitro, 48 hours of androgen deprivation led to significant increases in both cytoplasmic ($p=0.0258$) (Fig6A) and mitochondrial fraction total hexokinase activity relative to the androgen replete cells ($p=0.003$) (Fig6B). Regardless of DHT treatment the enzyme activity in the mitochondrial fraction was dramatically increased to approximately 6-7 fold of the levels in the cytoplasmic compartment ($p<0.0001$). The orthotopic tumors also demonstrated significant differences in hexokinase activities between androgen replete and androgen deprived tumors (Fig6C). The flash frozen tumor samples were fractionated into cytosolic and particulate fractions, as it was not possible to obtain pure mitochondrial fractions on the flash frozen tumors. The cytosolic hexokinase activity was approximately 35% greater in the androgen deprived tumors ($p=0.0308$). The particulate hexokinase activity was approximately 3.4 fold greater in the androgen deprived tumors, however there was a high degree of variability ($p=0.1231$). As the activity of the first enzyme in glycolysis (Hexokinase) was significantly increased in the androgen deprived tumors, we then assayed the activity of pyruvate dehydrogenase the final enzyme in the pathway linking

glycolysis and the TCA cycle. No significant differences were found between the pyruvate dehydrogenase activities of the cytosolic or particulate fractions of either the androgen replete or androgen deprived tumors (Figure 6D). In order to confirm that the large increase in HK II activity in the particulate cellular fraction of the orthotopic tumors was due to mitochondrial associated-HK II, we performed dual labeling confocal microscopy on 4% PFA fixed paraffin embedded orthotopic tumors to co-localize HK II and mitochondrial porin, a component of the VDAC on the outer mitochondrial membrane and the binding site for HK II (Figure 6E).

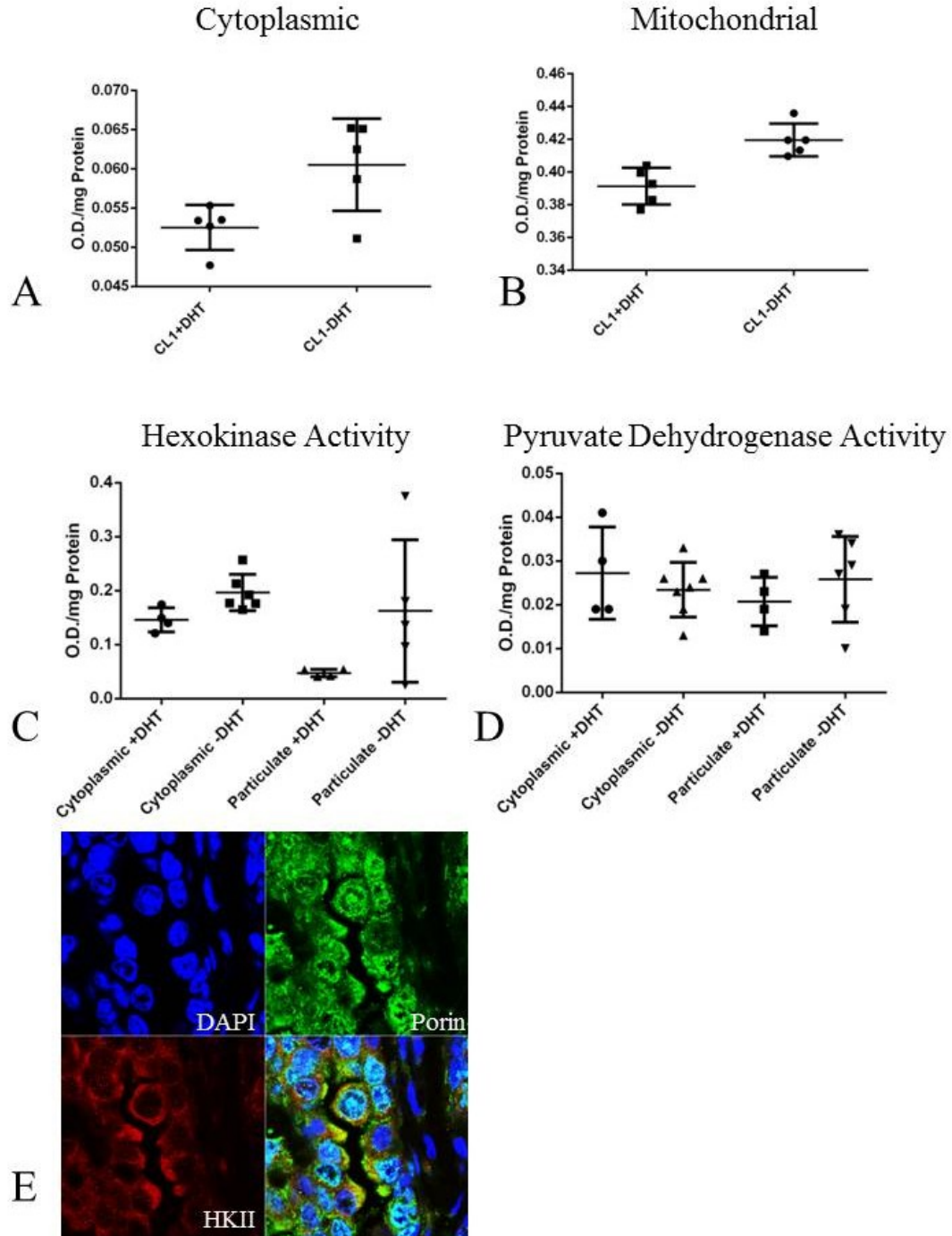


Figure 6. Increased in-vitro and in-vivo cytoplasmic and mitochondrial or particulate hexokinase activity in androgen deprived tumor cells. A) In-vitro 48 hours of androgen deprivation (-DHT) led to significant increases in both cytoplasmic (Fig 6A) and mitochondrial (Fig 6B) total hexokinase enzyme activity. Note the large increase in the

magnitude of the mitochondrial levels as compared to the cytoplasmic levels. Mean +/- S.D. C & D) Orthotopic tumor cytoplasmic and particulate hexokinase and pyruvate dehydrogenase enzyme activity in intact androgen replete (+DHT; n=4) and androgen deprived (-DHT; n=7) mice. Total enzyme activity was measured as an increase in optical density (O.D.) per mg total protein over a 45 minute colorimetric enzyme activity assay performed on the cytosolic and particulate cellular fractions. There is a significantly higher mean (+/- S.D.) hexokinase activity in the androgen deprived cytoplasmic fraction ($p=0.038$) and a trend towards a higher activity in the particulate fraction ($p=0.1231$). There is no significant difference in pyruvate dehydrogenase activity between the castrated and intact mice in either subcellular fraction. E) Confocal microscopy confirming the mitochondrial localization of HK II at the outer mitochondrial membrane porin/Voltage dependent anion channel (VDAC). Mouse anti-mitochondrial porin detected with goat anti-mouse-Alexa488 and rabbit anti-hexokinase II detected with goat anti-rabbit-Alexa568.

F. Androgen deprived cells have increased growth/survival under conditions of metabolic stress

As androgen deprived tumors and clone 1 cells grown in-vitro have increased levels of HK II, we hypothesized that they would have a survival advantage when subjected to metabolic stress. We used varying concentrations of 2-deoxyglucose in-vitro to metabolically stress the cells by simulating a low glucose environment. The MTT assay was used to determine if there were differences in cell viability (growth and survival) after 24 hours of androgen withdrawal in 0, 0.125mM, 0.25mM, 0.5mM, and 1mM of 2-deoxyglucose (Fig 7A). In normal metabolic conditions with no 2-

deoxyglucose there was no significant difference in viability between the androgen replete and the cells that were androgen deprived for 24hrs. In 0.125mM 2-deoxyglucose there was an approximate 25% increase in viability in the androgen deprived cells ($p=0.0085$). In 0.25mM 2-deoxyglucose there was an approximate 25% increase in viability in the androgen deprived cells ($p=0.016$). In 0.5mM 2-deoxyglucose there was an approximate 33% increase in viability in the androgen deprived cells ($p=0.016$). In 0.5mM 2-deoxyglucose there was an approximate 32% increase in viability in the androgen deprived cells ($p=0.0016$). In 1mM 2-deoxyglucose there was a trend towards increased viability in the androgen deprived cells (approximate 16% increase in cell viability), although this did not rise to the level of statistical significance ($p=0.185$).

We also used a competitive peptide inhibitor of HK II-mitochondrial binding to test the hypothesis that androgen deprived clone 1 cells will have increased resistance to the HK II-mitochondrial inhibitor due to higher total and mitochondrial levels of HK II. We also used this specific inhibitor of HK II to test the hypothesis that HK II-mitochondrial binding is necessary for optimal tumor growth. 12 hour incubation with two different concentrations of the HK II-inhibitor peptide demonstrated increased viability of the androgen deprived cells (Fig. 7B). At 0.5uM [HK II-inhibitor] there was an approximate 22% greater growth/survival in the androgen deprived cells ($p=0.0079$), and at 1uM there was an approximate 21% greater growth/survival in the androgen deprived cells ($p=0.0004$). The importance of the HK II-mitochondrial binding for optimal tumor growth regardless of androgen conditions was evident by the significant decrease in growth/viability at the 1uM concentration of the HK II-mitochondrial inhibitor in both androgen deprived and androgen replete cells.

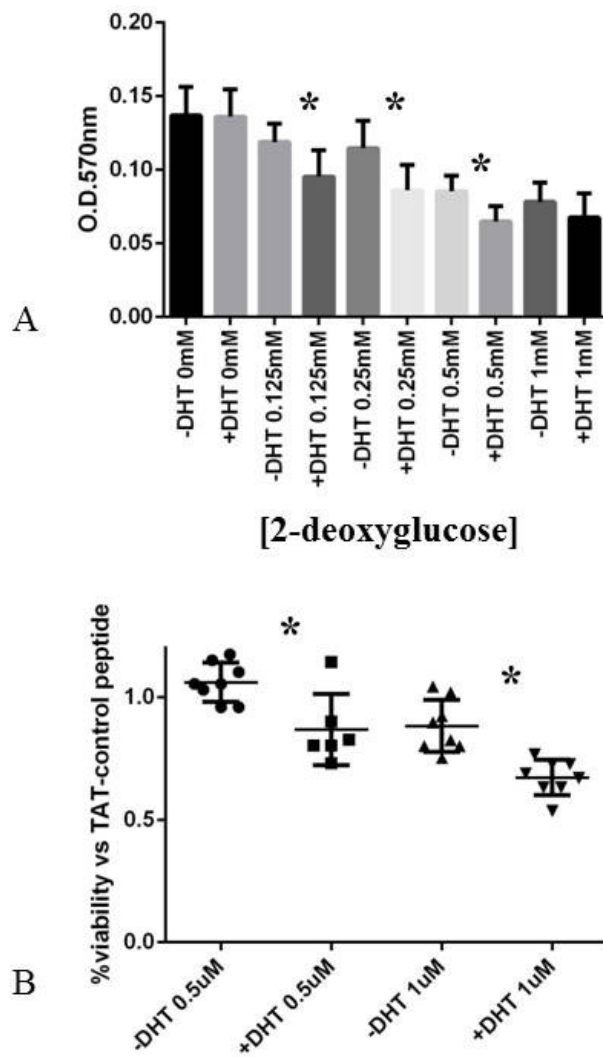


Figure 7. Increased cell viability in response to metabolic stress in androgen deprived Clone 1 cells in-vitro. A) Response to low glucose conditions (2-deoxyglucose treatment

for 24 hrs) in androgen replete (+DHT) and androgen deprived (-DHT) cells. Androgen deprived cells had significantly increased viability at 0.125mM, 0.25mM, and 0.5mM concentrations of 2-deoxyglucose relative to androgen replete cells. B) Response to HK II-mitochondrial binding competitive inhibitor in androgen replete (+DHT) and deprived (-DHT) cells. Cells were treated for 12 hours with either 0.5uM or 1uM of the competitive peptide inhibitor bound to HIV-TAT protein to allow for cellular uptake, or a random TAT-control peptide. At both concentrations of the inhibitor peptide there was significantly increased viability in the androgen deprived cells relative to the androgen replete cells. At 1uM both androgen replete and androgen deprived cells had decreased survival as compared to TAT-control peptide, demonstrating the survival benefit of mitochondrial-bound HK II in prostate carcinomas.

G. Metastatic castrate resistant human prostate cancer has significantly higher levels of Hexokinase II than primary tumors

The increased levels and activity of HK II in our *Pten*^{-/-}*Tp53*^{-/-} mouse model of castrate resistant prostate cancer led us to hypothesize that there will be increased levels of HK II in human CRPC as compared to primary androgen dependent tumors. In order to test this hypothesis we performed HK II immunohistochemistry on two tissue microarrays, one containing 54 samples of primary prostate adenocarcinoma and the other containing 45 samples from castrate resistant metastases. The tissue cores were semi-quantitatively scored based on the relative number of cells expressing HK II as well as the intensity of the immunolabeling: (no expression = 0, minimal = 1, mild = 2, moderate = 3, strong =4). The metastatic tumors had a dramatic increase in HK II levels ($p < 0.0001$, Mann-Whitney U test), as most metastases had strong levels of expression (Ave. Score = 3.7). Most of

the primary tumors were negative with occasional ones having minimal HK II levels, and rare tumors having mild levels (Ave. Score = 0.24) (Fig8).

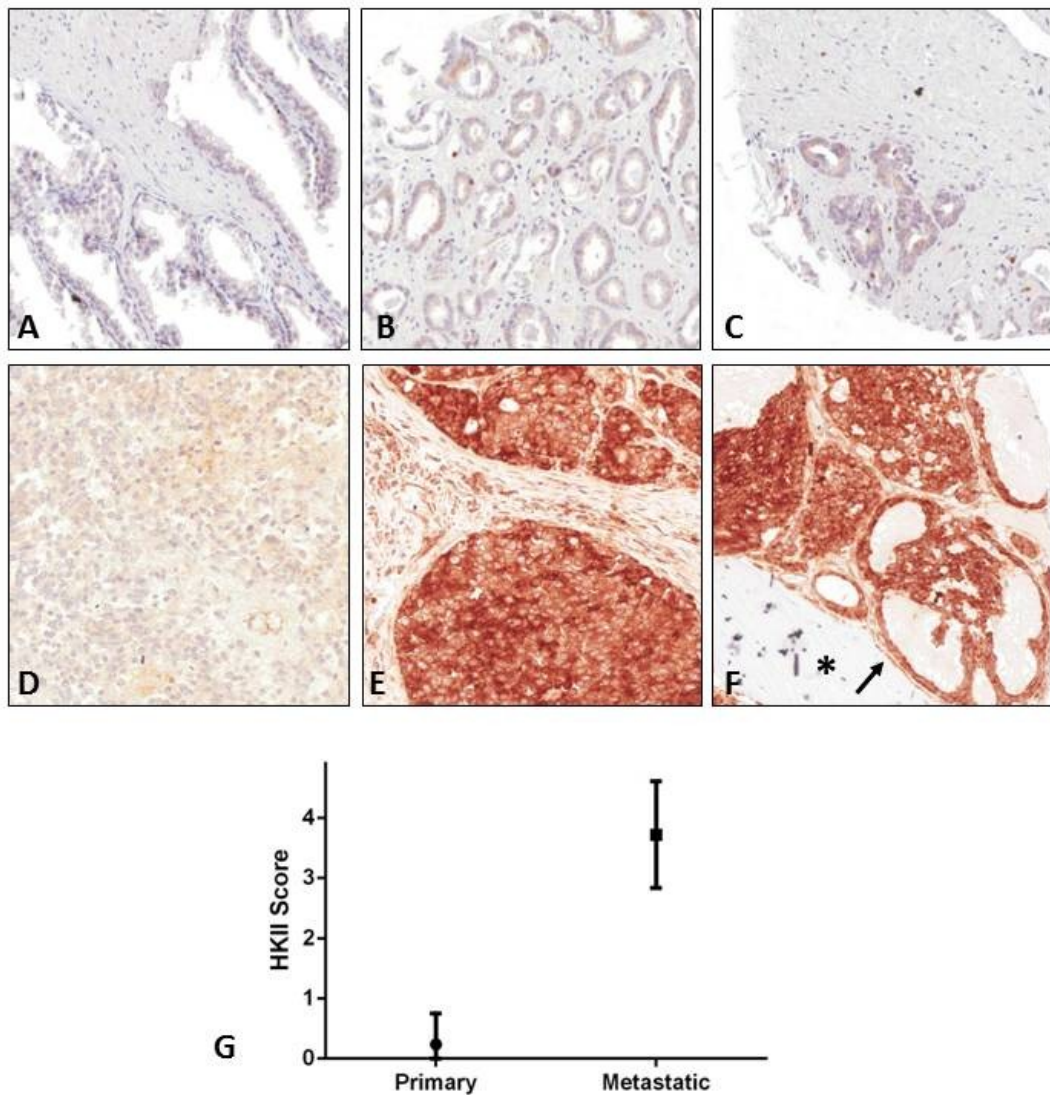


Figure 8. HK II levels in human prostate cancer primary and metastatic tumors. Tumors were scored semi-quantitatively for HK II levels detected by immunohistochemistry on human prostate cancer tissue microarrays. No expression = 0; minimal expression = 1; mild expression = 2; moderate expression = 3, strong expression = 4. A) Normal

prostate with no detectable HK II. B) Low grade primary prostate adenocarcinoma with minimal cytoplasmic HK II expression. C) Primary prostate adenocarcinoma with mild cytoplasmic HK II expression. D) Metastatic prostate carcinoma in unspecified lymph node with minimal cytoplasmic HK II. E) Metastatic prostate carcinoma in periaortic lymph node with high levels of HK II. F) Prostate adenocarcinoma bone metastasis in sacrum with high levels of HK II. Note bone spicule within sacrum marrow cavity(*) with adjacent adenocarcinoma glands (arrow) with high levels of HK II. G) Comparison of HK II IHC score between primary and metastatic tumors. Metastatic tumors have significantly higher levels of HK II than primary tumors ($p < 0.0001$; Mann-Whitney U test)

IV. Discussion

In this study we demonstrate an association between the development of castrate resistant prostate cancer (CRPC) and increased total and mitochondrial-associated HK II. This relationship between increased HK II and CRPC was validated in human metastatic prostate cancer specimens, as well as in a mouse model containing genetic alterations, *PTEN/TP53* deletions, commonly found in late stage human CRPC. Thus we propose an adaptive metabolic mechanism by which increased total and mitochondrial-associated HK II provide a selective advantage to prostate tumor cells in the androgen deprived environment and contribute to the evolution of CRPC. The adaptive significance of increased HK II was supported by a dramatic increase in HK II protein amounts in human metastatic/CRPC specimens relative to primary low grade prostate adenocarcinomas (Fig 8). This phenomenon was also reflected in the mouse model as there was increased HK II protein (Fig5) and enzyme activity in androgen deprived orthotopic mouse tumors as

compared to the androgen replete tumors in intact recipient mice (Fig 6). As we were unable to reliably produce pure mitochondrial fractionation from the particulate cellular fractions of our flash frozen tumor samples, we confirmed the mitochondrial localization of HK II using confocal microscopy to demonstrate co-localization with mitochondrial porin, a component of the VDAC on the outer mitochondrial membrane (Fig6E), and the HK II binding site. Mitochondrial localization was also confirmed in the parental cell line in-vitro, as producing pure mitochondrial fractions from cell pellets was possible (Fig6). Indirect evidence supporting this adaptive mechanism was provided by a metabolomics screen that suggested an increased reliance on carbohydrate metabolism in the androgen deprived tumors relative to the androgen replete tumors (Fig2), as well as increased expression of many genes involved in glycolysis, glycogen metabolism, the TCA cycle, and the pentose phosphate pathway (Fig4).

We confirmed the adaptive significance of increased total and mitochondrial HK II by demonstrating that androgen deprivation in-vitro increased HK II levels in mouse *Pten*^{-/-}*Tp53*^{-/-} prostate cancer cells (Fig5H), and this afforded them an increased ability to survive under conditions of metabolic stress. The androgen deprived *Pten*^{-/-}*Tp53*^{-/-} prostate cancer cells, which showed increased total and mitochondrial-associated HK II, were better able to survive the metabolic stress associated 2-deoxyglucose treatment, an inhibitor of glycolysis, than the same cells grown with DHT (Fig 7A). Androgen deprived cells also had an increased ability to withstand the growth inhibitory effects of a competitive peptide inhibitor of the HK II-mitochondrial association, suggesting a survival benefit of increased levels of residual mitochondrial-associated HK II that is associated with androgen deprivation (Fig 7B). Increasing concentrations of the HK II-

mitochondrial inhibitor (1 μ M) significantly decreased growth and survival of *Pten*^{-/-} *Tp53*^{-/-} prostate cancer cells regardless of androgen presence, demonstrating the survival benefit of HK II binding to the outer mitochondrial membrane (OMM). However the androgen deprived cells with elevated HK II had significantly increased HK II inhibitor peptide dose-dependent growth and survival relative to the androgen replete cells. These findings from the human prostate cancer specimens and our mouse model implicate increased HK II as an adaptive metabolic mechanism in CRPC. The fact that virtually all of the human metastatic samples had high HK II expression despite presumed genetic heterogeneity suggests that this metabolic mechanism may represent a unifying phenomenon and evolve through a number of different genetic alterations.

The most obvious adaptive significance of an increased total and mitochondrial HK II is an increased rate of glycolysis to fuel energy metabolism, as well as increased production of carbon precursors for anabolic processes such as nucleic acid synthesis via the pentose phosphate pathway and de-novo lipogenesis. Increased glycolysis in the androgen deprived tumors relative to the androgen replete tumors is supported by the increased protein levels (Fig 5) and activity (Fig 6) of HK II which is the rate limiting step in glycolysis. Increased glycolysis with androgen deprivation was also supported by the metabolomic data (Fig 2) which showed marked carbohydrate depletion and increased glycogen breakdown products. In addition to the energetic benefit, increased ribose 5-phosphate with androgen deprivation suggests that increased glycolysis was also providing increased carbon precursors for nucleic acid production. Increased FDG uptake in clinical PET imaging of CRPC metastases demonstrating an increased glycolytic flux [144] as well as our demonstration of increased HK II expression in

human metastatic lesions support the adaptive energetic benefit of increased carbohydrate utilization in CRPC. Genetically engineered mouse models (GEMs) of cancer have been used to demonstrate that increased HK II expression is critical for tumor energy production, increased flux of glucose into the pentose phosphate pathway (PPP) for nucleic acid production, and flow of carbon precursors into the Tricarboxylic Acid Cycle (TCA) as acetyl-CoA and citrate [151].

Our finding of decreased citrate provides preliminary evidence that in CRPC increased amounts of citrate are shuttled out of the mitochondria for de-novo lipogenesis in the cytoplasm. The finding of increased succinate, fumarate, and malate with increased aspartate and glutamate in androgen deprived tumors relative to androgen replete tumors, is consistent with replenishment of the TCA cycle intermediates through anaplerotic reactions. These anaplerotic reactions include glutaminolysis to replenish α -ketoglutarate, and aspartate conversion into oxaloacetate (Fig 2B). However, as metabolomic screening only gives a one time “snap-shot” of biochemical intermediate levels, rather than actual pathway flux, further research would be necessary to confirm these other interesting possible metabolic adaptations in CRPC. The similarities between metabolites that were increased with the development of CRPC in our model vs. those observed to be increased with disease progression in human primary prostate cancer specimens (Fig 3) support the relevance of this mouse model for dissecting the metabolic and molecular mechanisms associated with prostate cancer progression and CRPC. Notably we identified that androgen deprived tumors, relative to androgen replete tumors, had increased sarcosine, spermine, and amino acid metabolites which parallel the findings demonstrated with disease progression in primary human prostate cancer [130,

134, 136, 137, 152], although in the human prostate cancer samples comparisons between androgen dependent and androgen independent (CRPC) disease were not made. In addition to providing a massive energetic and anabolic benefit through the coupling of glycolysis and oxidative phosphorylation at the outer mitochondrial membrane, the binding of HK II at the VDAC also provides protection against the initiation of apoptosis by blocking the binding of pro-apoptotic factors such as bad and bax [59-61, 85, 90-92, 101, 102] Our study implicates this elegant pro-survival mechanism as one way that prostate cancer cells can evade the pro-apoptotic signals that occur with androgen deprivation. The high amount of HK II bound to the mitochondrial membrane may even provide protection against apoptosis induced by drug treatments as well.

Our finding of increased HK II in human metastatic CRPC, and increased total and mitochondrial HK II in our mouse model adds to the growing body of evidence supporting the importance of cancer metabolic adaptation through increased HK II levels and mitochondrial localization[58-61, 83-86, 88, 90-93, 100, 101, 151]. A potential role of PI3K-AKT signaling in promoting the mitochondrial-HK II association (Reviewed by Majewski, et al [102]) is likely in the *Pten*^{-/-}*Tp53*^{-/-} mouse model that showed high levels of pAKT activation due to the removal of the inhibitory effects of *Pten* expression. It has also been shown that elevated HK II expression in GEM cancer models is driven by both PI3K and MAPK signaling [83]. The orthotopic *Pten*^{-/-}*Tp53*^{-/-} tumors in our study in addition to expressing large amounts of pAKT, also express high cytoplasmic and nuclear levels of pERK indicating that MAPK signaling may also play a role in metabolic adaptation to CRPC. Blocking PI3K-AKT inhibits the HK II-mitochondrial association in human hepatocellular carcinoma cell lines [83]. In addition, these investigators

demonstrated that for human non-small cell lung cancer (NSCLC) and breast cancer clinical specimens, expression of HK2 via IHC on tissue microarrays was increased over adjacent normal tissues, and was positively correlated with increased pathological grade of the tumors as well as poor clinical outcomes. The association of PI3K-AKT and p-ERK/MAPK signaling in both human and mouse CRPC was also demonstrated by Kincade et. al, [11].

Several studies have shown that *Pten* loss with increased PI3K-AKT signaling is associated with CRPC in mouse models of prostate cancer as well as in human CRPC [11, 34, 40, 153-155]. The current study provides one specific metabolic mechanism that can explain adaptation to CRPC in the context of PI3K-pAKT and pERK-MAPK signaling: increased total and mitochondrial associated HK II. This finding also provides a mechanistic explanation for the common imaging results found in primary low grade prostate cancer (low FDG-PET uptake), while metastatic lesions often have increased FDG uptake [144] Indeed we showed that primary low grade prostate cancer rarely expressed HK II while most CRPC metastases had high levels of HK II (Fig 8). Exploiting the pro-survival metabolic mechanism of increased HK II may also have important implications for treatment of CRPC. Inhibition of HK II-mitochondrial association with compounds such as 3-bromopyruvic acid has already shown efficacy against tumors in animal models [95-98]. Targeting prostate cancer glycolysis with the inhibitory 2-Deoxyglucose has also been attempted in human clinical trials [99] however the results were unfavorable. Our results suggest that 2-Deoxyglucose treatment may be more effective when used at the initiation of androgen deprivation therapy, in order to inhibit the evolution of CRPC that we show is more dependent on glycolysis than

primary androgen dependent tumors. As androgen deprivation therapy alone can lead to a strong selection pressure for the evolution of CRPC, co-treatment with a glycolysis or HK II inhibitor may help to inhibit metabolic adaptation to the androgen independent milieu. In this study we have demonstrated that increased HK II and its association with the mitochondria likely afford both a metabolic and pro-survival benefit to prostate cancer cell survival in androgen deprived conditions. Thus improved treatments for CRPC may require not only targeting relevant cell signaling pathways, but targeting metabolic adaptations as well.

V. Materials and Methods

Cell Culture and Orthotopic Transplantation

Clone 1 tumor cells were derived from prostate adenocarcinomas of *Pb-Cre4⁺;Pten^{fl/fl};P53^{fl/fl}* mice and were injected into the anterior prostate of nude mice as described in Chapter 2 methods [40]. Briefly, mice were anesthetized with isoflurane and castrated through an abdominal incision, followed by orthotopic injection of 5×10^5 cells in 10ul, and implantation of a 5mg or 12.5mg subcutaneous testosterone pellet (Innovative Research of America, Sarasota, FL). Orthotopically injected nude mice were manually palpated weekly and removed from study upon signs of morbidity and/or when distended urinary bladders (indicative of urinary obstruction by prostate tumors) were easily palpable. For the high dose 12.5mg DHT experiment mice were randomized into two groups at week four post orthotopic injection. One group (n=9) had the subcutaneous testosterone pellets removed to simulate castration and allow for androgen independent tumor growth, while the other group (n=9) remained under the influence of

the testosterone pellet. For the low dose 5mg DHT experiment mice were randomized into two groups at week 7 post orthotopic injection as described in Chapter 2 methods. Cell culture conditions were as described in Chapter 2 methods.

Histology

Orthotopic tumors were harvested and fixed with 4% paraformaldehyde overnight, rinsed well in PBS, and transferred to 70% ethanol prior to standard histological processing, sectioning and staining (Histoserve Inc., Germantown, MD). All prostates and orthotopic tumors were sectioned as described (Shappell, et. al., 2004) allowing for the examination of all prostatic lobes, the seminal vesicles, bladder, and urethra. Several sections of the tumor, two sections through each lung lobe, and the sublumbar lymph nodes were placed together on the same slide. For the purpose of histopathological analysis of disease progression, for each mouse, two H&E sections separated by 200 um were analyzed. For the purposes of immunophenotyping the lesions, sequential serial sections were used for all immunohistochemical staining. Two serial sections (separated by 200 um) of the liver, kidneys, spleen, brain, head, and decalcified longitudinal sections of the lumbar spine as well as fore and hind limbs were analyzed from each animal to assay for metastasis. All slides were analyzed blindly and histopathological analysis was done by a board certified veterinary pathologist (P. Martin). To quantify the percentage of orthotopic tumor area with a certain histological pattern, the area was estimated by using the number of 200X fields comprised by the particular histological pattern/total 200X fields analyzed, averaged over the two 200 um step sections. Bright field images were taken using an upright Zeiss Axioplan microscope.

Immunohistochemistry

Unstained slides were deparaffinized, and antigen retrieval was performed in a citrate buffer (DAKO targeted antigen retrieval solution) in a steamer at 100°C for 15 min, followed by a 15 min incubation at room temperature. Blocking was performed with Cyto Q Background Buster reagent (Innovex Biosciences, Richmond, CA) for 30 min at room temperature for rabbit primary antibodies, and for 1hr for mouse primary antibodies. Primary antibody incubation was performed overnight at 4°C, followed by secondary antibody incubation at room temperature for 30 min. Secondary goat anti-rabbit biotinylated IgG (E0432), and goat anti-mouse biotinylated IgG (E0433), used at 1:200 dilution were from Dako (Carpinteria, CA). The ABC peroxidase kit (Vector Laboratories, Burlingame, CA) was used followed by DAB (Dako) for chromogen visualization, and ImmPACT NovaRED (Vector Laboratories). All slides were counterstained with hematoxylin. Primary antibodies and the concentrations used are as follows. The following primary antibodies were obtained from Abcam (Cambridge, MA): anti-Ki-67 (ab15580), 1/600; anti-CK8 (ab59400), 1:50; anti-synaptophysin (ab52636), 1:250; anti-Chromogranin A (ab15160), 1:10,000; and anti-*PTEN* (ab9559), 1:100. Additional antibodies were anti-CK5, 1:1000, from Covance (PRB-160P), San Diego, CA; anti-TP63, 1:400, from Millipore (MAB4135), Billerica, MA; anti-AR (sc-816), 1:200, from Santa Cruz Biotechnology, Santa Cruz, CA. The following antibodies were obtained from Cell Signaling (Danvers, MA): anti-E-cadherin (3195), 1:100; anti-pAKT (9271), 1:50; anti-TP53 (2527), 1:250, anti-Slug (9585), anti-Hexokinase II (2867).

Dual Color Immunohistochemistry

For dual color IHC to detect nuclear Ki67 in proliferating cells and cytoplasmic HK II, a sequential staining protocol was used for the two rabbit antibodies.

First slides were immunostained for Ki67 as described above, with a one hour primary incubation, followed by the standard Vector ABC IHC protocol with detection using ImmPACT NovaRED for 40 minutes. Slides were then washed for 5 minutes in PBST and then blocked with Cyto Q Background Buster for 20 minutes. Anti-Hexokinase II antibody was then applied and incubated overnight (approximately 12-16hrs) at 4C. Routine Vector ABC IHC protocol was used with DAB detection for 25 minutes.

For manual scoring of per cell HK II levels the slides were scanned with the Aperio™ system at 20x. Images were captured at 20X that comprised the entire tumor area. 100 Ki67+ were scored followed by 100 Ki67- cells. Each cell was scored according to this semi-quantitative scoring system: 0=negative, 1=minimal/mild labeling; 2=moderate labeling; 3=strong labeling. Data was analyzed using Graph Pad Prizm™, using T-test for statistical comparison of group means.

For automated detection using the Ariol™ scanning/analysis platform the slides were first scanned at 20X. The entire tumor region for each mouse was divided into equal 150um square regions of interest (ROI). Using the multi-stain assay the following features were counted for each ROI using the color and size parameters: number of positive Ki67 nuclei, number of negative hematoxylin counter stained nuclei, and % area positive for HK II DAB+ cytoplasm. For each ROI the % nuclei positive for Ki67 and the % area positive for HK II were plotted and analyzed using Graph Pad Prizm™.

Linear regression analysis was used to compare the slopes of the two linear equations describing the relationship between proliferation and %area + for HK II.

Reverse Transcriptase PCR

The Qiagen™ (Glucose Metabolism RT-PCR array was used to analyze the expression of 84 genes involved in glucose/TCA/glycogen/gluconeogenesis/and pentose phosphate pathway metabolism. In addition, separate RT-PCR reactions were performed using Qiagen RT-PCR assay primers for GLUT1, GLUT4, CPTa, CPTb, and PRL. For reverse transcription, 3ug of total RNA was used with the SuperScript III kit (Invitrogen, Carlsbad, CA). The amplification step used the SYBR green PCR master mix (Applied Biosystems, Bedford, MA). For all primer pairs, the thermocycler was run for 40 cycles with an initial 95°C incubation for 10 minutes, followed by 95°C melting for 15 seconds, 55°C annealing for 30 seconds, and 72°C extension for 30 seconds.

Western Blotting

For protein detection, the following primary antibodies at the indicated concentrations were used in an overnight 4C incubation: anti-rabbit CK8 (Abcam, ab59400), 1/1000; anti-rabbit AR (Millipore, #06-680), anti-rabbit AR (Epitomics), 1/500; anti-rabbit p-AKT (Cell Signaling, #4060), 1/1000; anti-rabbit AKT (Cell Signaling, #4691), 1/1000; anti-mouse TP63 (Millipore, NAB-4315), 1/500; anti-mouse GAPDH (Novus Biochemicals, Littleton, CO: NB300-221), 1/4000. Secondary antibodies (1:2000) were anti-rabbit IgG (#386325) or anti-mouse IgG (#381254) (GE Healthcare, Piscataway, NJ), incubated at room temperature for 1 hour.

For detection of metabolism enzymes the following primary antibodies at the indicated concentrations were used in an overnight 4C incubation: anti-mouse pyruvate

dehydrogenase E1a subunit (Abcam, Ab110334), 1/1000; anti-rabbit Aco1-cytoplasmic aconitase (Abcam, Ab126595); anti-rabbit Aco2-mitochondrial aconitase (Abcam, ab71440); anti-rabbit Aco2 (Kindly donated by Tracey Roualt); anti-rabbit Glutaminase (Abcam, ab93434); anti-rabbit Phosphofructokinase-1 (Abcam, ab37583).

Metabolomics

Flash frozen samples of each tumor were analyzed for global metabolite expression as described previously using mass spectroscopy (Metabolon™). All biochemical quantifications and bioinformatics analysis of metabolite changes were done by Metabolon™.

Enzyme Activity Assays

The enzyme activities of hexokinase and pyruvate dehydrogenase enzymes were determined using the hexokinase enzyme assay kit (E-111) and the Pyruvate dehydrogenase assay kit (E-109) from Biomedical Research Service and Clinical Application. University of Buffalo: <http://www.bmrservice.com/index.html>. Briefly flash frozen tumor sections were pulverized in glass dounce homogenizers under dry ice, prior to addition of ice cold lysis buffer. Tumor samples were homogenized with 10 strokes of the homogenizer and then lysates were transferred to 1.5ml Eppendorf tubes on ice. After following procedure detailed in enzyme assay kit, protein concentrations of lysates were determined by the BCA assay. For hexokinase assay 2ug of protein was used per sample.

Chapter 4: Conclusion

This dissertation research has succeeded in meeting its two major aims:

- 1) Develop and characterize a mouse model of *Pten/Tp53* deleted prostate cancer to investigate: the innate presence of castrate resistant prostate cancer (CRPC), the identity of tumor and metastasis initiating cells, and the lineage specific development of epithelial-to-mesenchymal transition.

Hypothesis: Orthotopically injected *Pten* and *Tp53* mouse prostate carcinoma will be capable of androgen independent (castrate resistant) growth and metastasis. The phenotypic heterogeneity: adenocarcinoma, adenosquamous carcinoma, basal/squamous carcinoma, and sarcomatoid carcinoma, each with occasional neuroendocrine differentiation, that are observed in primary tumors and metastases are due to a multi-potent tumor and metastasis initiating prostate progenitor cell that is capable of differentiating along basal and luminal lineages with occasional neuroendocrine differentiation.

Summary and Significance: By using a clonal cell line to produce orthotopic tumors with the full range of heterogeneity that was observed in the original genetically engineered mouse tumors, we confirmed that *Pten/Tp53* loss in the prostate epithelium can transform multipotential progenitor cells with a tumor and metastasis initiating capability of differentiating along each of the prostate epithelial lineages: luminal and basal, with occasional neuroendocrine marker expression. In addition, we show that *Pten/Tp53* loss leads to epithelial-to-mesenchymal transition in cells of the luminal lineage. The significance of these

findings is in defining two distinct tumor initiating cells which we used to produce clonal cell lines with different lineage differentiation potential, one capable of basal and/or luminal differentiation, and the other a luminal progenitor with EMT. Both of these clonal tumor initiating cell lines were capable of producing prostate adenocarcinoma that is similar in histological appearance and cytokeratin expression to most common human adenocarcinomas (CK8/18+, with occasional synaptophysin+ cells). We also provide an accurate and thorough characterization of a widely used mouse model of human prostate cancer.

- 2) Determine if there are metabolic differences between androgen dependent and castrate resistant prostate cancer that may serve as adaptations for the evolution and survival of CRPC.

Hypothesis: CRPC will be associated with increased glycolysis as an adaptation to survival in androgen independent conditions in contrast to the reliance on lipid metabolism in androgen replete conditions. This increased glycolysis is adaptive not only to compensate for energetic needs, but also to provide carbon precursors for anabolic processes such as lipogenesis and nucleic acid synthesis via the Pentose phosphate pathway, as well as to prevent metabolic stress induced apoptosis.

Summary and Significance: The discovery of the adaptive mechanism of increased cytoplasmic and mitochondrial associated hexokinase II in promoting prostate cancer progression to androgen independent growth is a novel finding that may help to develop new and improved treatment strategies for CRPC. Although this mechanism has been demonstrated to occur in carcinogenesis in

several tumor types, we are the first to demonstrate its role in androgen independent prostate cancer. The findings in our genotype specific mouse model mirrored the findings in human prostate cancer specimens which came from diverse genetic backgrounds. This suggests that we have identified a unifying metabolic mechanism that plays a significant role in the development of aggressive and/or androgen independent prostate carcinoma regardless of genotype. The mechanism of HK II binding to the outer mitochondrial membrane Voltage dependent Anion Channel (VDAC) provides an important pro-survival mechanism by blocking the binding of pro-apoptotic factors.

Our findings suggest that the significance of the increased phosphorylation of glucose afforded by the higher ATP supply from the outer mitochondrial anion exchange channel, that HK II can access when attached to the VDAC, not only increases energy production, but also provides increased carbon precursors for critical anabolic pathways: lipogenesis via shuttling of citrate back into the cytoplasm, and nucleic acid production via the pentose phosphate pathway. Our metabolic data also suggests that the androgen independent tumors can compensate for this loss of citrate for lipogenesis, by the anaplerotic reactions of glutaminolysis and aspartate conversion to oxaloacetate.

This study provides a new mechanistic understanding of the metabolic changes associated with the development of androgen independent prostate cancer and provides new targets for treatment of CRPC. The research presented in this work affirms the importance and relevance of using mouse models of human cancer as a powerful weapon in our growing arsenal to fight prostate cancer.

Bibliography

1. Stewart, S.L., et al., *Cancer mortality surveillance--United States, 1990-2000*. MMWR Surveill Summ, 2004. **53**(3): p. 1-108.
2. Levi, F., et al., *Leveling of prostate cancer mortality in Western Europe*. Prostate, 2004. **60**(1): p. 46-52.
3. Siegel, R., et al., *Cancer statistics, 2014*. CA Cancer J Clin, 2014. **64**(1): p. 9-29.
4. Gandaglia, G., et al., *Distribution of metastatic sites in patients with prostate cancer: A population-based analysis*. Prostate, 2014. **74**(2): p. 210-6.
5. Feldman, B.J. and D. Feldman, *The development of androgen-independent prostate cancer*. Nat Rev Cancer, 2001. **1**(1): p. 34-45.
6. Abate-Shen, C. and M.M. Shen, *Molecular genetics of prostate cancer*. Genes Dev, 2000. **14**(19): p. 2410-34.
7. Dong, J.T., *Chromosomal deletions and tumor suppressor genes in prostate cancer*. Cancer Metastasis Rev, 2001. **20**(3-4): p. 173-93.
8. Dahia, P.L., *PTEN, a unique tumor suppressor gene*. Endocr Relat Cancer, 2000. **7**(2): p. 115-29.
9. Suzuki, H., et al., *Interfocal heterogeneity of PTEN/MMAC1 gene alterations in multiple metastatic prostate cancer tissues*. Cancer Res, 1998. **58**(2): p. 204-9.
10. Taylor, B.S., et al., *Integrative genomic profiling of human prostate cancer*. Cancer Cell, 2010. **18**(1): p. 11-22.
11. Kinkade, C.W., et al., *Targeting AKT/mTOR and ERK MAPK signaling inhibits hormone-refractory prostate cancer in a preclinical mouse model*. J Clin Invest, 2008. **118**(9): p. 3051-64.
12. Gelmann, E.P., *Molecular biology of the androgen receptor*. J Clin Oncol, 2002. **20**(13): p. 3001-15.
13. Egan, A., et al., *Castration-resistant prostate cancer: adaptive responses in the androgen axis*. Cancer Treat Rev, 2014. **40**(3): p. 426-33.
14. Bennett, N.C., et al., *Molecular cell biology of androgen receptor signalling*. Int J Biochem Cell Biol, 2010. **42**(6): p. 813-27.
15. Velasco, A.M., et al., *Identification and validation of novel androgen-regulated genes in prostate cancer*. Endocrinology, 2004. **145**(8): p. 3913-24.
16. Wright, M.E., et al., *Identification of androgen-coregulated protein networks from the microsomes of human prostate cancer cells*. Genome Biol, 2003. **5**(1): p. R4.
17. Mostaghel, E.A., et al., *Intraprostatic androgens and androgen-regulated gene expression persist after testosterone suppression: therapeutic implications for castration-resistant prostate cancer*. Cancer Res, 2007. **67**(10): p. 5033-41.
18. Mellado, B., et al., *Molecular biology of androgen-independent prostate cancer: the role of the androgen receptor pathway*. Clin Transl Oncol, 2009. **11**(1): p. 5-10.
19. McNeal, J.E., *The zonal anatomy of the prostate*. Prostate, 1981. **2**(1): p. 35-49.
20. McNeal, J.E., *Normal histology of the prostate*. Am J Surg Pathol, 1988. **12**(8): p. 619-33.
21. Cunha, G.R., et al., *The endocrinology and developmental biology of the prostate*. Endocr Rev, 1987. **8**(3): p. 338-62.

22. Horoszewicz, J.S., et al., *LNCaP model of human prostatic carcinoma*. *Cancer Res*, 1983. **43**(4): p. 1809-18.
23. Kaighn, M.E., et al., *Establishment and characterization of a human prostatic carcinoma cell line (PC-3)*. *Invest Urol*, 1979. **17**(1): p. 16-23.
24. Brooks, C., et al., *Preclinical evaluation of sunitinib, a multi-tyrosine kinase inhibitor, as a radiosensitizer for human prostate cancer*. *Radiat Oncol*, 2012. **7**: p. 154.
25. Dozmorov, M.G., et al., *Unique patterns of molecular profiling between human prostate cancer LNCaP and PC-3 cells*. *Prostate*, 2009. **69**(10): p. 1077-90.
26. Hasegawa, N., et al., *A comparative study of protein profiling by proteomic analysis in camptothecin-resistant PC3 and camptothecin-sensitive LNCaP human prostate cancer cells*. *Urol Int*, 2006. **77**(4): p. 347-54.
27. Kumi-Diaka, J., *Chemosensitivity of human prostate cancer cells PC3 and LNCaP to genistein isoflavone and beta-lapachone*. *Biol Cell*, 2002. **94**(1): p. 37-44.
28. Laurenzana, A., et al., *Effectiveness of the histone deacetylase inhibitor (S)-2 against LNCaP and PC3 human prostate cancer cells*. *PLoS One*, 2013. **8**(3): p. e58267.
29. Rolfo, A., et al., *New perspectives for prostate cancer treatment: in vitro inhibition of LNCaP and PC3 cell proliferation by amnion-derived mesenchymal stromal cells conditioned media*. *Aging Male*, 2014.
30. Ross, R.K., et al., *Androgen metabolism and prostate cancer: establishing a model of genetic susceptibility*. *Cancer Res*, 1998. **58**(20): p. 4497-504.
31. Peehl, D.M., *Primary cell cultures as models of prostate cancer development*. *Endocr Relat Cancer*, 2005. **12**(1): p. 19-47.
32. Ittmann, M., et al., *Animal models of human prostate cancer: the consensus report of the New York meeting of the Mouse Models of Human Cancers Consortium Prostate Pathology Committee*. *Cancer Res*, 2013. **73**(9): p. 2718-36.
33. Shappell, S.B., et al., *Prostate pathology of genetically engineered mice: definitions and classification. The consensus report from the Bar Harbor meeting of the Mouse Models of Human Cancer Consortium Prostate Pathology Committee*. *Cancer Res*, 2004. **64**(6): p. 2270-305.
34. Wang, S., et al., *Prostate-specific deletion of the murine Pten tumor suppressor gene leads to metastatic prostate cancer*. *Cancer Cell*, 2003. **4**(3): p. 209-21.
35. Chen, Z., et al., *Crucial role of p53-dependent cellular senescence in suppression of Pten-deficient tumorigenesis*. *Nature*, 2005. **436**(7051): p. 725-30.
36. Di Cristofano, A., et al., *Pten and p27KIP1 cooperate in prostate cancer tumor suppression in the mouse*. *Nat Genet*, 2001. **27**(2): p. 222-4.
37. Kim, M.J., et al., *Cooperativity of Nkx3.1 and Pten loss of function in a mouse model of prostate carcinogenesis*. *Proc Natl Acad Sci U S A*, 2002. **99**(5): p. 2884-9.
38. Gao, H., et al., *A critical role for p27kip1 gene dosage in a mouse model of prostate carcinogenesis*. *Proc Natl Acad Sci U S A*, 2004. **101**(49): p. 17204-9.
39. Ding, Z., et al., *SMAD4-dependent barrier constrains prostate cancer growth and metastatic progression*. *Nature*, 2011. **470**(7333): p. 269-73.

40. Martin, P., et al., *Prostate epithelial Pten/TP53 loss leads to transformation of multipotential progenitors and epithelial to mesenchymal transition*. Am J Pathol, 2011. **179**(1): p. 422-35.
41. Vousden, K.H., *Functions of p53 in metabolism and invasion*. Biochem Soc Trans, 2009. **37**(Pt 3): p. 511-7.
42. Vousden, K.H., *Alternative fuel--another role for p53 in the regulation of metabolism*. Proc Natl Acad Sci U S A, 2010. **107**(16): p. 7117-8.
43. Vousden, K.H. and K.M. Ryan, *p53 and metabolism*. Nat Rev Cancer, 2009. **9**(10): p. 691-700.
44. Glinskii, A.B., et al., *Viable circulating metastatic cells produced in orthotopic but not ectopic prostate cancer models*. Cancer Res, 2003. **63**(14): p. 4239-43.
45. Wang, Y., et al., *Development and characterization of efficient xenograft models for benign and malignant human prostate tissue*. Prostate, 2005. **64**(2): p. 149-59.
46. Rembrink, K., et al., *Orthotopic implantation of human prostate cancer cell lines: a clinically relevant animal model for metastatic prostate cancer*. Prostate, 1997. **31**(3): p. 168-74.
47. Bastide, C., et al., *A Nod Scid mouse model to study human prostate cancer*. Prostate Cancer Prostatic Dis, 2002. **5**(4): p. 311-5.
48. Stephenson, R.A., et al., *Metastatic model for human prostate cancer using orthotopic implantation in nude mice*. J Natl Cancer Inst, 1992. **84**(12): p. 951-7.
49. Kubota, T., *Metastatic models of human cancer xenografted in the nude mouse: the importance of orthotopic transplantation*. J Cell Biochem, 1994. **56**(1): p. 4-8.
50. Jenkins, D.E., et al., *Bioluminescent imaging (BLI) to improve and refine traditional murine models of tumor growth and metastasis*. Clin Exp Metastasis, 2003. **20**(8): p. 733-44.
51. Irshad, S. and C. Abate-Shen, *Modeling prostate cancer in mice: something old, something new, something premalignant, something metastatic*. Cancer Metastasis Rev, 2013. **32**(1-2): p. 109-22.
52. Tomlins, S.A., et al., *Recurrent fusion of TMPRSS2 and ETS transcription factor genes in prostate cancer*. Science, 2005. **310**(5748): p. 644-8.
53. Shen, M.M. and C. Abate-Shen, *Pten inactivation and the emergence of androgen-independent prostate cancer*. Cancer Res, 2007. **67**(14): p. 6535-8.
54. Warburg, O., F. Wind, and E. Negelein, *The Metabolism of Tumors in the Body*. J Gen Physiol, 1927. **8**(6): p. 519-30.
55. Berg, J., Tymoczko JL, Stryer L, *Biochemistry*. 2007, New York: Freeman.
56. Schulze, A. and A.L. Harris, *How cancer metabolism is tuned for proliferation and vulnerable to disruption*. Nature, 2012. **491**(7424): p. 364-73.
57. Lunt, S.Y. and M.G. Vander Heiden, *Aerobic glycolysis: meeting the metabolic requirements of cell proliferation*. Annu Rev Cell Dev Biol, 2011. **27**: p. 441-64.
58. Golshani-Hebroni, S.G. and S.P. Bessman, *Hexokinase binding to mitochondria: a basis for proliferative energy metabolism*. J Bioenerg Biomembr, 1997. **29**(4): p. 331-8.
59. Pedersen, P.L., *Warburg, me and Hexokinase 2: Multiple discoveries of key molecular events underlying one of cancers' most common phenotypes, the "Warburg Effect", i.e., elevated glycolysis in the presence of oxygen*. J Bioenerg Biomembr, 2007. **39**(3): p. 211-22.

60. Mathupala, S.P., Y.H. Ko, and P.L. Pedersen, *Hexokinase II: cancer's double-edged sword acting as both facilitator and gatekeeper of malignancy when bound to mitochondria*. *Oncogene*, 2006. **25**(34): p. 4777-86.
61. Mathupala, S.P., Y.H. Ko, and P.L. Pedersen, *Hexokinase-2 bound to mitochondria: cancer's stygian link to the "Warburg Effect" and a pivotal target for effective therapy*. *Semin Cancer Biol*, 2009. **19**(1): p. 17-24.
62. Manning, B.D. and L.C. Cantley, *AKT/PKB signaling: navigating downstream*. *Cell*, 2007. **129**(7): p. 1261-74.
63. Vignot, S., et al., *mTOR-targeted therapy of cancer with rapamycin derivatives*. *Ann Oncol*, 2005. **16**(4): p. 525-37.
64. Morgensztern, D. and H.L. McLeod, *PI3K/Akt/mTOR pathway as a target for cancer therapy*. *Anticancer Drugs*, 2005. **16**(8): p. 797-803.
65. Hanada, M., J. Feng, and B.A. Hemmings, *Structure, regulation and function of PKB/AKT--a major therapeutic target*. *Biochim Biophys Acta*, 2004. **1697**(1-2): p. 3-16.
66. Guertin, D.A. and D.M. Sabatini, *An expanding role for mTOR in cancer*. *Trends Mol Med*, 2005. **11**(8): p. 353-61.
67. Downward, J., *PI 3-kinase, Akt and cell survival*. *Semin Cell Dev Biol*, 2004. **15**(2): p. 177-82.
68. Costello, L.C. and R.B. Franklin, *Novel role of zinc in the regulation of prostate citrate metabolism and its implications in prostate cancer*. *Prostate*, 1998. **35**(4): p. 285-96.
69. Huang, W.C., et al., *Activation of androgen receptor, lipogenesis, and oxidative stress converged by SREBP-1 is responsible for regulating growth and progression of prostate cancer cells*. *Mol Cancer Res*, 2012. **10**(1): p. 133-42.
70. Heemers, H.V., G. Verhoeven, and J.V. Swinnen, *Androgen activation of the sterol regulatory element-binding protein pathway: Current insights*. *Mol Endocrinol*, 2006. **20**(10): p. 2265-77.
71. Liu, Y., *Fatty acid oxidation is a dominant bioenergetic pathway in prostate cancer*. *Prostate Cancer Prostatic Dis*, 2006. **9**(3): p. 230-4.
72. Duvel, K., et al., *Activation of a metabolic gene regulatory network downstream of mTOR complex I*. *Mol Cell*, 2010. **39**(2): p. 171-83.
73. Lamming, D.W. and D.M. Sabatini, *A Central role for mTOR in lipid homeostasis*. *Cell Metab*, 2013. **18**(4): p. 465-9.
74. Bakan, I. and M. Laplante, *Connecting mTORC1 signaling to SREBP-1 activation*. *Curr Opin Lipidol*, 2012. **23**(3): p. 226-34.
75. Oyama, N., et al., *11C-acetate PET imaging of prostate cancer*. *J Nucl Med*, 2002. **43**(2): p. 181-6.
76. Oyama, N., et al., *11C-acetate PET imaging of prostate cancer: detection of recurrent disease at PSA relapse*. *J Nucl Med*, 2003. **44**(4): p. 549-55.
77. Jadvar, H., *Prostate cancer: PET with 18F-FDG, 18F- or 11C-acetate, and 18F- or 11C-choline*. *J Nucl Med*, 2011. **52**(1): p. 81-9.
78. Jadvar, H., *FDG PET in Prostate Cancer*. *PET Clin*, 2009. **4**(2): p. 155-161.
79. Nakashima, R.A., et al., *Hexokinase receptor complex in hepatoma mitochondria: evidence from N,N'-dicyclohexylcarbodiimide-labeling studies for the involvement of the pore-forming protein VDAC*. *Biochemistry*, 1986. **25**(5): p. 1015-21.

80. Graham, J.F., et al., *Regulation of hexokinase in cultured gliomas*. Neurosurgery, 1985. **17**(4): p. 537-42.
81. Gauthier, T., C. Denis-Pouxviel, and J.C. Murat, *Mitochondrial hexokinase from differentiated and undifferentiated HT29 colon cancer cells: effect of some metabolites on the bound/soluble equilibrium*. Int J Biochem, 1990. **22**(4): p. 419-23.
82. Miccoli, L., et al., *Intracellular pH governs the subcellular distribution of hexokinase in a glioma cell line*. Biochem J, 1996. **313** (Pt 3): p. 957-62.
83. Ahn, K.J., et al., *Evaluation of the role of hexokinase type II in cellular proliferation and apoptosis using human hepatocellular carcinoma cell lines*. J Nucl Med, 2009. **50**(9): p. 1525-32.
84. Arora, K.K., D.M. Parry, and P.L. Pedersen, *Hexokinase receptors: preferential enzyme binding in normal cells to nonmitochondrial sites and in transformed cells to mitochondrial sites*. J Bioenerg Biomembr, 1992. **24**(1): p. 47-53.
85. Pedersen, P.L., et al., *Mitochondrial bound type II hexokinase: a key player in the growth and survival of many cancers and an ideal prospect for therapeutic intervention*. Biochim Biophys Acta, 2002. **1555**(1-3): p. 14-20.
86. Rempel, A., P. Bannasch, and D. Mayer, *Differences in expression and intracellular distribution of hexokinase isoenzymes in rat liver cells of different transformation stages*. Biochim Biophys Acta, 1994. **1219**(3): p. 660-8.
87. Mathupala, S.P., A. Rempel, and P.L. Pedersen, *Aberrant glycolytic metabolism of cancer cells: a remarkable coordination of genetic, transcriptional, post-translational, and mutational events that lead to a critical role for type II hexokinase*. J Bioenerg Biomembr, 1997. **29**(4): p. 339-43.
88. Mayer, D., et al., *Hexokinase expression in liver preneoplasia and neoplasia*. Biochem Soc Trans, 1997. **25**(1): p. 122-7.
89. Rosano, C., *Molecular model of hexokinase binding to the outer mitochondrial membrane porin (VDAC1): Implication for the design of new cancer therapies*. Mitochondrion, 2011. **11**(3): p. 513-9.
90. Robey, R.B. and N. Hay, *Mitochondrial hexokinases, novel mediators of the antiapoptotic effects of growth factors and Akt*. Oncogene, 2006. **25**(34): p. 4683-96.
91. Pastorino, J.G., N. Shulga, and J.B. Hoek, *Mitochondrial binding of hexokinase II inhibits Bax-induced cytochrome c release and apoptosis*. J Biol Chem, 2002. **277**(9): p. 7610-8.
92. Pastorino, J.G. and J.B. Hoek, *Hexokinase II: the integration of energy metabolism and control of apoptosis*. Curr Med Chem, 2003. **10**(16): p. 1535-51.
93. Azoulay-Zohar, H., et al., *In self-defence: hexokinase promotes voltage-dependent anion channel closure and prevents mitochondria-mediated apoptotic cell death*. Biochem J, 2004. **377**(Pt 2): p. 347-55.
94. Lynch, R.M., K.E. Fogarty, and F.S. Fay, *Modulation of hexokinase association with mitochondria analyzed with quantitative three-dimensional confocal microscopy*. J Cell Biol, 1991. **112**(3): p. 385-95.
95. Geschwind, J.F., et al., *Recently elucidated energy catabolism pathways provide opportunities for novel treatments in hepatocellular carcinoma*. Expert Rev Anticancer Ther, 2004. **4**(3): p. 449-57.

96. Geschwind, J.F., et al., *Novel therapy for liver cancer: direct intraarterial injection of a potent inhibitor of ATP production*. *Cancer Res*, 2002. **62**(14): p. 3909-13.
97. Ko, Y.H., P.L. Pedersen, and J.F. Geschwind, *Glucose catabolism in the rabbit VX2 tumor model for liver cancer: characterization and targeting hexokinase*. *Cancer Lett*, 2001. **173**(1): p. 83-91.
98. Ko, Y.H., et al., *Advanced cancers: eradication in all cases using 3-bromopyruvate therapy to deplete ATP*. *Biochem Biophys Res Commun*, 2004. **324**(1): p. 269-75.
99. Stein, M., et al., *Targeting tumor metabolism with 2-deoxyglucose in patients with castrate-resistant prostate cancer and advanced malignancies*. *Prostate*, 2010. **70**(13): p. 1388-94.
100. Shulga, N., R. Wilson-Smith, and J.G. Pastorino, *Hexokinase II detachment from the mitochondria potentiates cisplatin induced cytotoxicity through a caspase-2 dependent mechanism*. *Cell Cycle*, 2009. **8**(20): p. 3355-64.
101. Robey, R.B. and N. Hay, *Mitochondrial hexokinases: guardians of the mitochondria*. *Cell Cycle*, 2005. **4**(5): p. 654-8.
102. Majewski, N., et al., *Hexokinase-mitochondria interaction mediated by Akt is required to inhibit apoptosis in the presence or absence of Bax and Bak*. *Mol Cell*, 2004. **16**(5): p. 819-30.
103. Roudier, M.P., et al., *Phenotypic heterogeneity of end-stage prostate carcinoma metastatic to bone*. *Hum Pathol*, 2003. **34**(7): p. 646-53.
104. Sircar, K., et al., *PTEN genomic deletion is associated with p-Akt and AR signalling in poorer outcome, hormone refractory prostate cancer*. *J Pathol*, 2009. **218**(4): p. 505-13.
105. Taylor, B.S., et al., *Integrative genomic profiling of human prostate cancer*. *Cancer Cell*. **18**(1): p. 11-22.
106. Agell, L., et al., *KLF6 and TP53 mutations are a rare event in prostate cancer: distinguishing between Taq polymerase artifacts and true mutations*. *Mod Pathol*, 2008. **21**(12): p. 1470-8.
107. Schlomm, T., et al., *Clinical significance of p53 alterations in surgically treated prostate cancers*. *Mod Pathol*, 2008. **21**(11): p. 1371-8.
108. Weinberg, R.A., *Mechanisms of malignant progression*. *Carcinogenesis*, 2008. **29**(6): p. 1092-5.
109. Goldstein, A.S., T. Stoyanova, and O.N. Witte, *Primitive origins of prostate cancer: In vivo evidence for prostate-regenerating cells and prostate cancer-initiating cells*. *Mol Oncol*.
110. Bubendorf, L., et al., *Metastatic patterns of prostate cancer: an autopsy study of 1,589 patients*. *Hum Pathol*, 2000. **31**(5): p. 578-83.
111. Shah, R.B., et al., *Androgen-independent prostate cancer is a heterogeneous group of diseases: lessons from a rapid autopsy program*. *Cancer Res*, 2004. **64**(24): p. 9209-16.
112. van Leenders, G.J., et al., *Expression of basal cell keratins in human prostate cancer metastases and cell lines*. *J Pathol*, 2001. **195**(5): p. 563-70.

113. Wang, S., et al., *Pten deletion leads to the expansion of a prostatic stem/progenitor cell subpopulation and tumor initiation*. Proc Natl Acad Sci U S A, 2006. **103**(5): p. 1480-5.
114. Korsten, H., et al., *Accumulating progenitor cells in the luminal epithelial cell layer are candidate tumor initiating cells in a Pten knockout mouse prostate cancer model*. PLoS One, 2009. **4**(5): p. e5662.
115. Wang, X., et al., *A luminal epithelial stem cell that is a cell of origin for prostate cancer*. Nature, 2009. **461**(7263): p. 495-500.
116. Abou-Kheir, W., et al., *Characterizing the contribution of stem/progenitor cells to tumorigenesis in the Pten+/-TP53+/- prostate cancer model*. Stem Cells, 2010. **In press**.
117. Cao, Y.A., et al., *Molecular imaging using labeled donor tissues reveals patterns of engraftment, rejection, and survival in transplantation*. Transplantation, 2005. **80**(1): p. 134-9.
118. Meletis, K., et al., *p53 suppresses the self-renewal of adult neural stem cells*. Development, 2006. **133**(2): p. 363-9.
119. Zhao, T. and Y. Xu, *p53 and stem cells: new developments and new concerns*. Trends Cell Biol. **20**(3): p. 170-5.
120. Zheng, H., et al., *p53 and Pten control neural and glioma stem/progenitor cell renewal and differentiation*. Nature, 2008. **455**(7216): p. 1129-33.
121. Signoretti, S., et al., *p63 regulates commitment to the prostate cell lineage*. Proc Natl Acad Sci U S A, 2005. **102**(32): p. 11355-60.
122. Gu, G., et al., *Prostate cancer cells with stem cell characteristics reconstitute the original human tumor in vivo*. Cancer Res, 2007. **67**(10): p. 4807-15.
123. Ansieau, S., et al., *Induction of EMT by twist proteins as a collateral effect of tumor-promoting inactivation of premature senescence*. Cancer Cell, 2008. **14**(1): p. 79-89.
124. Smit, M.A. and D.S. Peeper, *Deregulating EMT and senescence: double impact by a single twist*. Cancer Cell, 2008. **14**(1): p. 5-7.
125. Hansel, D.E. and J.I. Epstein, *Sarcomatoid carcinoma of the prostate: a study of 42 cases*. Am J Surg Pathol, 2006. **30**(10): p. 1316-21.
126. Molchadsky, A., et al., *p53 plays a role in mesenchymal differentiation programs, in a cell fate dependent manner*. PLoS One, 2008. **3**(11): p. e3707.
127. Cardiff, R.D., *The pathology of EMT in mouse mammary tumorigenesis*. J Mammary Gland Biol Neoplasia. **15**(2): p. 225-33.
128. Jonkers, J., et al., *Synergistic tumor suppressor activity of BRCA2 and p53 in a conditional mouse model for breast cancer*. Nat Genet, 2001. **29**(4): p. 418-25.
129. Yin, J., et al., *Activation of the RalGEF/Ral pathway promotes prostate cancer metastasis to bone*. Mol Cell Biol, 2007. **27**(21): p. 7538-50.
130. Giskeodegard, G.F., et al., *Spermine and citrate as metabolic biomarkers for assessing prostate cancer aggressiveness*. PLoS One, 2013. **8**(4): p. e62375.
131. Jordan, K.W. and L.L. Cheng, *NMR-based metabolomics approach to target biomarkers for human prostate cancer*. Expert Rev Proteomics, 2007. **4**(3): p. 389-400.
132. Kobus, T., et al., *In vivo (1) H MR spectroscopic imaging of aggressive prostate cancer: Can we detect lactate?* Magn Reson Med, 2014. **71**(1): p. 26-34.

133. Maxeiner, A., et al., *Retrospective analysis of prostate cancer recurrence potential with tissue metabolomic profiles*. Prostate, 2010. **70**(7): p. 710-7.
134. McDunn, J.E., et al., *Metabolomic signatures of aggressive prostate cancer*. Prostate, 2013. **73**(14): p. 1547-60.
135. Santos, C.F., et al., *Metabolic, pathologic, and genetic analysis of prostate tissues: quantitative evaluation of histopathologic and mRNA integrity after HR-MAS spectroscopy*. NMR Biomed, 2010. **23**(4): p. 391-8.
136. Serkova, N.J., et al., *The metabolites citrate, myo-inositol, and spermine are potential age-independent markers of prostate cancer in human expressed prostatic secretions*. Prostate, 2008. **68**(6): p. 620-8.
137. Sreekumar, A., et al., *Metabolomic profiles delineate potential role for sarcosine in prostate cancer progression*. Nature, 2009. **457**(7231): p. 910-4.
138. Swanson, M.G., et al., *Proton HR-MAS spectroscopy and quantitative pathologic analysis of MRI/3D-MRSI-targeted postsurgical prostate tissues*. Magn Reson Med, 2003. **50**(5): p. 944-54.
139. Trock, B.J., *Application of metabolomics to prostate cancer*. Urol Oncol, 2011. **29**(5): p. 572-81.
140. Sellers, W.R., and Sawyers, C.L., *Somatic Genetics of Prostate Cancer: Oncogenes and Tumore Suppressors* 2002, Philadelphia:: Lippincott Williams & Wilkins.
141. Mulholland, D.J., et al., *Cell autonomous role of PTEN in regulating castration-resistant prostate cancer growth*. Cancer Cell, 2011. **19**(6): p. 792-804.
142. Jadvar, H., et al., *Glucose metabolism of human prostate cancer mouse xenografts*. Mol Imaging, 2005. **4**(2): p. 91-7.
143. Ozcan Kara, P., et al., *Comparison of bone scintigraphy and 18F-FDG PET-CT in a prostate cancer patient with osteolytic bone metastases*. Rev Esp Med Nucl, 2011. **30**(2): p. 94-6.
144. Yu, E.Y., et al., *C11-acetate and F-18 FDG PET for men with prostate cancer bone metastases: relative findings and response to therapy*. Clin Nucl Med, 2011. **36**(3): p. 192-8.
145. Morris, M.J., et al., *Fluorodeoxyglucose positron emission tomography as an outcome measure for castrate metastatic prostate cancer treated with antimicrotubule chemotherapy*. Clin Cancer Res, 2005. **11**(9): p. 3210-6.
146. Swinnen, J.V., et al., *Androgens, lipogenesis and prostate cancer*. J Steroid Biochem Mol Biol, 2004. **92**(4): p. 273-9.
147. Barfeld, S., et al., *Androgen-regulated metabolism and biosynthesises in prostate cancer*. Endocr Relat Cancer, 2014.
148. Massie, C.E., et al., *The androgen receptor fuels prostate cancer by regulating central metabolism and biosynthesis*. EMBO J, 2011. **30**(13): p. 2719-33.
149. Putluri, N., et al., *Metabolomic profiling reveals a role for androgen in activating amino acid metabolism and methylation in prostate cancer cells*. PLoS One, 2011. **6**(7): p. e21417.
150. Capano, M. and M. Crompton, *Biphasic translocation of Bax to mitochondria*. Biochem J, 2002. **367**(Pt 1): p. 169-78.

151. Patra, K.C., et al., *Hexokinase 2 is required for tumor initiation and maintenance and its systemic deletion is therapeutic in mouse models of cancer*. *Cancer Cell*, 2013. **24**(2): p. 213-28.
152. Jung, K., *Words of wisdom. Re: the metabolites citrate, myo-inositol, and spermine are potential age-independent markers of prostate cancer in human expressed prostatic secretions*. *Eur Urol*, 2008. **54**(5): p. 1198-9.
153. Gao, H., et al., *Combinatorial activities of Akt and B-Raf/Erk signaling in a mouse model of androgen-independent prostate cancer*. *Proc Natl Acad Sci U S A*, 2006. **103**(39): p. 14477-82.
154. Gao, H., et al., *Emergence of androgen independence at early stages of prostate cancer progression in *Nkx3.1*; *Pten* mice*. *Cancer Res*, 2006. **66**(16): p. 7929-33.
155. Jiao, J., et al., *Murine cell lines derived from *Pten* null prostate cancer show the critical role of *PTEN* in hormone refractory prostate cancer development*. *Cancer Res*, 2007. **67**(13): p. 6083-91.